A Computational Approach to the Synthesis of Chiral Sulfoxides

PhD Thesis

David Balcells Badia

2006

Supervised by Feliu Maseras Cuní and Gregori Ujaque Perez

Departament de Química

Facultat de Ciències

Universitat Autònoma de Barcelona

Acknowledgments

Six years ago I was finishing the industry practicals in a pharmaceutical company called Combino Pharm S.L.; I was feeling very well there, there was a very good atmosphere and also HPLC, a very interesting method of analysis that gave me the opportunity of working with computers; I was close to get the bachelor degree in Chemistry and they offered to me a position; but at that time I had other things in mind, I was interested in research; in fact, few months before, I attended a seminar in which a couple of prefossors with a peculiar but interesting look, Feliu and Agustí, talked about doing research by means of computed-assisted simulations; I get very interested on that and especially with the possibility of exploring methods of asymmetric synthesis with that tools; so I went to meet Feliu in his office and I told him that I wanted to study *in silico* enantioselective synthesis; and well, here you have this thesis.

Since I started my thesis I have done a lot of interesting things, including my preferred activity now: travelling; in the last years of my thesis I have been in nine different countries, in most cases thanks to my research activities (Syria, France, Russia, Canada, UK, Japan and USA) and in other cases thanks to my addiction to climbing (India and Thailand); I also learned a lot of things related with theoretical and experimental chemistry, computer science, and I managed to reach an acceptable level of english.

I should acknowledge a lot of people for their support and guidance in the long way of this thesis; but first of all, I want to thank my parents just to be able of being here now, in front of my laptop, writing these words; without them, I guess I would have a different form, I would be another person or animal; or maybe I would be something undefined, scattered among a cluster of living beings or objects; or maybe, I would just not be; I want to acknowledge all the people at Química Física, in UAB, that helped me from the beginning: Maria, Jaume, Laura, Prat, Galí, Oriol, Xavi, Erika, Marc, Adrià, Ataualpa, Alfons, Ismael, Edu, Raquel,...; and all my friends that decided to do research in other fields: Ona, Úrsula, Sílvia, Montse, Manu, Jordi,...; and also the support given by the supervisers of this thesis: Gregori and Feliu; and

the company and guidance of Agustí; and my new colleagues at ICIQ: Pere, Eva, Marta, Campa, Joan, Torstein, Fabienne, Oriol, Manolo, Núria,...; and the support and company of the Tous sect, before and during the thesis; the guidance of Tom Ziegler in Calgary, and of Shigeyoshi Sakaki in Kyoto; and the nice people I met in Calgary: Kumar, Anastasia, Jashek, Roger, Miclosh, Artur, Elizabeth, David, Shengyong, Zithao, ...; and in Kyoto: Ima, Shimizu, Yoko,...; and to the Kinesiology of climbing, and to all I learned in the the walls and boulders that I climbed in Montserrat, Escales, Cavallers, Prades, Fontainebleau, Albarracín, Sant Joan de Vilatorrada, Squamish, Lake Louis, ...; and to Ainara, for being with me, so close; and to all the good people and energy I met during the thesis and that I forgot to mention here.

Thank you very much, and please,

we should take care of ourselfs

Sant Martí de Tous, 23/4/06

Contents

Part I

General Introduction, Objectives, Discussion of the Results and Conclusions

Chapter 1

General Introduction

1.1 Chirality and Asymmetric Synthesis

1.1.1 The Concept of Chirality

Chirality is the property found in those objects that cannot be overlapped with their mirror images.[1] The word chirality was derived from the greek term *chiros* which means hands, and hands are an example of chiral objects (see Figure 1.1). In contrast with this, soccer balls and spheres in general are not chiral since their mirror images are absolutely equal. The concept of chirality applies to chemistry and thousands of molecules with this property have been characterized. Like the *cis* and *trans* isomers of olefins, enantiomers are one type of stereoisomers, *i.e.* molecules characterized by the same connectivity that only differ in their spatial arrangement.

Alanine is the smallest chiral aminoacid (see Figure 1.1). Alanine and its mirror image, alanine', are apparently equal and in fact they are, with the sole exception of not being superimposable. In contrast with this, methane is a non chiral molecule since it is equal to its mirror image, methane'. Alanine and alanine' are said to be enantiomers of each other. Each enantiomer is labeled as R or S following the Cahn-Ingold-Prelog arbitrary rules. According to these rules alanine is (R)-alanine and alanine' is (S)-alanine. In biochemistry, the D and L labels are used to distinguish amino acid and carbohydrate enantiomers applying other rules. From the physical point of

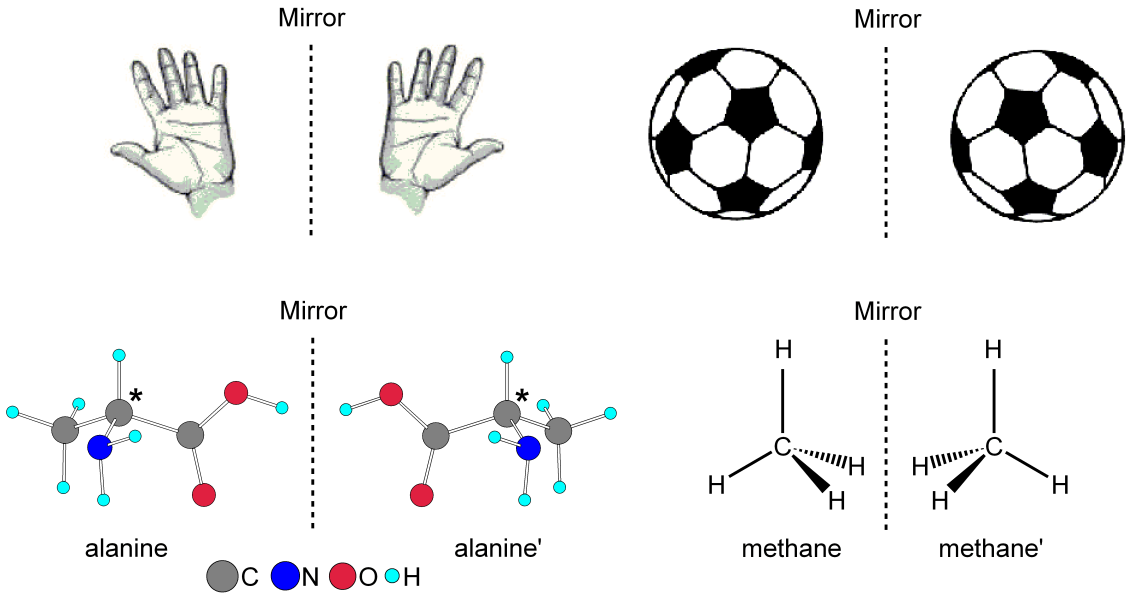

Figure 1.1: Chiral (left) and non chiral (right) objects and molecules.

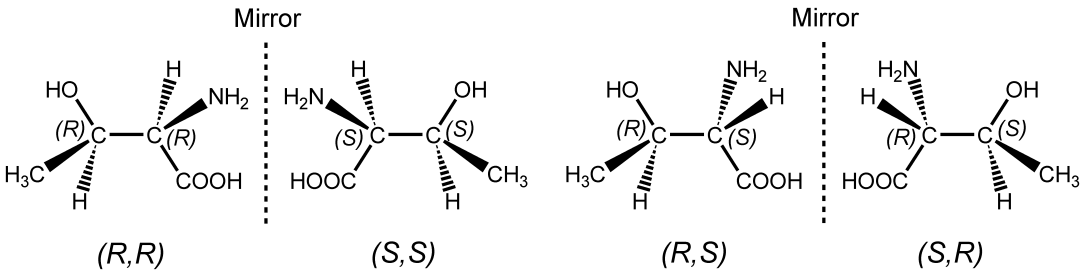

Figure 1.2: Stereoisomers of treonine.

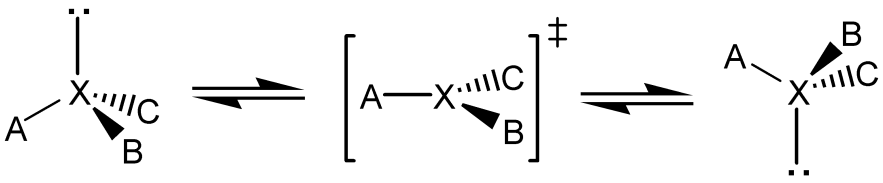

Figure 1.3: Pyramidal inversion.

view, chiral compounds have the property of rotate the plane of polarized light by an angle of α°. Since α is proportional to the length of the cell containing the chiral compound (l) and the concentration of the sample (c), $[\alpha]$, known as specific rotation, is defined as follows:

$$[\alpha] = \frac{\alpha(^{\circ})}{\mathrm{l(dm)c(gml^{-1})}} \tag{1.1}$$

The value of $[\alpha]$ depends on the wavelength and temperature and when is different of zero for some compound, the latter is said to be optically active. Furthermore, if one enantiomer induces a clockwise rotation of $+\alpha^{\circ}$ then the other does exactly the same but in the opposite (counterclockwise) direction by -α°. Hence, a couple of enantiomers have the same absolute value of $[\alpha]$ but with opposite signs. The sign of $[\alpha]$ is also used to label enantiomers. Taking into account the specific rotations of (R)-alanine (-14.5°) and (S)-alanine (+14.5°) these enantiomers would be labeled as (-)-alanine and (+)-alanine respectively. R/S and D/L labels are determined following arbitrary rules, while specific rotation is a physical property. Thus, there is no systematic correlation between the (+)/(-) and the R/S nor the D/L labels. The specific identity of one enantiomer, regardless of the labeling used, is referred to as absolute configuration.

Alanine and any other organic molecule having an sp^3 carbon with four different substituents is chiral. In coordination and organometallic chemistry, metal complexes can be also chiral. For instance, a square pyramidal complex with five different substituents is chiral. In general, the chirality introduced by an atomic center attached to different substituents is known as central chirality. Such atomic center is referred to as the stereogenic center or stereocenter (usually marked with an asterisk as in Figure 1.1). From the point of view of symmetry, the existence of non equivalent enantiomers is associated with the lack of improper axis of symmetry (S_n), including symmetry planes (S_1) and centers of inversion (S_2). The origin of this asymmetry is found in the stereogenic center itself. Two other types of chirality not involving stereocenters also exist: axial and planar chirality. All chiral compounds studied in this thesis have central chirality.

Enantiomers have exactly the same energy, and this applies to poten-

tial, internal, enthalpic and free energies. Hence, when (R)-alanine and (S)-alanine are in equilibrium both molecules are mixed in a 50:50 ratio. These mixtures are known as racemic mixtures or racemates. In contrast with this, a sample containing a single enantiomer is said to be enantiopure. From the pysical point of view, racemates are characterized by a specific rotation of 0° and they are thus optically inactive.

Two or more stereogenic centers might be combined within a single molecule giving rise to different isomers. For instance, the two asymmetric carbons of the treonine aminoacid (see Figure 1.2) give rise to four different isomers, namely (R,R), (R,S), (S,R) and (S,S). (R,R)/(S,S), and also (R,S)/(S,R), are mirror images and thus isoenergetic enantiomers because the absolute configuration of both stereocenters is reversed. In contrast with this, the molecules of each (R,R)/(R,S), (R,R)/(S,R), (S,S)/ (S,R) and (S,S)/(R,S) pairs are neither superimposable nor mirror images. The relationship among these molecules is called diastereisomery. Enantiomers and diastereomers are two different types of stereoisomers. One of the most important differences between them is that unlike enantiomers, diastereomers have clearly different energies and chemical and physical properties. Introduction of diastereoisomery by combining different stereocenters is of fundamental importance in asymmetric synthesis as will be shown below.

Some enantiomers have temperature-depending optical activity because they are transformed into their mirror images by a relatively fast reaction. This process is known as racemization since it involves the transformation of a pure chiral compound into a racemate. In the case of sp^3 central chirality, when the stereocenter has lone electronic pairs (amines and sulfoxides) both enantiomers can be interconverted through a process known as pyramidal inversion (see Figure 1.3). In such process the tetrahedral mirror images are interconverted through a trigonal planar transition state. When the racemization of a chiral compound is not possible or it only happens in extreme conditions then it is said to be optically stable.

1.1.2 The Importance of Chirality

Most drugs are chiral compounds with some biological activity based on their interaction with a given enzyme. Enzymes, and most biological systems, are able to recognize both enantiomers of a chiral compound. This is because such natural species, which are chiral themselves, stablish non-degenerate diastereomeric interactions with each enantiomer. Thus, it usually happens that one enantiomer of a drug is very efficient whereas the other one is totally inactive, and the same happens for many agrochemicals.[2] Furthermore, in some cases the non efficient enantiomer induces undesirable effects. For instance, the comercialization of a drug known as thalidomide in its racemic form caused a tragedy in the late 1950s.[3] This drug, with sedative properties, was prescribed to pregnant women. Nevertheless, while one enantiomer of thalidomide had this effect, the other one induced malformations in the fetus. Since the thalidomide affair new laws concerning the enantiomeric purity of drugs have been aproved and applied around the world.[4,5] Due to these laws, in most pharmaceutical industries the preparation of their products as single enantiomers is a duty. Furhtermore, as will be explained below, optically active compounds are not only the final goal but also the tool to achieve it. Two different strategies are used to produce optically active compounds: asymmetric synthesis and resolution of racemates.

1.1.3 Asymmetric Synthesis

Asymmetric synthesis consists of transforming a non chiral substrate by generating new stereogenic centers with a particular configuration. From the conceptual point of view, the goal achieved by asymmetric synthesis is not trivial if we keep in mind that enantiomers have the same energy. In the reaction pathway of an asymetric transformation, chirality is created at some point and then such pathway diverges in two enantiomeric paths, one leading to the R enantiomer and the other to the S enantiomer. If these paths are strictly enantiomeric, that is, interconverted through a mirror, then they are isoenergetic and then the reaction gives rise to a racemic mixture (see Figure 1.4).

Enantiopure reaction products are obtained taking advantage of the same

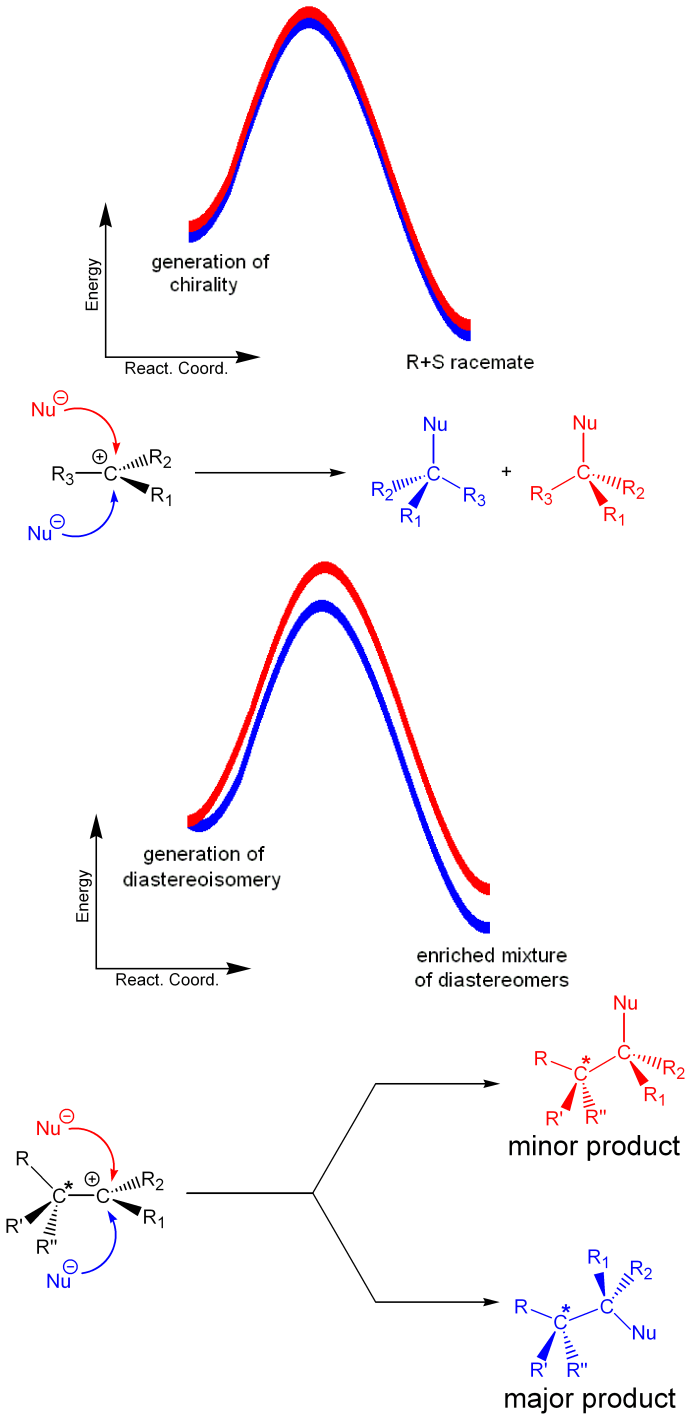

Figure 1.4: Enantiomeric (above) and diastereomeric (below) energy profiles in the S_N1 mechanism.

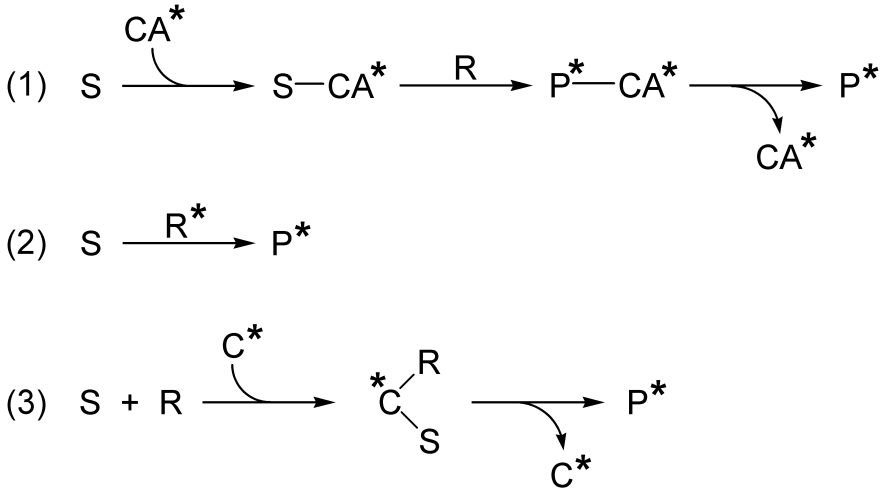

Figure 1.5: Asymmetric synthesis by means of chiral auxiliaries (1), chiral reagents (2) and asymmetric catalysts (3). S=Substrate, CA=Chiral Auxiliary, R=Reagent, C=Catalyst, P=Product.

property desired in the final reaction product: chirality. A chiral entity with a well defined and stable configuration is introduced into the reaction system. As in the enantiomeric pathways, a stereogenic center with two different configurations is created but now in the presence of an additional stereocenter with a fixed configuration. Hence, the system now evolves along two diastereomeric non degenerate pathways towards a mixture of diastereomers out of the 1:1 ratio (see Figure 1.4). In this case, the overall reaction is said to be stereoselective. In some methods of asymmetric synthesis the external source of chirality inducing stereoselectivity is only temporarily attached to the substrate and the possible reaction products are a couple of enantiomeric structures. This is the case of enantioselective synthesis for which stereoselectivity is particulary referred to as enantioselectivity. In other synthetic methods the external source of chirality is still present in products or two or more stereocenters are created. In this case the reaction product consists of a mixture of two or more diastereomers. This is the case of diastereoselective synthesis for which stereoselectivity is particulary referred to as diastereoselectivity.

Enantioselectivity and diastereoselectivity are quantified by computing

enantiomeric excess (ee) and diastereomeric excess (de) respectively as follows:

$$\frac{[A]-[B]}{[A]+[B]}100\% \text{ ee or de} \tag{1.2}$$

where [A] and [B] are the concentrations of the product isomers (enantiomers or diastereomers). For instance, a reaction giving rise to a couple of enantiomers has an enantioselectivity of 0% ee if it produces a racemate but of 100% ee if it leads to a single pure enantiomer.

The concepts mentioned above can be illustrated considering a simple and classic organic transformation: the nucleophilic substitution through the S_N1 mechanism (see Figure 1.4). In the initial step of the mechanism a trigonal planar carbocation intermediate is formed. In a subsequent reaction, a nucleophilic anion (Nu^-) attacks the cationic carbon forming a new stereogenic center. Such attack can occur on either face of the carbocation giving rise to the two possible enantiomers of the final product. If substituents R_1, R_2 and R_3 do not contain any chiral center, then both attacks are absolutely equivalent and a racemate is obtained. The energy profiles of the two possible pathways are enantiomeric and thus degenerate. Hence, the reaction proceeds with 0% ee. Nevertheless, the degenerate energy profiles can be separated introducing an additional stereocenter with a fixed configuration. In the approach represented in red, Nu^- interacts with R while in the attack depicted in blue it comes into close proximity with R' and R". Thus the two possible facial approaches will follow non degenerate paths because each one is characterized by different stereoelectronic interactions. Associating the blue and red colors of the energy profiles and chemical equations, the low-energy blue reaction channel leads to the blue diastereomer that will be obtained as the major product of the reaction. On the other hand, the red diastereomer would be the major reaction product if the absolute configuration of C^* is reversed.

The diastereoisomery needed to achieve stereoselective transformations can be introduced into the reaction pathways following three different strategies: 1) using a chiral auxiliary 2) using a chiral reagent 3) using a chiral catalyst. A general representation of each strategy is given in Figure 1.5. In the first approach an optically active compound (the chiral auxiliary) is

previously bound to the reactant. The presence of the auxiliary stereocenter introduces the diastereosimery needed to create the new chiral center stereoselectively in a subsequent reaction. In a final step the chiral auxiliary is removed from the diasteromer obtained as the major product in order to obtain the target chiral product. In the diastereoselective S_N1 reaction represented in Figure 1.4, the chiral center introduced in the R_3 substituent can be considered as a chiral auxiliary. A classical example of chiral auxiliary that has been widely used in asymmetric synthesis is menthol and its derivatives.[6–8] In the second method a chiral reagent transfers a molecular fragment to the substrate creating a new stereocenter. An example of this methodology is the asymmetric hydroxylation of enolates with chiral oxaziridines.[9] The synthetic approaches based on chiral auxiliaries and reagents require stoichiometric amounts of these compounds. In the third method, known as asymmetric catalysis, diastereoisomery is introduced by a chiral catalyst which in most cases is a metal complexed with an optically active ligand. Biocatalysts such as enzymes[10,11] and catalytic antibodies[12] have been used as well.

Asymmetric catalysis is in principle the most convenient method because it does not require stoichiometric amounts of optically active reagents that are usually expensive. Thanks to this, one molecule of a chiral catalyst assists the formation of millions of chiral product molecules. Moreover, the accelerating effect of the catalyst allows to obtain higher yields in shorter reaction times. Since the early 1970s the field of asymmetric catalysis has experienced an explosive development and the number of publications has increased exponentially each year. The most relevant methods that have been developed include the hydrogenation of dehydroamino acids by Knowles,[13,14] later applied to the industrial production of L-DOPA,[15] the Sharpless epoxidation,[16,17] and the asymmetric hydrogenation processes developed by Noyori,[18,19] all of them based on synthetic catalysts consisting of chiral metal complexes. These catalytic methods had a great impact in the field of asymmetric synthesis both in academic and industrial laboratories. This fact was recognized in 2001 when the Nobel prizes of chemistry were given to Knowles,[20] Sharpless[21] and Noyori[22] "for their work on chirally catalyzed hydrogenation and oxidation reactions". A number of catalytic asymmet-

ric methods have been also implemented in industry[23] like the "Monsanto process" (asymmetric hydrogenation), the "Takasago process" (asymmetric isomerization), the "Sumitomo process" (asymmetric cyclopropanation), and the "Arco process" (asymmetric Sharpless epoxidation). One of the main concerns in industry regarding the implementation of these processes is the elimination of metal-related impurities in the final product.[24]

1.1.4 Resolution of Racemates

Another important method used in the preparation of enantiopure compounds is the resolution of racemates, in which both enantiomers of a racemic mixture are separated. In this process, stereogenic centers are not created *de novo* since they are already present in the starting racemate. Hence, resolution is not considered as a method of asymmetric synthesis. Resolution of racemates is nowadays the most important synthetic method to produce chiral compounds in industry due to the patents that affect most efficient catalytic systems.[25] The resolution of racemates is applied to the obtention of chiral compounds preparing the desired reaction product in its racemic form. In a subsequent step the target enantiomer is separated from the other one. This separation, referred to as resolution, is achieved introducing diastereoisomery by means of an optically active compound. This compound, referred to as resolving agent, is attached temporarily to the substrate through a reversible chemical reaction that gives rise to a mixture of diastereomers. In the final step, the diastereomers are separated and the resolving agent is removed in order to obtain the desired enantiomer of the product. Diastereomeric interactions are also applied in the resolution of racemates by means of cromatography and SFC (Supercritical Fluid Cromatography) with chiral stationary phases is nowadays widely used in industry.[26] Furthermore, the preparation of an optically active compound by an irreversible chemical transformation of a racemic mixture is also referred to as resolution.

The resolution of racemates is in many cases based on the kinetic properties of the system and proceeds through either kinetic resolution (KR) or dynamic kinetic resolution (DKR). In KR, both enantiomers of the initial racemate react with the resolving agent with different speeds and the tar-

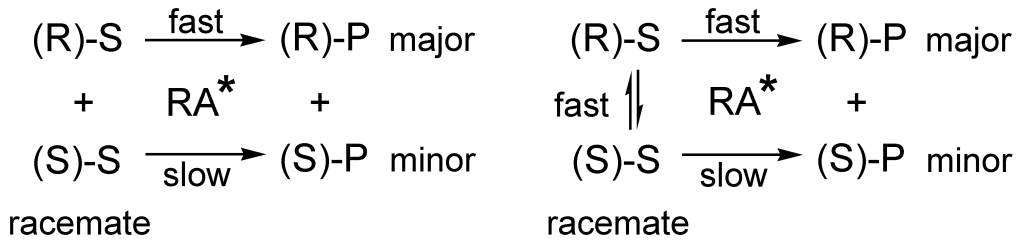

Figure 1.6: Kinetic resolution (left) and dynamic kinetic resolution (right) of racemates. S=Substrate, P=Product, RA=Resolving Agent.

get compound is obtained as the reaction product of the fastest reaction (see Figure 1.6). The main drawback of this method is that the maximum overall yield affordable is 50% because both enantiomers of the starting reactants are in a 1:1 ratio. This limitation is overcome by DKR in which both enantiomers of the racemate are somehow interconnected allowing maximum yields of 100%. Both KR[27,28] and DKR[29,30] are used as synthetic tools in modern organic synthesis.

1.1.5 Computational Studies on Asymmetric Synthesis

Enantioselective reactions are performed under kinetic control. If thermodynamic control is forced both enantiomers of the product (isoenergetic) are then equilibrated giving rise to a racemate. In diastereoselective reactions the selectivity can be thermodynamically controlled since the products have different stabilities. Nevertheless, in most cases the combination of a significant energy barrier with negative values of ΔG makes the overall reaction irreversible and the equilibration of the products is only possible at very high temperatures. From the theoretical point of view, assuming kinetic control, both ee and de can be computed (see equation 1.2) assuming that the final A:B ratio (of enantiomers or diastereomers) is given by the Boltzmann distribution at a certain temperature of the transition states leading to each isomer. Such distribution is easily computed from the free energy difference between these transition states ($\Delta G^{\ddagger}_{AB}$):

$$\frac{[A]}{[B]} = e^{-\Delta G^{\ddagger}_{AB}/RT} \tag{1.3}$$

The tools provided by modern computational chemistry[31] can be applied to estimate ΔG_{AB} and this can be useful not only to predict the enantioselectivity of a given asymmetric transformation but also to rationalize it, predict tendences and thus tackle the optimization of a given method of asymmetric synthesis or resolution in a rational fashion.

Three different types of computational methods are mainly used: quantum mechanics (QM), molecular mechanics (MM) and hybrid QM/MM. QM methods, which are based on quantum chemistry,[32] provide the most accurate description of the system and can be used to modelize bond formation and cleavage and thus reactivity. The main drawback of these methods is that they are very time-consuming especially when the system is big. MM methods,[33] which are based on classic mechanics, are fast and give a good description of steric effects. Nevertheless, their application to the study of reactivity, although is possible,[34,35] is also very fuzzy. When the system under study is big, QM/MM methods[36–39] offer the best deal giving a good description in a reasonable time. These methods are applied by dividing the system in two parts, one computed at a QM level (QM part) and the other at a MM level (MM part). The QM part includes the site of chemistry, in which bonds are formed and broken, while the rest of the system, likely to play mainly a steric role, is embedded within the MM part.

QM methods like density functional theory[40] (DFT) have been used as a powerful tool in the study of reaction mechanisms.[41,42] These methods have been successfully used to study asymmetric organocatalysis[43] and to clarify the mechanism of several metal-catalyzed reactions used in organic synthesis like σ-bond activation,[44] hydrogenation of carbon dioxide,[45] olefin polymerization,[46] isomerization of double and triple C-C bonds,[47] oxygen transfer reactions,[48] benzannulation[49] and coupling reactions (Heck,[50] Suzuki[51] and Stille[52] reactions).

In the particular case of asymmetric synthesis, the reaction mechanism is usually explored in a previous study at a QM level in a model system. In this study the step controlling the stereochemical outcome of the reac-

tion is identified. The value of $\Delta G^{\ddagger}_{AB}$ for this step is then computed with a QM/MM method considering the real system and the origin of enantioselectivity is rationalized. This strategy has been successfully applied in the study of several catalytic systems used in asymmetric hydrogenation,[53,54] olefin dihydroxylation,[55,56] hydroformylation[57,58] and hydrosylylation.[59]

1.2 Chiral Sulfoxides: Applications and Synthesis

1.2.1 Chirality in Sulfoxides

A sulfoxide (SO(R)(R')) with R≠R' is chiral since it contains a sp^3 sulfur (referred to as stereogenic sulfinyl sulfur) bound to four different substituents: one oxygen, one lone electron pair, R and R'. The term sulfoxide is reserved to those compounds in which R and R' are alkyl or aryl substituents. When these compounds contain substituents bound to sulfur through atoms more electronegative than carbon, such as nitrogen (SO(R)(NR')) or oxygen (SO(R)(OR')), they are usually referred to as sulfinyl compounds. As commented above, sulfoxides might undergo racemization through pyramidal inversion (see Figure 1.3). Nevertheless, whereas most chiral amines racemize quickly in mild conditions, the racemization of enantiopure sulfoxides occurs only at high temperatures.[60]

1.2.2 Applications of Chiral Sulfoxides

Many compounds with biological activity are chiral sulfoxides (see Figure 1.7). For instance omeprazole,[61] an antiulcer agent that was the highest selling drug in 2000, is a chiral sulfoxide sold in both racemic and S enantiopure (esomeprazole[62,63]) forms. Other relevant drugs with stereogenic sulfinyl sulfurs are the anticancer drugs sulforaphane[64,65] and sparsomycin[66,67] and the platelet adhesion inhibitor OPC-29030.[68,69]

Chiral sulfoxides have been widely used in organic asymmetric synthesis[70,71] both as chiral auxiliaries and ligands. The successful application of chiral sulfoxides in asymmetric synthesis is based on their high optical

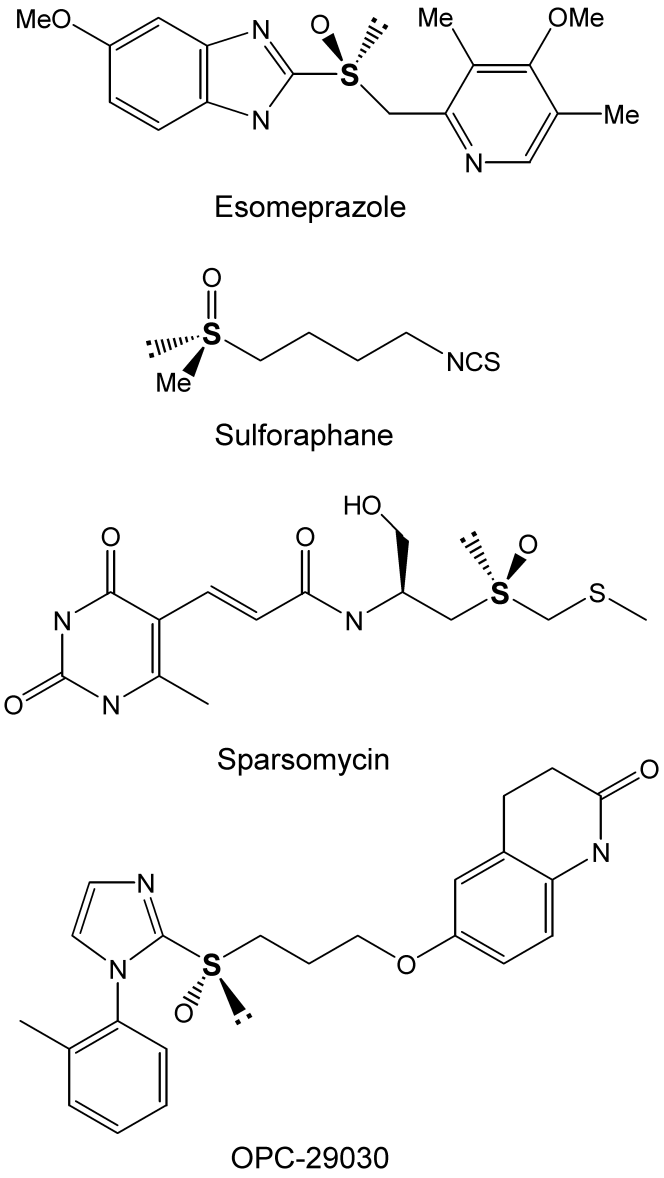

Figure 1.7: Biologically active chiral sulfoxides.

stability. The thermal racemization of chiral sulfoxides by pyramidal inversion occurs with significant rates only above 200 °C.[60] Furthermore, the stereogenic sulfinyl sulfur induces a strongly asymmetric environment since it contains three types of substituents (oxygen, lone electron pair and organic substituents) very different from each other both at the electronic and steric levels. Hence, this stereogenic center is in principle able to introduce diastereomeric interactions characterized by clearly different energies, *i.e.* significant values of $\Delta G^{\ddagger}_{AB}$ in equation 1.3. From a more pragmatic point of view, an additional advantage is given by the fact that both enantiomers of most sulfoxides are accessible in high enantiopurities. Thus, the two possible enantiomers of the target reaction product synthetized by means of chiral sulfoxides can be in principle obtained.

Thanks to the properties mentioned above, optically active sulfoxides have been efficiently used as chiral auxiliaries in the asymmetric synthesis of biologically active compounds[70] (see Figure 1.8). One general example is the asymmetric reduction of β-keto sulfoxides leading to diastereopure β-hydroxy sulfoxides. This method has been applied in the synthesis of optically active methyl carbinols,[72,73] 1,2-diols[74,75] and epoxides.[76,77] One example of this methodology is the synthesis by the group of Kosugi of epoxide **P1**,[78] a chiral precursor of juvenile hormone II. Asymmetric C-C[79,80] and C-N[81,82] bond forming reactions have been performed by means of conjugate additions to α,β-unsaturated sulfoxides. An interesting example of this method is the synthesis by Posner of **P2**,[83] a precursor of a stereoid (11-oxoequilenin methyl ether). Carbanions stabilized by chiral sulfoxides have been used in asymmetric addition reactions to carbonyls[84,85] and α,β-unsaturated compounds[86,87] that involve the formation of C-C bonds. This synthetic approach was used by the group of Hua to obtain **P3**,[88] that was subsequently tranformated into alkaloid elaeokanine B. Stereogenic sulfinyl centers have been also used as chiral auxiliaries in the Pummerer rearrangement[89,90] in which sulfoxides are converted into α-acyloxy sulfides. This transformation was used by Marino to obtain the compound **P4**,[91] which is a chiral precursor of (-)-physostigmine alkaloid. Sulfoxides have been also used as chiral auxiliaries in Diels-Alder cycloadditions either in dienophiles[92,93] or dienes.[94,95] The research group of Koizumi prepared the cyclic compound **P5**[96] by means

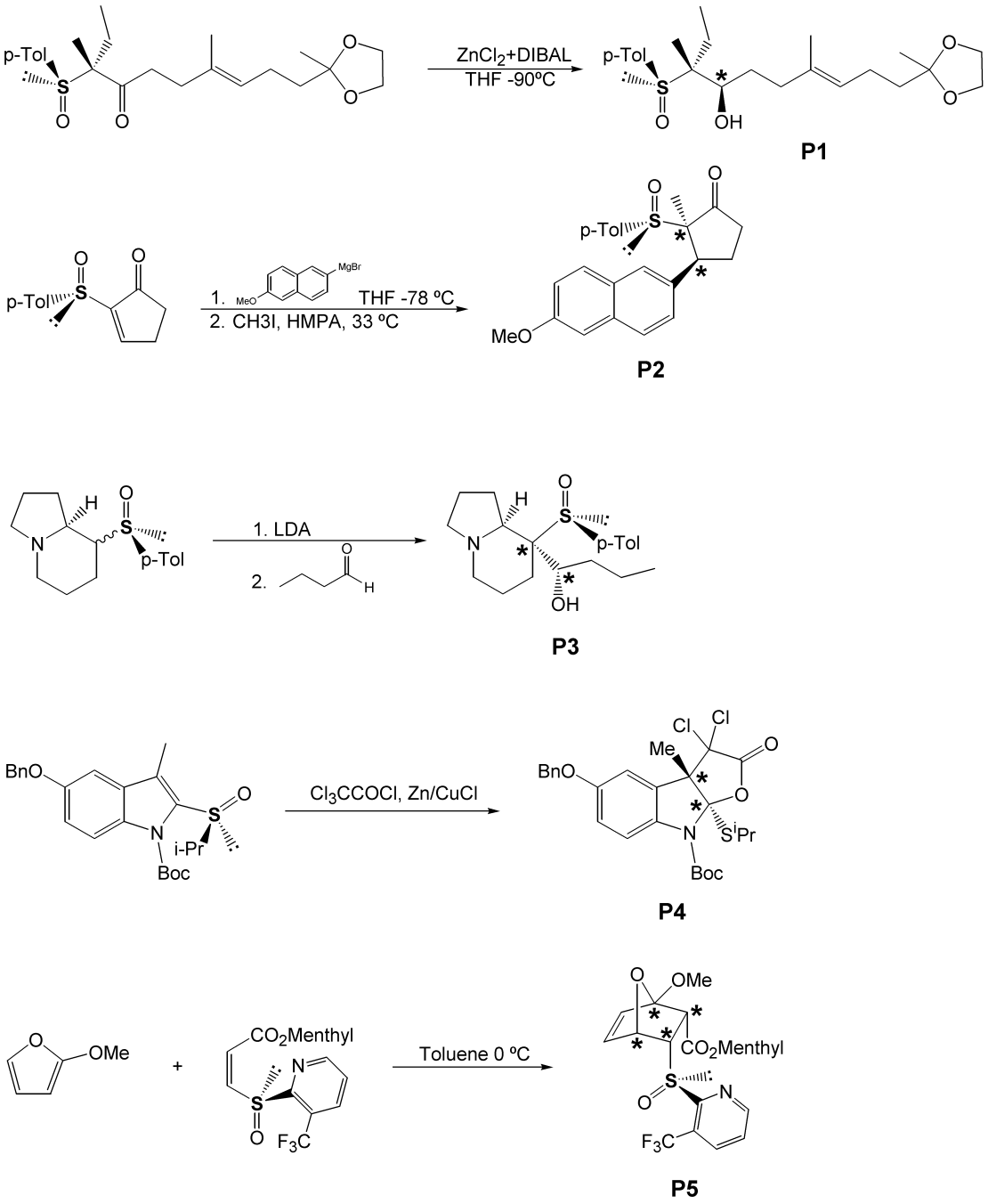

Figure 1.8: Sulfoxides as chiral auxiliaries in asymmetric synthesis.

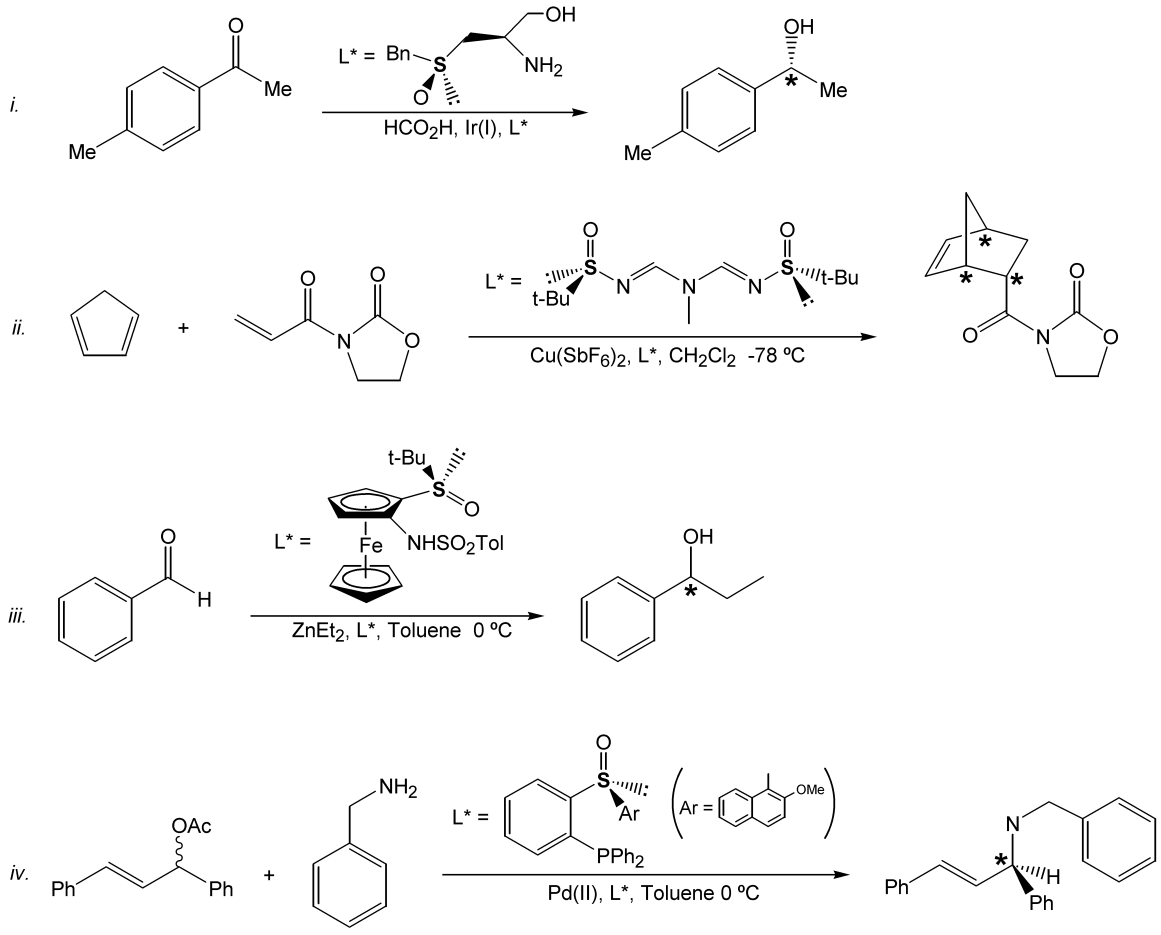

Figure 1.9: Sulfoxides as chiral ligands in asymmetric synthesis.

of a Diels-Alder cycloaddition, and used this compound in the synthesis of a glyoxalase I inhibitor.

Chiral sulfoxides have been also used in asymmetric catalysis as chiral ligands.[71] James and co-workers reported the first example of a metal-catalyzed asymmetric hydrogenation using this kind of ligands.[97] Nevertheless very low enantioselectivities (<25% ee) were obtained. Higher selectivities (up to 65% ee) were achieved by van Leeuwen's research group with an iridium catalyst[98] (example *i* in Figure 1.9). Enantiopure sulfoxide ligands were used in Lewis acid catalyzed Diels-Alder cycloadditions with moderate success (36-56% ee) in a pioneer work by Khiar.[99] The best sulfoxide-based chiral catalyst for this reaction reported to date, was recently developed by the group of Ellman[100] and gave enantioselectivities up to 98% ee (example *ii* in Figure 1.9). Asymmetric addition of diethyl zinc to aldehids in the presence of chiral sulfoxides was originally reported by the group of Garcia Ruano.[101] Chiral bidentate β-hydroxy sulfoxides were used as ligands but low enantioselectivities were achieved (<46% ee). The group of Carretero developed chiral sulfoxide ligands for this reaction derived from ferrocene[102] (example *iii* in Figure 1.9) and obtained higher selectivities (up to 88% ee). Optically active sulfoxides have been also used as ligands in catalytic allylic substitution. The research groups of Williams[103] (pioneer) and Hiroi[104] (example *iv* in Figure 1.9) have used optically active sulfoxides as ligands in this transformation obtaining enantioselectivities up to 97% ee.

1.2.3 Synthesis of Chiral Sulfoxides

Due to the relevant applications of optically active sulfoxides, several synthetic methods have been developed in order to obtain these compounds.[71] Two general methods are used: 1) asymmetric oxidation of prochiral sulfides, known as sulfoxidation, and 2) nucleophilic substitution on optically active sulfur derivatives. In the first approach a prochiral sulfide, *i.e.* a sulfide with two different substituents, is enantioselectively oxidized. In biological sulfoxidations, this process is done by means of enzymes,[105–107] microorganisms,[108–110] or catalytic antibodies.[111,112] Another option is the utilization of enantiopure oxidants, like chiral oxaziridines[113,114] and peroxides.[115,116]

Asymmetric sulfoxidations have been performed by means of optically active metal catalysts as well. In the synthetic methods based on nucleophilic substitution, enantiopure sulfoxides are obtained through the addition of a nucleophilic reagent to an optically active sulfur compound. In the following two subsections, the asymmetric metal-catalyzed sulfoxidation and the nucleohilic substitution on sulfur compounds are reviewed since the particular reactions studied in this thesis belong to these general synthetic methods.

Asymmetric Metal-Catalyzed Sulfoxidation

Optically active sulfoxides can be prepared by metal-catalyzed enantioselective oxidation of prochiral sulfides.[117] In this synthetic approach, that has been used in industry,[118] some stoichiometric oxidizing agent is used in combination with a catalyst consisting of a metal complexed with a chiral ligand which makes the oxidation enantioselective (see Figure 1.10). In most cases, the oxidant is a peroxidic compound activated by the metal. C_2-symmetric chelating bidentate tartrate ligands were used in combination with titanium as a first approach. C_2-symmetric diol, C_3-symmetric triol, salen and Schiff base ligands were afterwards introduced. The ligand evolution was followed by a diversification of the metal center and other elements like vanadium, manganese or iron were also used.

The very good performance of the Sharpless epoxidation of allylic alcohols catalyzed by titanium alcoholates[119] stimulated the research groups of Kagan and Modena to apply the same type of metal complexes to the asymmetric oxidation of sulfides. Kagan found that the mixture Ti(*i*-PrO)$_4$/(R,R)-DET/H_2O in a 1:2:1 ratio at -20°C in CH_2Cl_2 was able to promote asymmetric sulfoxidation using *tert*-butyl hydroperoxide (TBHP) as oxidant[120] (example *i* in Figure 1.10). Several dialkyl sulfides were oxidized with this mixture but high yields (70-98%) and enantioselectivities (74-95%ee) were only obtained with alkyl aryl sulfides. The main drawback of this system was that stoichiometric amounts of the titanium complex were needed in order to obtain optimal results. This problem was partially solved by Kagan using cumene hydroperoxide (CHP=Ph-C(CH$_3$)$_2$-OOH) as oxidant instead of TBHP[121] and substituting the original titanium mixture by Ti(*i*-

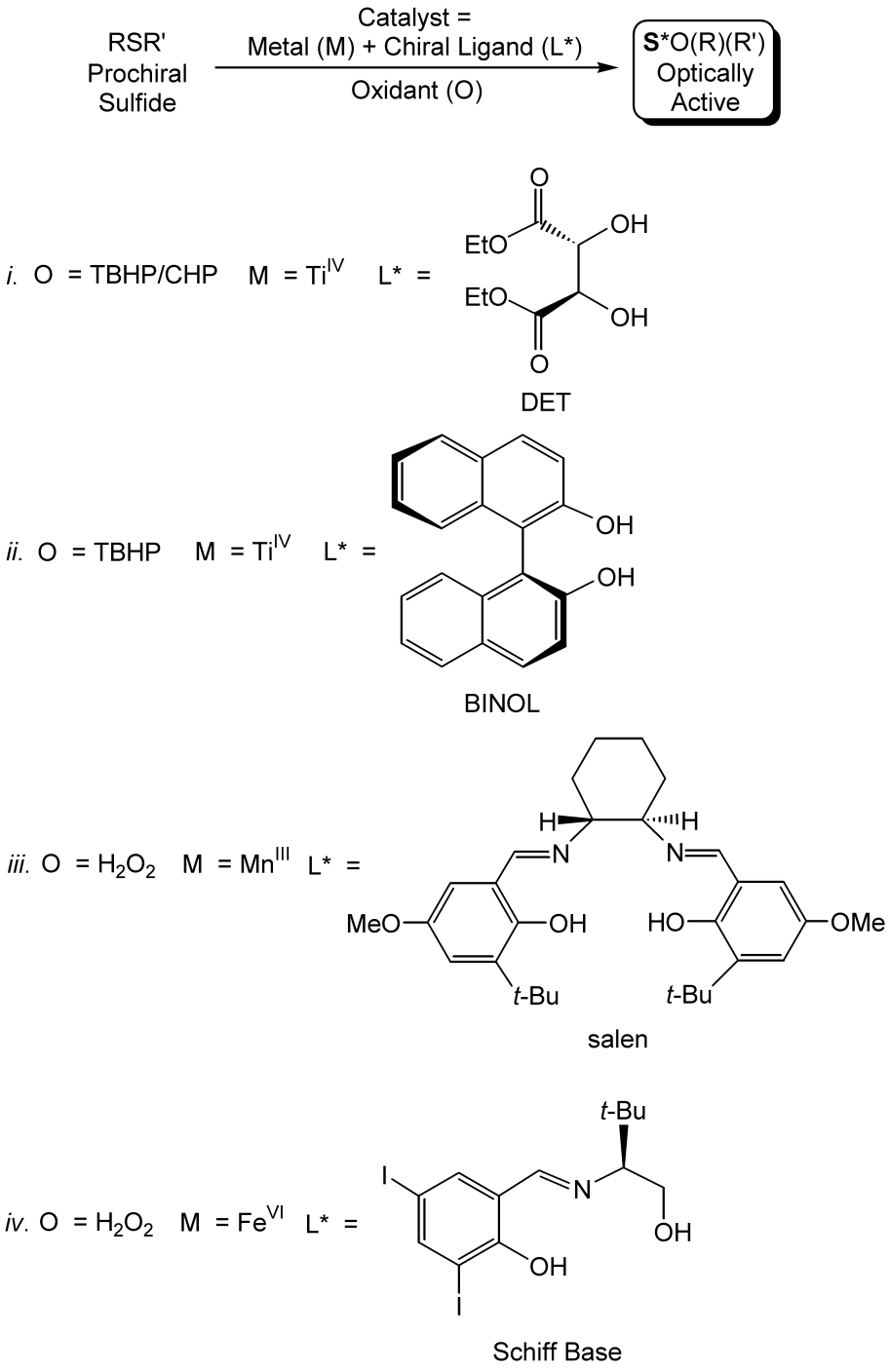

Figure 1.10: Metal-catalyzed sulfoxidation.

PrO)$_4$/(R,R)-DET/i-PrOH 1:4:4 in the presence of molecular sieves.[122] The Kagan's system has been used in pharmaceutical industries like Rhone Polenc, AstraZeneca or Synthex for the production of biologically active chiral sulfoxides. Some examples are the preparation of the hypocholesterolemic agent RP73163,[123] the hypotensive agent RP52891,[124] the antiulcer agent esomeprazole[63] (see Figure 1.7) and some cardiovascular drugs.[125,126] Modena developed a very similar catalytic system almost at the same time as Kagan. The Modena's system consists of a Ti(i-PrO)$_4$/(R,R)-DET/TBHP oxidizing mixture in a 1:1:4 ratio at -20°C in CH_2Cl_2 or toluene.[127,128] The yields and enantioselectivities obtained with this method were in general similar to those achieved by Kagan.

A second generation of catalysts inspired on the Kagan's and Modena's systems was developed by other research groups that introduced C_2-symmetric diols and C_3-symmetric triols as ligands. The main goal was to reduce as much as possible the amount of chiral controller keeping or increasing the good yields and enantioselectivities already obtained. The group of Uemura obtained good results by substituting the diethyl tartrate ligands by BINOL[129] (example *ii* in Figure 1.10). Following this pioneering work other research groups developed alternative catalysts based on Ti(IV) and C_2-symmetric diols with different electronic and steric features.[130,131] Other catalytic systems with higher activities were also developed using C_3-symmetric chiral trialkanolamines as ligands and either titanium[132] or zirconium[133] (IV) as metals.

Metallo-(salen) complexes were found to be a good alternative to the modified Sharpless methods described above. Salen ((Salicylidene)-ethylendiamine) compounds are tridentate chelating O-N-N-O-donor ligands (see example *iii* in Figure 1.10). Metallo-(salen) complexes have also been used as catalysts in other important reactions like CO_2/epoxide copolymerization[134] and epoxidation of alkenes[135] with remarkable success. Pasini reported the first example of a metallo-(salen)-catalyzed sulfoxidation.[136] This catalytic system was based on a chiral Ti(IV)-(salen) complex and in comparison with the Sharpless-modified methods it offered much higher activity but lower enantioselectivity. Fujita solved this problem using a binuclear version of a very similar titanium complex.[137] Jacobsen also reported an alternative

catalyst consisting of a chiral manganese-salen complex[138] originally developed for the asymmetric epoxidation of alkenes (example *iii* in Figure 1.10). The main advantage aported by the Jacobsen's catalyst was the utilization of hydrogen peroxide as oxidant. Hydrogen peroxide is a very clean and thus convenient oxidant because it produces water as the only by-product of the oxidation. Furthermore, while toxic organic solvents should be used when TBHP or CHP are the oxidants, water is the solvent with hydrogen peroxide. The main drawback of this method was the low enantioselectivity obtained. Katsuki improved this aspect of the reaction but at the cost of using PhIO as oxidant[139] instead of H_2O_2. The same group also developed a metal-(salen) catalyst based on titanium and H_2O_2 as oxidant.[140]

The first exemple of a vanadium-catalyzed asymmetric sulfoxidation was also given by Fujita.[137] Salen ligands analogous to those reported by Pasini, Jacobsen and Katsuki were used but low enantioselectivities were obtained. One of the best metal catalysts for asymmetric sulfoxidation was later reported by Bolm.[141] This catalyst is a vanadium complex generated *in situ* from a mixture of $VO(acac)_2$ with a chelating O-N-O chiral Schiff base. The details of this catalytic system will be further commented in the third and fourth chapthers. Recently Bolm reported a new version of this catalytic system based on iron[142] (example *iv* in Figure 1.10). With respect to other metals cited above, iron presents the advantatges of being less toxic and expensive. In a first approach, the catalyst was analogous to that of vanadium and only the metal source, $VO(acac)_2$, was replaced by $Fe(acac)_3$. Good enantioselectivities up to 90% *ee* were obtained but with low yields (44% in the best case). The catalytic system was later improved by means of carboxilic acid additives which enhanced both the yield and the enantioselectivity of the reaction.[143,144] Bryliakov developed an alternative iron system with chiral salen ligands and PhIO as oxidant and detected a reaction intermediate in which the oxidant is directly bound to the metal.[145] Other iron catalysts based on dinuclear complexes have been developed by Fontecave.[146]

Nucleophilic Substitution on Sulfur Derivatives

In this approximation chiral sulfoxides are prepared by nucleophilic addition of a metal organic reagent to a chiral electrophilic sulfinyl compound (see Figure 1.11). The latter compound, referred to as sulfinylating agent, is usually a sulfynate ester with the general formula S*O(R)(OR'*). This ester contains two stereogenic centers: the sulfur of the sulfinyl group and a chiral carbon within the OR' group. In a first step, the sulfinylating agent is diastereoselectively obtained through dynamic kinetic resolution of sulfinyl chloride (SO(R)(Cl)) racemates. In this process, Cl is displaced by OR'* through the addition of a chiral resolving agent. In a subsequent step, the major diastereomer of the sulfinylating agent is purified and a metal organic reagent, usually a Grignard compound (R'MgBr), is added to it in orther to obtain chiral sulfoxides. The latter transformation follows a S_N2 mechanism with total inversion of configuration, *i.e.* the absolute configuration of sulfur in the sulfinylating agent is completely reversed, and the resulting sulfoxide is thus optically active. The successfull application of this synthetic approach requires the synthesis of the sulfinyl precursor with high diastereoselectivity. In principle, this method presents an important limitation in comparison with the asymmetric oxidations promoted by chiral catalysts described above: the necessity of a chiral source of OR'* in stoichiometric amounts. This problem has been recently solved by the group of Ellman[147] as will be commented below.

The are two main synthetic approaches depending on whether the chiral sulfinylating agent is cyclic or acyclic. The latter approach is the most widely used because acyclic sulfinylating agents are in general more easy to prepare with high yield and diastereomeric excess than the cyclic. In fact, the first example of this synthetic methodology is based on acyclic reagents. This pioneering work was done by Andersen who reported that the nucleophilic substitution of diastereomerically pure menthyl sulfinate ester with Grignard reagents leads to enantiopure sulfoxides with good yields[148,149] (example *i* in Figure 1.11). It was later demostrated by Mislow that this reaction proceeds with total inversion of configuration at the sulfinyl sulfur,[150,151] which is consistent with an S_N2 mechanism. At the begining, the limitation of the An-

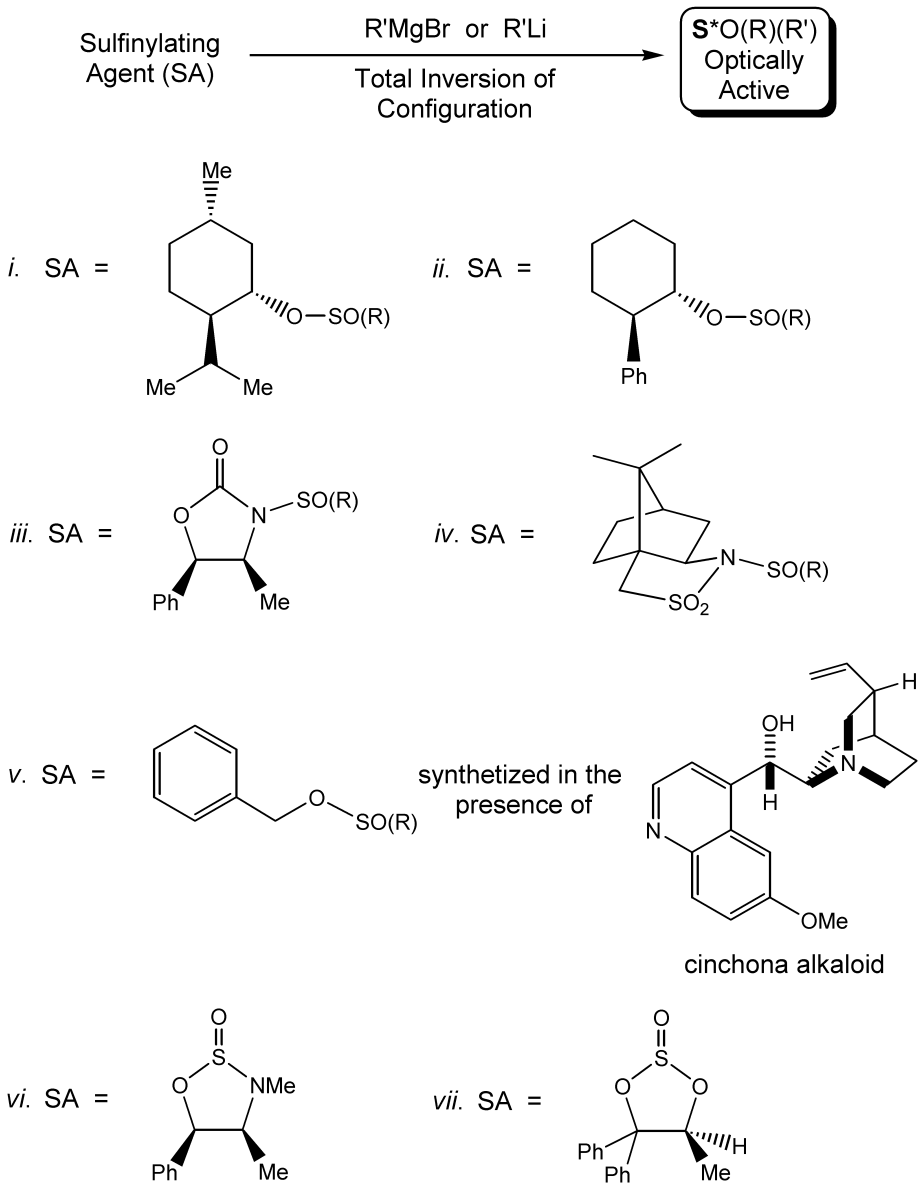

Figure 1.11: Nucleophilic substitution on sulfur derivatives.

dersen's method was the difficulty to synthetize the sulfinate esters with high yield and diastereoselectivity. This problem was solved by Mioskowski and Solladié that improved the synthesis of the sulfinate ester[152,153] and prepared several chiral sulfoxides.[154] Nevertheless the narrow scope of the method remained as an important limitation: only some aryl sulfoxides were obtained and dialkyl sulfoxides could not be prepared. This problem prompted several research groups to develop new and more general methods.

Whitesell reported the synthesis of *trans*-2-phenylcyclohexanol. The sulfinate esters obtained with the reaction of this compound with SO(R)(Cl) (example *ii* in Figure 1.11) were used to prepare several chiral sulfoxides by means of the addition of Grignard reagents.[155] This method was successfully applied to the synthesis of the anticancer compound Sulforaphane[156] (see Figure 1.7). Evans introduced N-sulfinyloxazolidinones as chiral sulfinylating agents[157,158] (example *iii* in Figure 1.11). These compounds were prepared from SO(R)(Cl) racemates and chiral oxazolidinones. Addition of Grignard reagents afforded enantiopure sulfoxides in good yields (>75%) and enantioselectivities (>90%). Garcia Ruano applied this method to the synthesis of biologically active compounds.[159] Oppolzer prepared N-sulfinylsultams from bornane-10,2-sultam and used these compounds as sulfinylating agents[160,161] (example *iv* in Figure 1.11). The reaction with Grignard reagents provided optically active sulfoxides in good yields.

Khiar developed one of the most powerful synthetic approaches to chiral sulfoxides: the DAG method.[162–164] In this approach, a sulfinyl chloride racemate is transformed into chiral sulfinate esters in the presence of nitrogenated organic bases and a chiral alcohol. Interestingly, the absolute configuration of sulfur in the sulfinate ester product can be reversed just changing the nature of the non chiral base. In a subsequent step, the addition of Grignard reagents leads to optically active sulfoxides. Recently, Ellman developed a catalytic system resembling the DAG method in which enantiopure sulfinate esters were prepared mixing *tert*-butyl sulfinyl chlorides with non chiral alcohols in the presence of catalytic amounts of optically active bases[147] (example *v* in Figure 1.11). Enantioselectivities were later improved (>99% ee) using cinchona alkaloids as catalysts.[165] This method introduced an important advantatge: the source of chirality was used only in small catalytic amounts.

Similar synthetic methods have been reported by Shibata[166] and Lu[167] but using cinchona alkaloids in stoichiometric amounts as chiral auxiliaries. The details and applications of these synthetic methods will be presented in further detail in the fifth and sixth chapters.

Aminosulfites and sulfites have been used as cyclic sulfinylating agents. These compounds are prepared by the reaction of a chiral precursor with the highly reactive and inexpensive sulfur compound $SOCl_2$. Wudl and Lee synthetized aminosulfites using ephedrine as starting chiral material (example *vi* in Figure 1.11). Subsequent reaction with two equivalents of metal organic reagents leads to optically active sulfoxides in low yields.[168] Yields were later improved by Snyder and Benson[169] but the method has still the important limitation of not being able to afford diaryl sulfoxides. Cyclic sulfites were introduced by Kagan[170–173] (example *vii* in Figure 1.11). These compounds are synthetized by means of the reaction of a chiral diol with $SOCl_2$. The subsequent addition of two equivalents of Grignard or organolithium reagents affords chiral sulfoxides in good yields and enantioselectivities. Although a broad range of sulfoxides can be prepared, the practical application of the Kagan's sulfite method is hampered by the difficult preparation of the cyclic sulfite in high diastereomeric excess.

Chapter 2

Objectives

The main goal of this thesis is the computational determination of the reaction mechanism and the origin of enantioselectivity of advanced synthetic methods used in the experimental obtention of chiral sulfoxides. Representative examples of the two main synthetic methods are studied: 1) the vanadium-catalyzed asymmetric oxidation of sulfides with hydrogen peroxide and 2) the DAG synthetic method. The study of both reactions was divided in two parts.

The particular objectives in the study of the vanadium-catalyzed asymmetric sulfoxidation were:

- Clarify the nature of the catalyst. Available experimental data were compatible with two different forms, namely the hydroperoxo and peroxo isomers.

- Determine the reaction mechanism. Two reaction mechanisms can be proposed, namely the direct oxygen transfer and the insertion mechanisms, depending on whether sulfur binds to vanadium during the catalytic cycle.

- Rationalize the origin of enantioselectivity. This requires the identification of the enantioselectivity-determining step, and calculation of all possible isomeric forms of the corresponding transition state leading to the R and S products.

- Explain the effect of the nature of the catalyst on the enantiomeric excess. Experimental data showed an unexpected simultaneous sensibility of enantiomeric excess on the identity of two different substituents of the ligand coordinating vanadium which are quite far away from each other.

The particular objectives in the study of the DAG synthetic method were:

- Clarify the the identity and the mechanism of the interconversion step. The DAG method involves dynamic kinetic resolution (DKR) which requires a low energy path between the two enantiomeric forms of the system at some point in the reaction mechanism. The nature of this step was not known.

- Determine the reaction mechanism of the base-assisted displacement of chlorine by alcohol in sulfinyl chlorides. Two possible reaction pathways, namely the neutral and ion pair mechanisms are in principle possible.

- Rationalize the effect of the nature of the base in the sign of enantioselectivity. The use of different non-chiral bases of similar electronic characteristics, like pyridine or collidine, induced the obtention of opposite enantiomers of the product, in an unexpected and puzzling experimental result.

Chapter 3

Mechanism of the Vanadium-Catalyzed Sulfoxidation

The vanadium-catalyzed sulfoxidation reported by Ellman,[174] in which 1,2-bis(*tert*-butyl)-disulfide was enantioselectively oxidized using hydrogen peroxide as oxidant and a mixture of $VO(acac)_2$ with a chiral Schiff base as catalyst (see Figure 3.1), was theoretically studied. The final goal of our study was to elucidate the origin of enantioselectivity. Nevertheless, the particular step of the mechanism in which enantioselectivity is induced and the nature of the catalytic species were essentially unknown. We thus decided to start our investigations with a computational study on a model system in orther to clarify the reaction mechanism. The results of this preliminar work, published in **article I**, are relevant not only for our subsequent study on enantioselectivity (**article II**), but also for other catalytic systems like: 1) other metal-catalyzed sulfoxidations, 2) oxidations catalyzed by vanadium haloperoxidases[175,176] and 3) metal-catalyzed epoxidation of alkenes.[135]

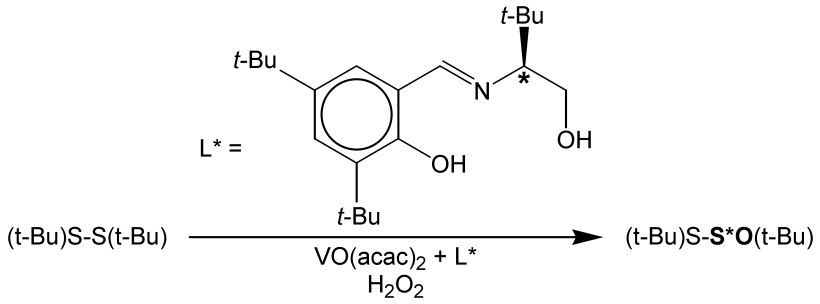

Figure 3.1: Vanadium-catalyzed sulfoxidation by Ellman studied in this thesis.

3.1 Introduction

3.1.1 The catalytic system

One of the best metal catalysts for asymmetric sulfoxidation was originally reported by Bolm.[141,177,178] In this catalytic system, the oxidant is hydrogen peroxide and the catalyst is a vanadium complex generated *in situ* from a 1:1 mixture of $VO(acac)_2$ with a chiral Schiff base (see Figure 3.2). The Schiff base is a chelating tridentate O-N-O donor ligand that can have different R1 and R2 substituents in the phenyl ring and also a variable R3 substituent attached to a chiral carbon in the N-C*-C-OH fragment. This vanadium catalyst presents several advantatges: 1) low catalyst loads and good yields in reasonable reaction times due to high catalytic activity, 2) mild and simple conditions: the reaction is performed at room temperature under air-open atmosphere and using water as solvent, 3) H_2O_2 as a very convenient oxidant since it is cheap and produces water as a unique by-product and 4) modular chiral ligands: several Schiff bases with different substituents R1, R2 and R3 can be easily prepared from accessible precursors and used as ligands. Several sulfides were oxidized to the corresponding chiral sulfoxides with good yields and enantioselectivities. One of the best results achieved by Bolm (yield of 94% with 70% ee) was obtained in the oxidation of methyl phenyl sulfide (thioanisole) using the Schiff base **SB1**[141] (see Figure 3.2).

Several research groups directed their efforts towards the study, optimization and application of the Bolm's catalyst. The group of Berkessel

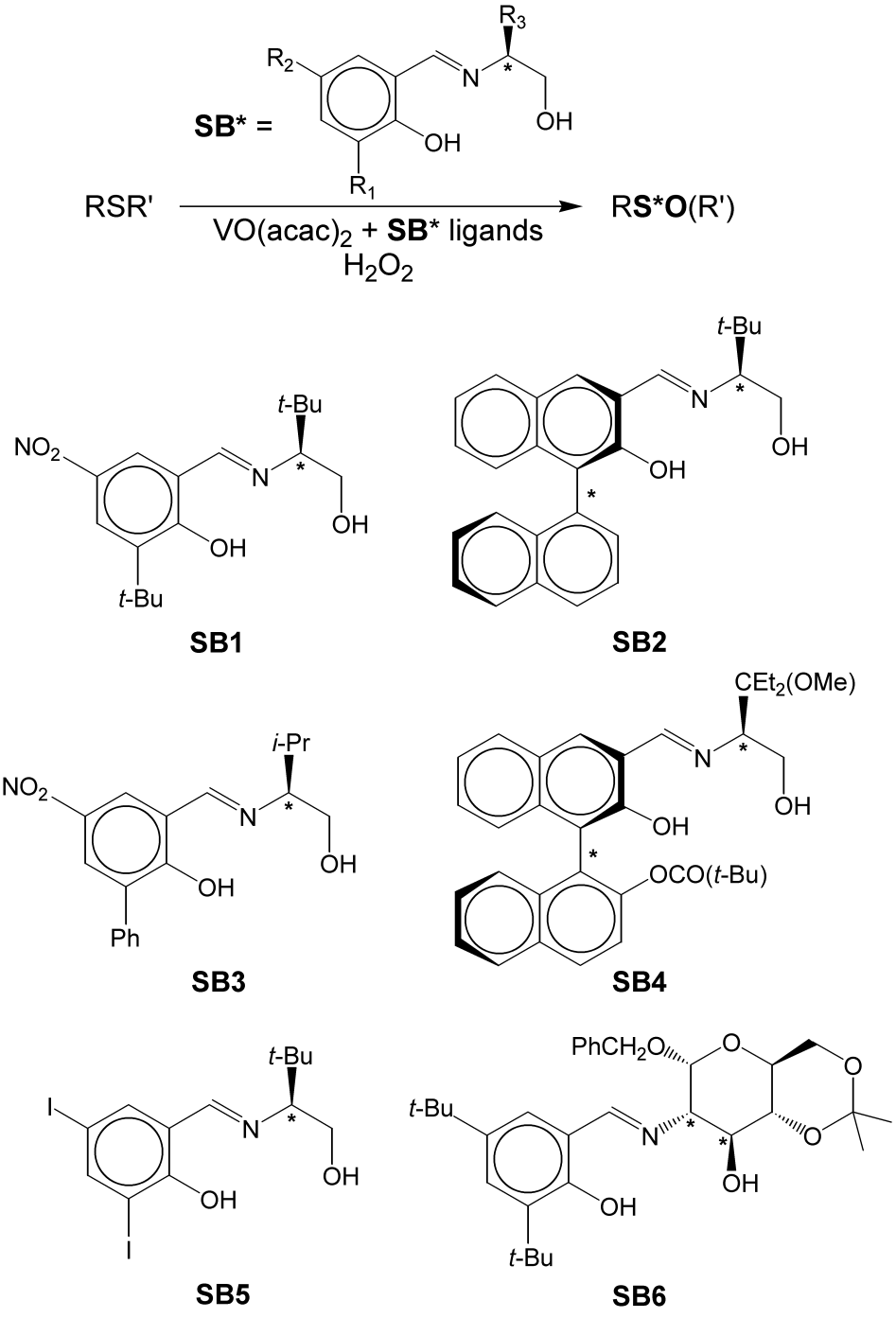

Figure 3.2: Vanadium-catalyzed sulfoxidations with H_2O_2.

introduced a new series of chiral Schiff bases incorporating additional centers of chirality that improved enantioselectivity in some cases.[179] Using ligand **SB2** methyl phenyl sulfoxide was obtained with good yield (92%) and enantioselectivity (78% ee). Skarzewski applied the Bolm's system to the synthesis of C_2-symmetric chiral sulfoxides[180] and the sulfoxidation of homoallylic sulfides.[181] One of the best results was obtained in the oxidation of bis(*o*-methoxyphenylthiomethane) using the Schiff base ligand **SB3**.[180] The research group of Ahn tested different BINOL-derived Schiff base ligands similar to **SB2** in the asymmetric oxidation of benzyl phenyl sulfide.[182,183] Ligand **SB4**[183] gave high yield (78%) and enantioselectivity (99% ee). The Bolm catalyst was successfully combined with kinetic resolution by Jackson.[184] Methyl 2-naphthyl sulfide was oxidized with good yield (73%) and excellent enantioselectivity (99% ee) by means of ligand **SB5**. Very recently, the group of Ruffo reported moderate enantioselectivities (42-60% ee) using the carbohydrate-derived ligand **SB6**.[185]

The asymmetric oxidation of 1,2-bis(*tert*-butyl)-disulfide done by Ellman[174] (see Figure 3.1) is probably the most interesting application of the Bolm's catalyst. The chiral sulfoxide obtained with this reaction is of particular interest since it has a wide range of synthetic applications.[186] In a later work, the reaction was adapted to operate in the kilogram-scale.[187] As will be analyzed in detail in the next chapter, interesting effects of the Schiff base ligand structure on enantioselectivity were observed.[174] The best results (yield of 98% with 91% ee) were obtained with the ligand represented in Figure 3.1 (R1=R2=R3=*t*-Bu). This particular reaction was studied in this thesis as one of the most relevant examples of vanadium-catalyzed sulfoxidation.

3.1.2 Previous Studies on the Reaction Mechanism

The first speculations on the reaction mechanism of metal-catalyzed sulfoxidations were given for the Kagan's system.[120] Dimeric[188] and monomeric[122] complexes of titanium were proposed as the key catalytic species. Such species were octahedral complexes of titanium(IV) coordinated to the tridentate chiral DET ligand and to the peroxidic oxidant (ROO^-) in a η^2 fashion. The mechanism of titanium-catalyzed sulfoxidation with chiral tri-

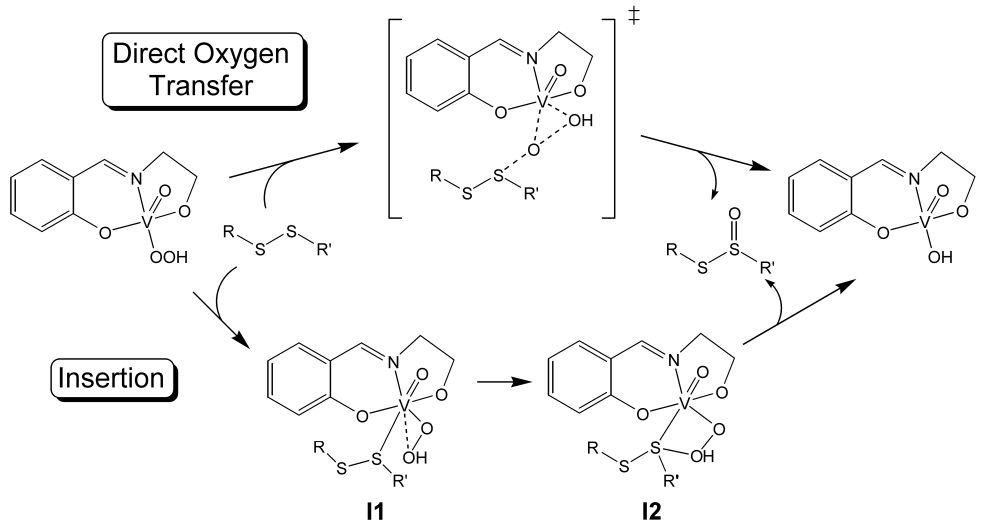

Figure 3.3: Direct oxygen transfer and insertion mechanisms.

alkanolamines as ligands and cumene hydroperoxide as oxidant[132] was also studied both theoretically[189] and experimentally.[190] In this case, monomeric trigonal bipyramid complexes of titanium were proposed as the catalytic species. In these intermediates, the metal is coordinated to cumene hydroperoxide and to the tridentate trialkanolamine.

Metal-catalyzed sulfoxidation systems are also found in nature. Vanadium haloperoxidases[175,176] are natural enzymes found in *algae* and *fungi* that are able to catalyze the oxidation of sulfides.[191,192] The active site of these enzymes contains a oxovanadium(V) fragment coordinated to a histidine aminoacid. Vanadium is also bound to a O-O fragment that can be either a peroxo or hydroperoxo ligand depending on the pH. In a recent theoretical study, Pecoraro proposed that the most reactive form of the active site is the peroxo.[193]

Mechanistic studies on sulfoxidations catalyzed by synthetic vanadium complexes suggested that the catalytic species are peroxidic complexes of vanadium(V).[194] Kinetic studies by Modena suggested that the key intermediate of the catalytic cycle is a hydroperoxovanadium complex.[195] Catalytic hydroperoxo species were also postulated in a experimental study by Ellman for the reaction represented in Figure 3.1.[196] In contrast with this, Karpy-

shev and Bryliakov proposed that the catalytic species is a peroxovanadium complex on the basis of ^{13}C and ^{51}V NMR studies.[197,198] All these investigations and also other studies,[141,174] indicated that the key intermediate is a mononuclear neutral oxovanadium(V) complex in which the metal is coordinated to the Schiff base (L) and the oxidant (O) in a V:L:O ratio of 1:1:1. Nevertheless, these studies did not clarify whether the oxidant coordinates to vanadium as a hydroperoxo (HOO^-) or peroxo (OO^{2-}) ligand.

The main issue considered in all the mechanistic studies commented above is the nature of the catalyst. Nevertheless, there is an additional important question to answer: how these catalytic species catalyze the sulfoxidation process, or in other words, which is the reaction mechanism? This question has been tackled for metal-catalyzed epoxidations. In this catalytic process, which is very similar to metal-catalyzed sulfoxidation, alkenes, instead of sulfides, are oxidized by peroxidic metal complexes. This reaction has been theoretically studied by the groups of Rösch,[199,200] Wu,[201,202] Frenking[203,204] and Thiel.[205] Two relevant topics were object of discussion in these studies: 1) the nature of the catalyst: as in metal-catalyzed sulfoxidations, both hydroperoxo and peroxo complexes were proposed depending on the identity of the metal center, and 2) the reaction mechanism: two different mechanisms, namely the direct oxygen transfer and insertion mechanisms, were proposed. These mechanisms are represented in Figure 3.3 for a generic neutral hydroperoxovanadium(V) complex bearing a Schiff base ligand. In the direct oxygen transfer mechanism, one of the peroxidic oxygens is transferred to the sulfide in a single concerted step leading to the sulfoxide product. In the insertion mechanism, the sulfide coordinates to vanadium in a preliminary step and then inserts into the V-OOH bond. Two intermediates, **I1** and **I2**, are formed in this mechanism, both characterized by V-S bonds.[206] In the final step **I2** decomposes giving rise to the sulfoxide product. In most cases, the theoretical studies on metal-catalyzed epoxidations pointed out that the reaction follows the direct oxygen transfer mechanism. In contrast with this, the only computational study on metal-catalyzed sulfoxidation suggested the existence of intermediates of type **I1**.[207]

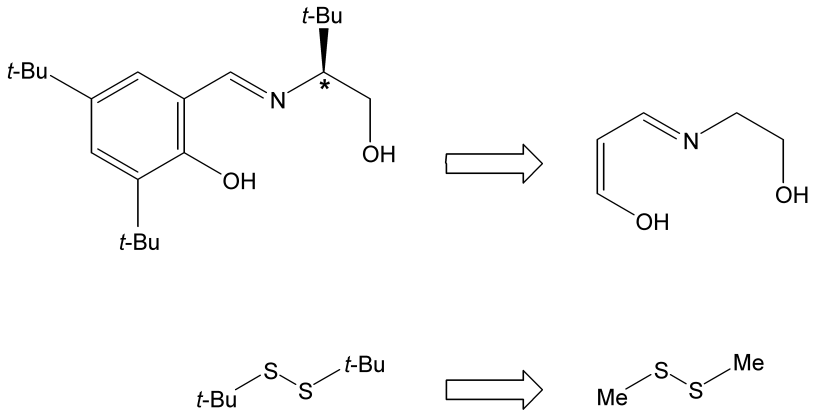

Figure 3.4: Modelization of the real system.

3.2 Computational Details

All calculations were carried out using the Becke3LYP[208,209] density functional as implemented within the Gaussian98 program.[210] The 10 internal electrons of vanadium[211] and sulfur[212] were described with effective core potentials. The valence double-ζ basis set associated to the pseudopotential in the program,[210] with the contraction labeled as LANL2DZ, was used for these two elements and suplemented with a d shell in the case of sulfur.[213] The 6-31G(d) basis set was used for oxygen and nitrogen[214,215] and 6-31G for carbon and hydrogen.[214] All elements of the system were thus described with a double-ζ basis set plus an additional polarization shell for those atoms bound to the metal or directly involved in the oxidation process. All geometry optimizations were full, wihout any geometrical constrain. All stationary points located in the energy hypersurface were characterized as minima or transition states through vibrational analysis. This analysis was also used to obtain the absolute free energies. All the energies given in the following sections are relative free energies at 25 °C and 1 atm. The electronic structures of some stationary points were explored inspecting the NPA (Natural Population Analysis[216,217]) charges.

The validity of the computational method described above was assessed considering two different improvements: 1) utilization of a larger basis set and 2) introduction of solvent effects. The basis set was expanded using the

all-electron 6-31+G(d) basis set for sulfur.[218] This basis set was also used for oxygen and nitrogen.[219] The effect of solvent (water) was considered by means of the continum PCM model.[220] Both improvements of the method were introduced recomputing the energies of the key stationary points with single-point calculations. The results did not change in any case the conclusions of our study. Furthermore, we found good agreement between the optimized geometry of the catalyst found in our study and an X-Ray structure of a similar complex reported by Ellman.[196]

The catalytic system represented in Figure 3.1 is too big for a systematic mechanistic study at the quantum mechanical level described above. Thus, the real system was modeled as shown in Figure 3.4. The disulfide susbtrate was simplified replacing the *tert*-butyl substituents by methyls, and the size of the Schiff base ligand was reduced supressing the phenyl ring and the *tert*-butyl substituent. The resulting dangling bonds were capped with hydrogens. The simplification of the ligand preserves its chelating tridentate character but implies the loss of its chirality. Thus, our model catalytic system is not enantioselective. Nevertheless, we think that our model retains the main electronic factors controlling the reaction mechanism.

3.3 Results and Discussion

3.3.1 Isomers of the Catalyst

Experimental studies suggested that the key intermediate involved in the catalytic cycle is a neutral vanadium(V) oxo complex with a V:Ligand:Peroxide ratio of 1:1:1. Nevertheless, such studies did not clarify whether hydrogen peroxide is bound to the metal as a hydroperoxo (OOH) or peroxo (OO) ligand. In the former case, the formula of the complex would be VO(L)(OOH) while in the latter case would be VO(LH)(OO), where L stands for the model Schiff base ligand (L=$O(CH)_3N(CH_2)_2O$; see Figure 3.4). The stability and reactivity of both isomers were explored in detail since in principle, each one can be the most active catalytic species as it has been reported in the case of olefin epoxidation.[199]

In the hydroperoxo complex, VO(L)(OOH), the combination of the neu-

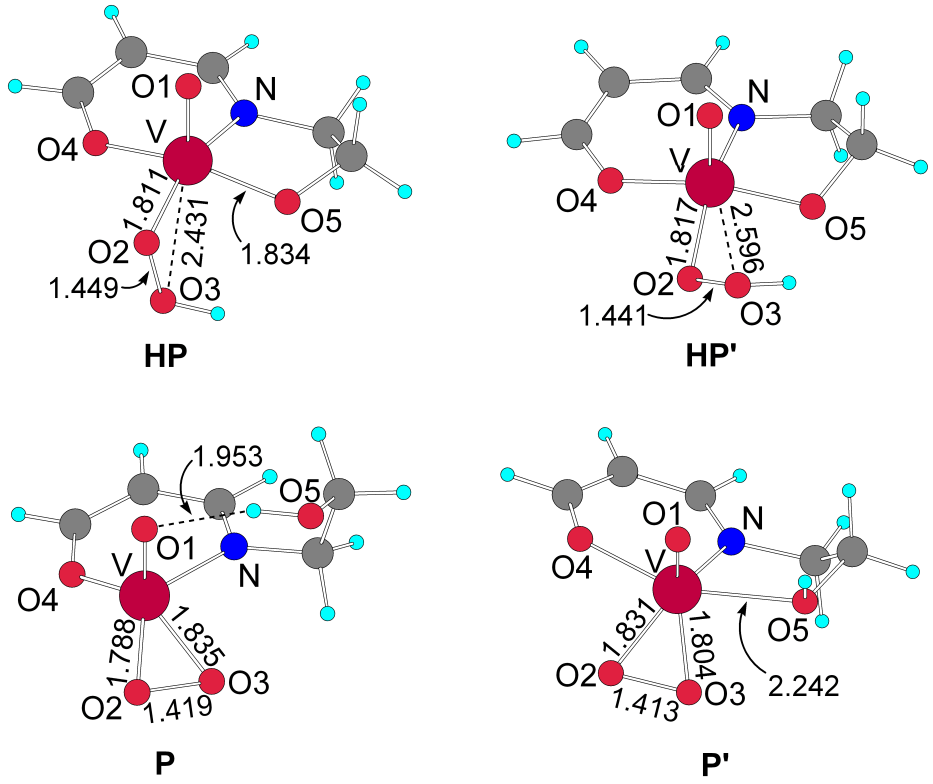

Figure 3.5: Most stable hydroperoxo (above) and peroxo (below) isomers.

trality of the complex with the formal oxidation states of vanadium (+5), and the oxo (-2) and hydroperoxo (-1) ligands requires that the Schiff base coordinates as a dianionic ligand through its oxygens in deprotonated alkoxy form. The optimized structure of such isomer, labeled as **HP**, is represented in Figure 3.5. The geometry of this complex is square pyramidal with the oxo ligand occupying the axial position, as the O1-V-X angles close to 90° point out. Other isomers of **HP** with the oxo ligand on basal positions were searched without success. Another relevant feature of **HP** is that the hydroperoxo ligand is coordinated in η^1 fashion, *i.e.* only the O2 oxygen is strongly bound to vanadium. This is clearly indicated by the short V-O2 distance of 1.811 Å and the long V-O3 distance of 2.431 Å.

Our calculations showed that complex **HP** has a significant degree of fluxionality. Four different conformations of this complex were found associated with the rotation of the V-OOH bond. The **HP** and **HP'** geometries (see Figure 3.5) correspond to the first and second most stable conformations respectively. These complexes can be easily distinguished inspecting the O5-V-O2-O3 dihedral angle which has a value of -113.3° in **HP** and 59.1° in **HP'**. As it can be seen comparing **HP** with **HP'** these conformations have the same key features: they are square pyramidal geometries with O1 in the apical position bearing a η^1-OOH ligand. The four conformations have similar stabilities within a range of 5 kcal/mol and, for instance, **HP'** is less stable than **HP** by 4.1 kcal/mol. The interconversion of **HP** into **HP'** was explored and the corresponding transition state was found. The imaginary frequency of this saddle point consists of the rotation of the V-O2 bond and implies a free energy barrier of only 7.5 kcal/mol from **HP**. We thus concluded that these conformations are quickly interconverted through σ-bond rotation. An additional fluxional process was also characterized, consisting of the flipping of the five-membered metallacycle containg V, N and O5. In this case, we found very small energy differences: the free energy of **HP** rises only 0.2 kcal/mol by this flipping. Moreover, the energy barrier of this process is very low, only 2.3 kcal/mol from **HP**. We thus decided to ignore this conformational equilibrium in the rest of our study of the model system.

In the peroxo complex, VO(L)(OO), the metal-coordinated hydrogen peroxide is now a dianionic O-O^{2-} ligand. Thus, in orther to mantain the neu-

trality of the complex, the Schiff base should act as a monoanionic ligand with only one of its oxygens deprotonated. At least two distinct peroxo isomers would exist depending on whether O4 or O5 are the anionic alkoxy oxygens. In fact, three isomers with O4 deprotonated and one with O5 deprotonated were characterized. The latter compound was directly discarded due to its very low stability (30.4 kcal/mol above **HP**). The other three isomers were only remarkably stable in two cases. The optimized geometries of these two isomers, labeled as **P** and **P'**, are represented in Figure 3.5. In isomer **P** H(O5) is bound to O1 through a hydrogen bond with a distance of 1.953 Å, while in **P'** is bound to vanadium through a long V-O5 bond of 2.242 Å. The weakness of these bonds with resepect to the V-O5 bond of **HP** (1.834 Å) indicated that the strength of the V-L bond is reduced by the protonation of L. The relative energies of these species showed that isomer **P** is more stable than **P'** by 1.2 kcal/mol.

In all peroxo isomers, the peroxo ligand is coordinated to vanadium in a η^2 fashion, *i.e.* both O2 and O3 are bound to the metal, as the V-O2 and V-O3 distances of 1.788 Å and 1.835 Å indicate in structure **P**. This coordination mode is more rigid than the η^1 mode found in **HP** and any additional conformers were found associated to the rotation of the V-O2 and V-O3 bonds. As in the hydroperoxo complexes, the coordination geometry around vanadium is square pyramidal with the oxo ligand in the apical position in all cases. In comparison with **HP**, **P** has a stronger η^2 bond between the metal and the oxidant but a weaker coordination with the Schiff base. The latter factor seems to be critical since we found that **HP** is more stable than **P** by 4.4 kcal/mol. The interconversion of these species was also explored and the transition state connecting **HP** with **P** was found. The transition vector of this saddle point consists of a proton transfer from O3 to O5 coupled with the formation of the V-O3 bond and the partial cleavage of the V-O5 bond. The energy barrier of this process from **HP** is 14.8 kcal/mol which makes this reaction feasible from the kinetic point of view.

In summary, our calculations showed that the catalyst consists of a mixture of different η^1-hydroperoxo and η^2-peroxo complexes that in solution will probably be in equilibrium due to their similar stabilities and fast interconversion. All these species are in principle candidates to be the most

active catalytic intermediates and thus they were all considered in the reactivity studies. The oxidation of the model disulfide mediated by the most stable complex (**HP**) was initially explored in detail. The data obtained in this preliminary analysis was then applied to the study of all other isomers.

3.3.2 Reaction Mechanism: Insertion or Direct Oxygen Transfer?

The oxidation of 1,2-dimethyl disulfide by **HP** can follow two distinct reaction mechanisms: insertion or direct oxygen transfer (see Figure 3.3). In the insertion mechanism, the disulfide would coordinate to vanadium and then insert into the V-OOH bond. This mechanism is characterized by the formation of intermediates **I1** and **I2** with V-S bonds. The insertion to both V-O2 and V···O3H bonds was explored but all efforts to optimize intermediates of type **I1** and **I2** were unsuccessful. In the case of **I1** the optimization lead to the rupture of the V-S bond, while it evolved to products in the case of **I2**. Our calculations thus suggest that as in most metal catalyzed epoxidations,[199] the insertion mechanism is not relevant in vanadium-catalyzed sulfoxidations.

The exploration of the direct transfer mechanism was more successful. The structures of the model substrate (MeSSMe) and **HP** were put together and the transition state **HP-TS**, corresponding to an attack of S upon O2, was found (see Figure 3.6). The approach of S to O3 was also explored without success. The unique imaginary frequency of **HP-TS** revealed that this stationary is a concerted transition state in which the cleavage of the peroxidic O2-O3 bond and the formation of the new bond between S and O2 are simultaneous. This process is consistent with the oxidation of 1,2-dimethyl disulfide by **HP**. The O2-O3 bond in **HP-TS** (1.829 Å) is clearly longer than in **HP** (1.449 Å) indicating that such bond is being broken in the transition state. On the other hand, the relatively short S-O2 distance of 2.149 Å in **HP-TS** points out the formation of the S-O2 bond. Moreover, as a result of the cleavage of the peroxidic bond, a new bond between V and O3 is also formed, as the shortening of the V-O3 distance, from 2.431 Å in **HP-TS** to 2.097 Å in **HP-TS** indicates. The relaxation of **HP-TS**

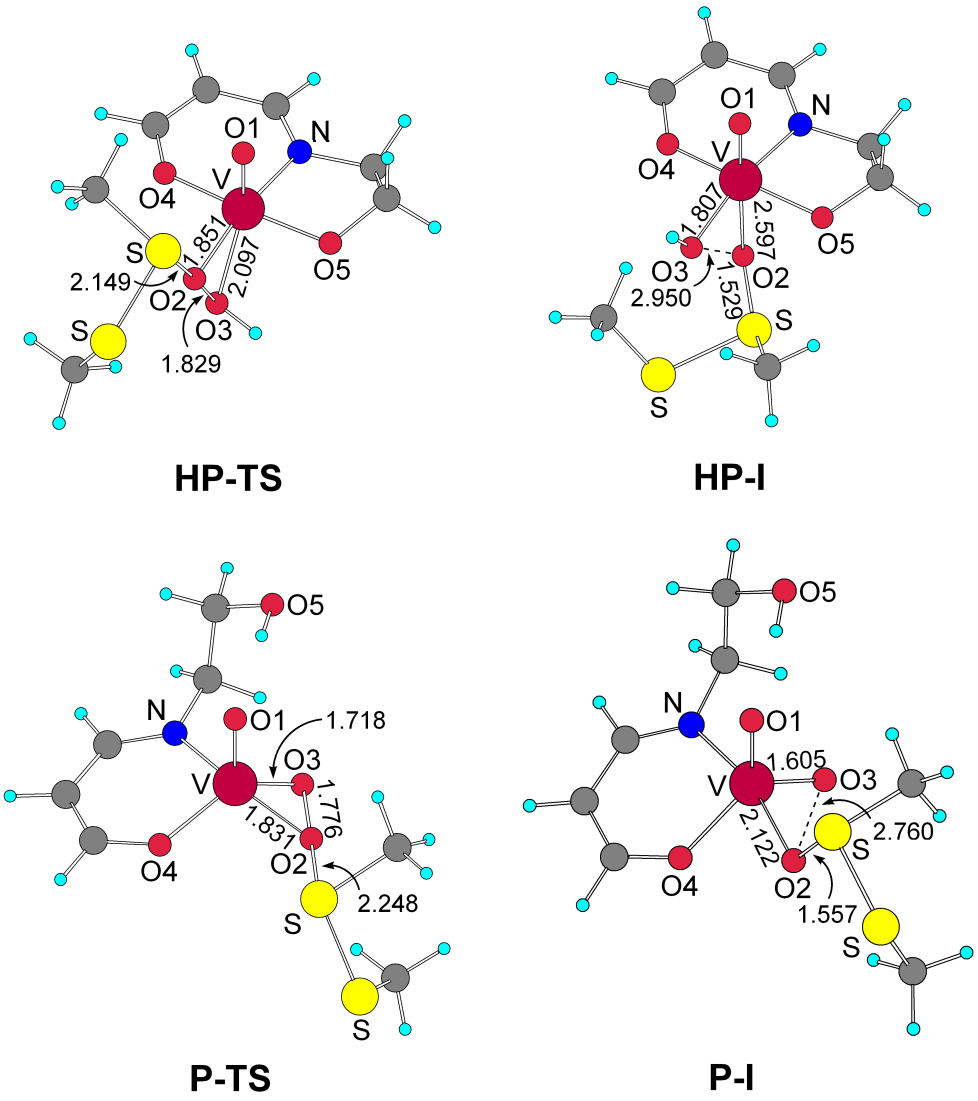

Figure 3.6: Most stable hydroperoxo (above) and peroxo (below) transition states and intermediates.

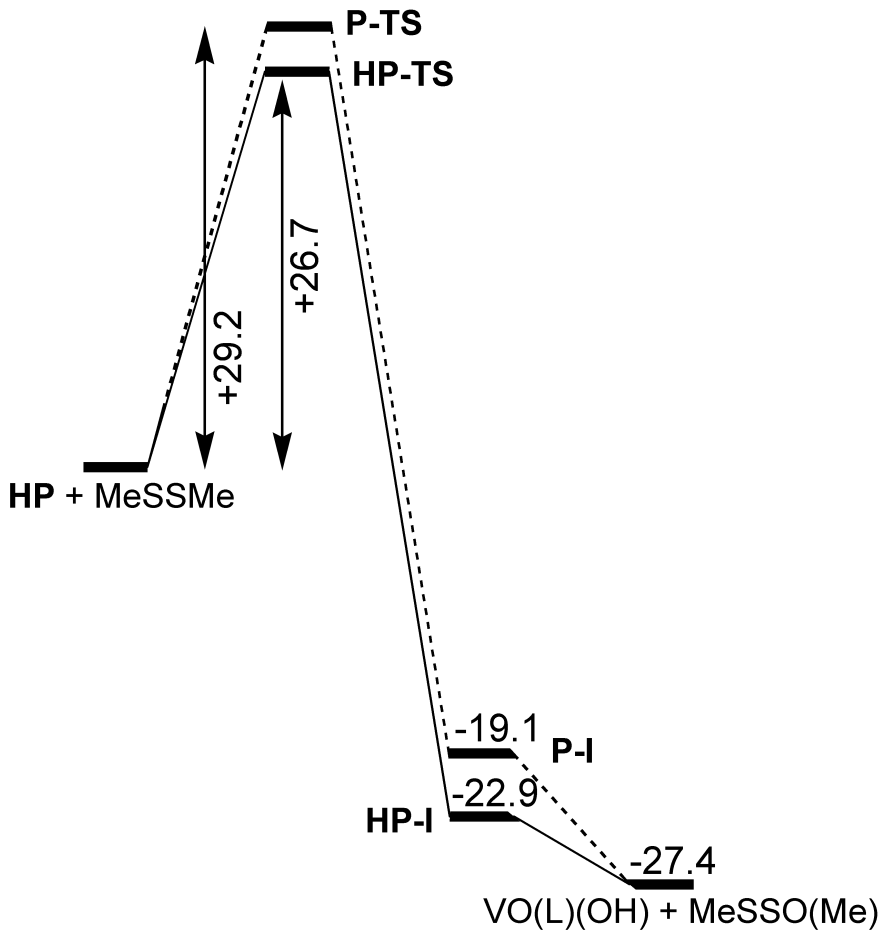

Figure 3.7: Free energy profile for the hydroperoxo (solid line) and peroxo (dotted line) reaction pathways.

towards products converged into **HP-I** (see Figure 3.6). This intermediate can be considered as a vanadium complex with the formula VO(L)(OH) coordinated to the final reaction product (Me-S-SO(Me)) through a weak V-O2 bond (2.597 Å). Moreover, the O2-O3 (2.950 Å) and V-O3 (1.807 Å) bonds are clearly broken and formed respectively. The coordination geometry of vanadium in **HP-I** is octahedral with O1 *trans* to O2 and N *trans* to O3. Overall, the **HP** + MeSSMe $\longrightarrow$ **HP-I** transformation can be considered as a S_N2 reaction in which the disulfide and O3H are the nucleophile and the leaving group respectively. The nucleophilic and electrophilic characters of S and O2 respectively were confirmed inspecting the NPA charges, which indicated a charge loss on S and a charge gain on O2. We found that the oxidation transition state can be converged only when S-O2-O3 are in a linear arrangement. This is consistent with an important participation of the σ^* orbital of the electrophilic O2-O3 bond,[221] as already found in other studies.[222] The absolute configuration of sulfur in **HP-TS** is retained in **HP-I** and we can thus conclude that the stereochemical outcome of the reaction is controlled in this oxidation step.

The free energy profile of the oxidation step is represented in Figure 3.7. The formation of the intermediate, **HP-I**, is clearly exergonic by 22.9 kcal/mol. This intermediate dissociates giving rise to the final reaction product, Me-S-SO(Me), and a hydroxy vanadium complex, VO(L)(OH), with a free energy release of 4.5 kcal/mol. In the final step, the catalytic cycle is closed by the reaction of VO(L)(OH) with the stoichiometric oxidant, H_2O_2, giving rise to the catalyst, VO(L)(OOH), and water. The energy profiles show that the oxidation barrier is 26.7 kcal/mol. This value is probably overestimated by the unfavourable entropic factor associated to the bimolecularity of the reaction, which is higher in gas phase than in solution. The uncatalyzed reaction was also theoretically characterized and an oxidation barrier of 40.4 kcal/mol was found. We can thus conclude that vanadium catalyzes the reaction by reducing the energy barrier *ca.* 15 kcal/mol.

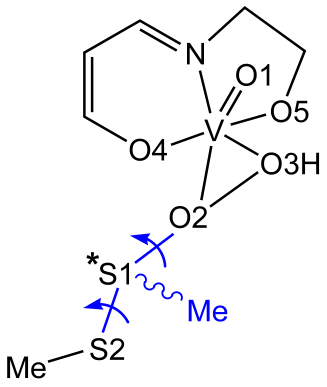

Figure 3.8: Sources of structural flexibility in the oxidation transition state.

3.3.3 Conformations of the Transition State

The **HP-TS** transition state has two bonds that are likely to rotate with low energy barriers and give rise to distinct conformations. They are the S1-O2 bond under formation and the S1-S2 bond (see Figure 3.8). The rotation of the former bond is associated with the orientation of the substrate with respect to the catalyst. The other rotation corresponds to the internal conformation of the substrate. Rigid energy scans revealed that the rotation of the S1-O2 and S1-S2 bonds would generate three and two conformations respectively. Furhtermore, S1 is a chiral center with two possible absolute configurations. The existence of these three sources of structural flexibility implies that **HP-TS** has in principle twelve possible conformations.

The conformational space of the oxidation transition state was sistematically scrutinized considering all the possibilities commented above, and ten different conformations were found. The other two hypothetic structures did not converge due to strong steric repulsions between the substrate and the catalyst. The most stable conformation found was **HP-TS** (see Figure 3.6). Our results indicated that: 1) the preferred orientation of the substrate, controlled by the rotation of the nascent S-O2 bond, is that with the S2-Me fragment in *anti* position with respect the catalyst, 2) the most stable internal conformation of the substrate in the transition state is that in which O2 is eclipsed with the methyl attached to S2 and 3) the inversion of S1* in **HP-TS** leads to an energy rise of only 0.8 kcal/mol, indicating the

poor stereodiscriminating ability of the model system in which the sterically demanding *tert*-butyl substituents of the real ligand are missing (see Figure 3.4).

3.3.4 Other reaction pathways

The reactivity of the other isomers of **HP** was also explored. The oxidation transition states connected to these species were searched taking into account the conformational preferences found for **HP-TS**. Two additional saddle points were found associated to other conformations of **HP** derived from the rotation of its V-O2 bond. One of this transition states is directly connected to **HP'**. The geometrical features of these stationary points are analogous to those found for **HP-TS** and their vibrational analysis showed that they also correspond to the oxidation of MeSSMe. Moreover, the associated energy barriers are in both cases clearly lower than the barrier of the uncatalyzed reaction. Hence, the catalytic properties of **HP** are preserved in the rotation of its V-O2 bond. Nevertheless, the relative energies of these transition states showed that they are less stable than **HP-TS** by *ca.* 7 kcal/mol. The relaxation of these transition states towards products converged into vanadium complexes with the general formula VO(L)(OH)(MeSSO(Me)) in which the final reaction product appears weakly coordinated to vanadium through its sulfinyl sulfur. The geometry of these intermediates is octahedral as in **HP-I**, but with a different relative distribution of the ligands around vanadium. In both cases, one of the oxygens of the model Schiff base lies *trans* to the oxo ligand. Such oxygen is O4 in one intermediate and O5 in the other. These intermediates are clearly less stable than **HP-I**, as their relative energies with respect to reactants (+1.5 kcal/mol and -0.1 kcal/mol) indicate. The isomerization of these species giving rise to **HP-I** was explored and low barriers (9.1 and 7.7 kcal/mol) were found.

The oxidation of MeSSMe by η^2-peroxo vanadium species was also investigated. The search of transition states was only successful in the case of isomer **P**. Both attacks to O2 and O3 were considered and one saddle point was found in each case, corresponding to the oxidation of MeSSMe. The most stable geometry, labeled as **P-TS** and represented in Figure 3.6, cor-

responds to the O2-attack. The free energy profiles (see Figure 3.7) indicate that **P-TS** is 2.5 kcal/mol above **HP-TS**. We can thus conclude that the η^2-peroxo **P** complex is also catalytic but less active than the η^1-hydroperoxo **HP** species. The relaxation of **P-TS** towards reactants converged into **P-I** (see Figure 3.6), a reaction intermediate with two V=O double bonds. The formation of this octahedral intermediate is exergonic by -19.1 kcal/mol. As in the hydroperoxo mechanism, the dissociation of **P-I** leads to the release of the reaction product, MeSSO(Me), and the regeneration of the catalyst in a subsequent step. The electrophilic attack of O3 upon the substrate was also characterized but the corresponding transition state and intermediate are 4.2 and 5.1 kcal/mol less stable than **P-TS** and **P-I** respectively.

In summary, we found that the conformers derived from the rotation of the V-OOH bond in **HP** also catalyze the oxidation of MeSSMe with the formation of an additional intermediate but through higher energy barriers. Starting from **P** complex, a catalytic pathway analogous to that starting from **HP** was characterized, but also with larger barriers. We can thus conclude that the most stable catalytic species, the η^1-hydroperoxo **HP** complex, also leads to the lowest energy reaction path. This compound catalyzes the sulfoxidation of MeSSMe through a direct oxygen transfer mechanism.

Chapter 4

Origin of Enantioselectivity in the Vanadium-Catalyzed Asymmetric Sulfoxidation

4.1 Introduction

The application of the vanadium-catalyzed sulfoxidation developed by Ellman[174] is of particular interest due to the wide variety of Schiff base ligands that were tested (see Figure 4.1). In this reaction, 1,2-bis(*tert*-butyl) disulfide was enantioselectively oxidized with hydrogen peroxide. The R enantiomer of (*t*-Bu)S-S*O(*t*-Bu) was obtained as the major reaction procuct in all cases, regardless of the ligand used. Nevertheless, a strong dependence of enantioselectivity on the structure of the chiral Schiff base was observed. This dependence is clearly illustrated by the **A**-**D** set of ligands. With ligand **A** (R1=R2=R3=*t*-Bu) the chiral sulfoxide product was obtained with 82% ee. The replacement of the *tert*-butyl in the R2 position by hydrogen (ligand **B**) indicated that this substituent has no effect on the stereochemical outcome of the reaction since the enantioselectivity was almost the same (83% ee). Contrary to this, both R1 and R3 were found to have a strong influence upon enantioselectivity. In the case of R3, the replacement of *t*-Bu (ligand **A**) by *i*-Pr (ligand **C**) implies a reduction of the enantioselectivity from 82% ee to 60% ee. For R1, the replacement of *t*-Bu (ligand **A**) by hydrogen (lig-

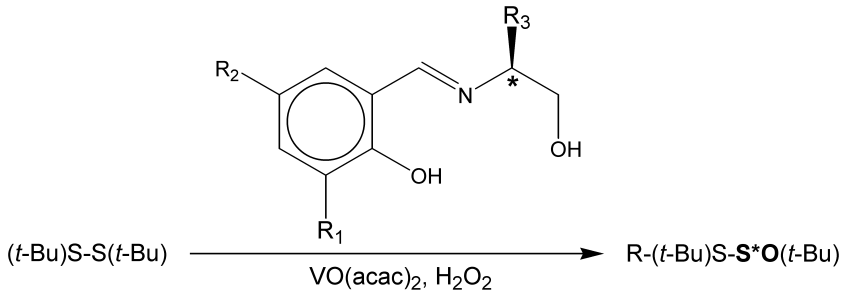

Ligand	R1	R2	R3	Enantioselectivity
A	*t*-Bu	*t*-Bu	*t*-Bu	82% ee
B	*t*-Bu	**H**	*t*-Bu	83% ee
C	*t*-Bu	*t*-Bu	***i*-Pr**	60% ee
D	**H**	H	*t*-Bu	46% ee

Figure 4.1: Vanadium-catalyzed sulfoxidation by Ellman. Influence of the Schiff base ligand structure on enantioselectivity.

and **D**) has a much stronger effect since enantioselectivity drops down to 46% ee. These results indicated that the high steric hindrance offered by the *tert*-butyl groups is needed in both the R1 and R3 positions of the Schiff base ligand in order to achieve high enantioselectivities.

The puzzling question derived from the experimental evidence commented above is how both R1 and R3, seemingly far from each other in the ligand, can have such dramatic influence upon enantioselectivity. On the other hand, the rigidity of the ligand hampers an eventual aproximation between R1 and R3 through conformational transformations. As recently demonstrated in a theoretical account by Lipkowitz,[223] the success of asymmetric catalysis is based not only in the ability to create a strongly asymmetric environment in the catalyst, but also in introducing it as close as possible to the site of chemistry where the new stereogenic center is created. Taking into account the model study presented in the previous chapter (**article I**), the strong effect of R1 seems reasonable since this substituent is relatively close to one of the oxygens connected to vanadium and thus close to the site of chemistry

(see section 3.3.2). In contrast with this, although R3 is directly attached to the chiral center of the ligand, is difficult to understand its strong effect on enantioselectivity since it stands appearently far from the region where the chiral sulfinyl sulfur is generated.

The vanadium-catalyzed sulfoxidation developed by Ellman was theoretically studied considering the real system at a QM/MM level (**article II**). The origin of enantioselectivity was explored considering the **A**, **B**, **C** and **D** ligands in order to rationalize the dependence of enantioselectivity on the structure of the chiral Schiff base. This study was carried out taking into account the main conclusion of the previous mechanistic study (**article I**): the key intermediate is a neutral η^1-hydroperoxovanadium(V) complex that catalyzes the oxidation of the disulfide through a direct oxygen transfer mechanism.

4.2 Computational Details

4.2.1 Methodology

The study on the real system was carried out by means of the IMOMM method.[224] This hybrid QM/MM method is applied by dividing the system in two parts: one is computed at a high quantum mechanical (QM) level (QM part) and the other is computed with a molecular mechanics (MM) method (MM part). The calculations were done using the mmabin98 code wich consists of a combination of the Gaussian98[210] and mm3(92)[225] programs. The former program is used to compute the QM part while the latter is used in the calculation of the MM part. The calculations were done at the IMOMM(Becke3LYP:MM3) level, *i.e.* the QM part was computed with the hybrid Becke3LYP density functional[208,209] and the MM part was computed using the MM3 force field.[226]

The QM/MM partition of the system used in our calculations is represented in Figure 4.2. The QM part corresponds to the model system considered in our previous study (**article I**) and it was described with the same basis set. The accuracy of this basis set was not explored since it was already confirmed in the model study (see section 3.2). The rest of the system,

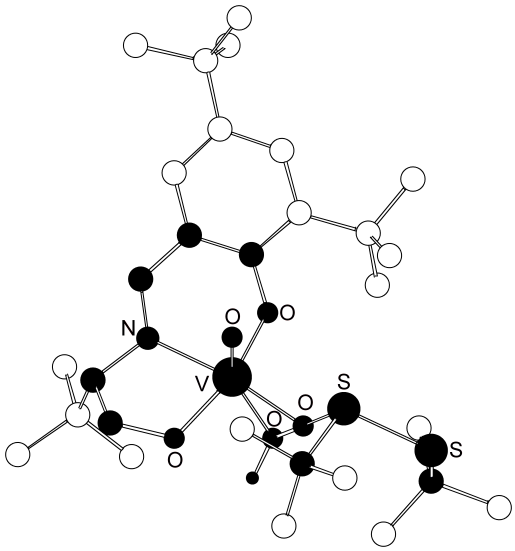

Figure 4.2: QM (black) and MM (white) parts in the IMOMM calculations. All hydrogens, except the peroxidic, were removed for clarity.

which contains the enantioselectivity-modulating R1 and R3 substituents, was included in the MM part of the calculation. The purely aliphatic nature of R1 and R3 suggested that the role of these substituents will be mostly steric and thus, their influence upon enantioselectivity is likely to be well reproduced with a MM method.[227] On the other hand, systematic theoretical studies demonstrated that mm3 is among the most accurate force fields.[228] The MM calculations were performed using the standard set of parameters of the MM3 force field with two exceptions: 1) the van der Waals parameters of vanadium were extracted from the UFF force field[229] and 2) as will be explained below, an additional hydrogen bond potential was introduced to get a correct description of the conformational properties of the system.[230]

The geometry optimizations were full except for the bond distances across the QM/MM partition. The distances of these bonds were kept frozen to the following values: 1.100 Å (C_{sp^2}-H) and 1.070 Å (C_{sp^3}-H) for the QM calculations and 1.400 Å (C_{sp^2}-C_{sp^2}) and 1.550 Å (C_{sp^3}-C_{sp^3}) for the MM calculations. The frequency analysis was not done since the calculation of analytical frequencies with the IMOMM method is not implemented in mmabin98.

Nevertheless, the nature of all stationary points was confirmed comparing the optimized geometries with those found for the model system (see section 3.3) which were characterized inspecting their analytical frequencies. All the relative energies given in the following sections are potential energies in gas phase. This is a reasonable approach since the previous study on the model system proved that entropic and solvent effects did not affect substantially the energy profile. Theoretical enantioselectivities were computed using equations 1.2 and 1.3 (see sections 1.1.3 and 1.1.5), taking into account the energy difference between the most stable pro-R and pro-S transition states.

4.2.2 Force Field Tuning

The model study (**article I**) revealed that the rotation of the S1-S2 bond gives rise to two distinct conformations of the transition state (see section 3.3.3). In one of these conformations (referred here as the closed conformation), the methyl attached to S2 is eclipsed with O2 while in the other (referred here as the open conformation) is in *anti* position with respect to O2. In the real system, although the methyls are replaced by *tert*-butyls, these two conformations are also possible (see Figure 4.3). Nevertheless, contrary to what we found for the model system, the IMOMM calculations predicted that the open conformation is more stable than the closed one. The inversion of the relative stabilities of these conformations can be rationalized considering that the much bulkier *tert*-butyl group attached to S2 introduce steric repulsions with O2 that make the closed conformation less stable than the open. However, these steric interactions are also possible in the model when S2 is attached to a methyl. We thus decided to explore this issue in more detail considering the oxidation of (*t*-Bu)S-S(*t*-Bu) with hydrogen peroxide:[230]

$$(t\text{-Bu})\text{S1-S2}(t\text{-Bu}) + \text{H}_2\text{O}_2 \longrightarrow [\text{HO}\cdots(\text{H})\text{O}\cdots\text{S1}(t\text{-Bu})\text{-S2}(t\text{-Bu})]^{\ddagger} \longrightarrow (t\text{-Bu})\text{S1(O)-S2}(t\text{-Bu}) + \text{H}_2\text{O}$$

The closed and open conformations of the [HO···(H)O···S1(*t*-Bu)-S2(*t*-Bu)]‡ transition state were optimized at the IMOMM(Becke3LYP:MM3) level using the default MM3 force field parameters and including the *tert*-butyls

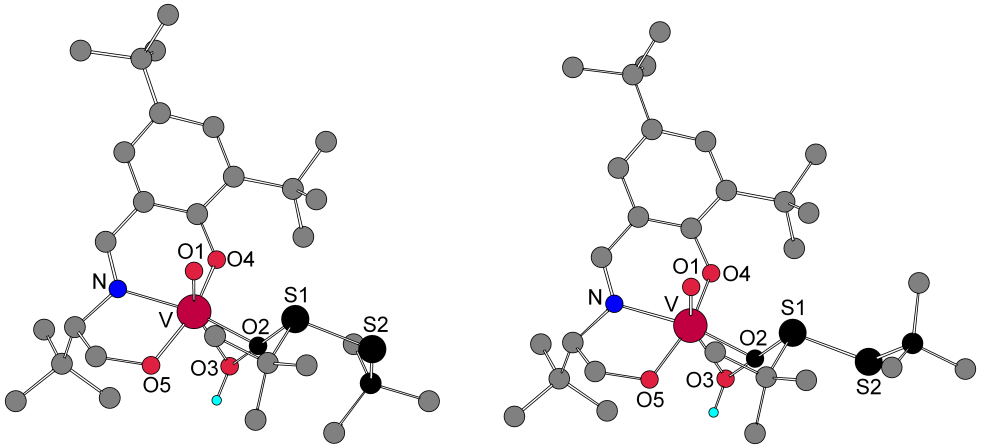

Figure 4.3: Closed (left) and open (right) conformations of the oxidized substrate in the transition state. All hydrogens, except the peroxidic, were removed for clarity.

of the substrate in the MM part as indicated in Figure 4.2. As for the vanadium-catalyzed sulfoxidation, the results showed that the open conformation is more stable than the closed by 0.39 kcal/mol. In contrast with this, the full-QM reoptimization of these saddle points with the hybrid Becke3LYP densitiy functional indicated that the closed arrangement is more stable than the open by 1.35 kcal/mol. This result was further confirmed by single point CCSD(T) calculations, which predicted that the closed conformation is the most stable by 2.12 kcal/mol. All these data pointed out that our IMOMM model was wrong. The analysis of the Mulliken charges showed that the higher stability of the closed conformation is due to hydrogen bond interactions between the C-H groups of the *tert*-butyl attached to S2 and the peroxidic oxygens of H_2O_2, which are highly polarized in the transition state. The existence of CH···O interactions has been proposed in several studies.[231–233] These interactions were computed at the MM level in our QM/MM study. Hence, the lack of a hydrogen bond potential between an aliphatic CH and a hydroxylic oxygen in the MM3 force field explains the wrong predictions of our initial IMOMM calculations. This problem was fixed introducing such potential in the force field. Only two parameters are needed: 1) the equilibrium distance of the CH···O hydrogen bond (d) and 2) the energy

released in the formation of the hydrogen bond from infinitely separed reactants (ϵ). The d parameter was computed as the optimized distance of the hydrogen bond in the $[CH_4 \cdots OH]^-$ model system computed at a very high QM level (MP2[234]/6-311++G(3d,3p)[235]). The ϵ parameter was fitted to reproduce the Becke3LYP energy difference between the closed and open conformers. The closed and open transition states were recomputed at the IMOMM(Becke3LYP:MM3) level using the hydrogen bond potential mentioned above (d=2.00 Å and ϵ=1.4 kcal/mol), and the results were that the closed conformation is more stable than the open by 1.29 kcal/mol. Hence, the rest of the IMOMM calculations presented in this chapter were carried out using this CH···O hydrogen bond potential implemented in the MM3 force field.

4.3 Results and Discussion

4.3.1 Ligand A. Diastereomers of the Real Catalyst

C_2-symmetrical chiral ligands like BINOL,[236,237] BINAP[238,239] and salen[240,241] derivatives have been widely used in asymmetric catalysis. The symmetry of these ligands reduces by a factor of two the number of isomers of the catalytic species and their associated reaction pathways. This effect improves enantioselectivity in many cases since the supressed pathways lead to the non desired enantiomer of the product. Nevertheless, in some cases the highest degree of discrimination between the pro-R and pro-S pathways is achieved by means of C_1 asymmetric ligands. This is the case of vanadium-catalyzed asymmetric sulfoxidation in which the C_1 asymmetric ligand **A** (see Figure 4.1) induced higher enantioselectivities[141,174] than C_2-symmetric salen ligands.[137] However, the lack of symmetry increases the structural complexity of the system. This fact can be clearly illustrated considering vanadium-catalyzed sulfoxidations. The $VO(OOH)^{2+}$ fragment can be combined with a chiral salen or Schiff base planar ligand in two different ways depending on which face of the ligand is occupied by the apical oxo ligand (see Figure 4.4). In principle, these two approaches lead to distinct isomers of the catalytic hydroperoxo complexes, namely **a** and **b**. With C_2-symmetric salen

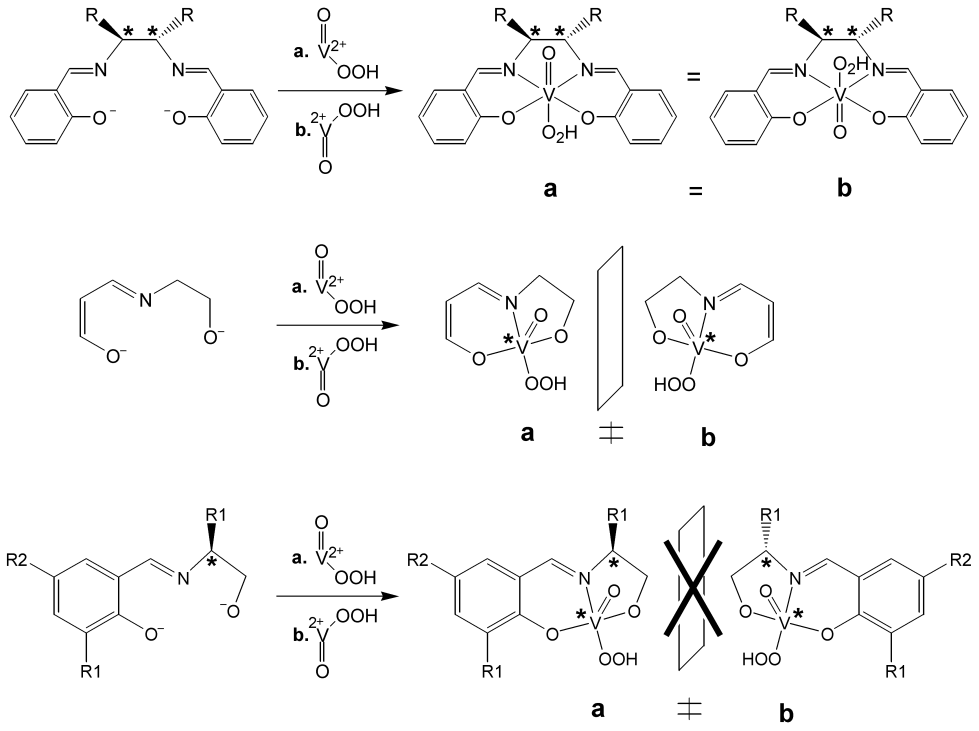

Figure 4.4: Equal (top), enantiomeric (middle) and diastereomeric (bottom) forms of the catalyst in vanadium-catalyzed sulfoxidations.

ligands these isomers are equal. With the model Schiff base analyzed in the previous chapter (**article I**), the C_2-symmetry is lost and vanadium becomes a stereogenic center. In this case, **a** and **b** are the two possible enantiomers given by the chiral metal center. In contrast with this, with a C_1 asymmetric chiral Schiff base like the one represented in Figure 4.1, the chiral metal center is combined with the asymmetric carbon of the ligand. Hence, **a** and **b** are now a couple of diastereomers in which the absolute configurations of vanadium and the ligand are reversed and retained respectively. The existence of two diastereomers of the catalyst in vanadium-catalyzed sulfoxidations is in total agreement with the NMR studies conducted by Bryliakov and Karpyshev.[197,198] Furthermore, as will be explained in the following sections, the existence of diastereomers **a** and **b** is the key to the full understanding of the origin of enantioselectivity.

The optimized geometries of diastereomers **a** and **b** with ligand **A**, la-

beled as **a-AC** and **b-AC** respectively, are represented in Figure 4.5. The main structural difference between both species is that in **a-AC**, which is 1.9 kcal/mol more stable than **b-AC**, the *tert*-butyl in the R3 position is in the face opposite to the oxo ligand, while in **b-AC** both fragments are on the same side. Appart from this, both **a-AC** and **b-AC** have essentially the same features found in the model **HP** catalyst: the oxidant is coordinated in a η^1-hydroperoxo fashion and the conformation of the V-OOH bond is the same (see section 3.3.1). These structural features are clearly indicated in **a-AC** by the V-O2 and V-O3 bond distances of 1.812 Å (1.811 Å in the model) and 2.444 Å (2.431 Å in the model) respectively, and the O5-V-O2-O3 dihedral angle of 96.5° (95.8° in the model).

The consideration of the real ligand introduces additional sources of conformational flexibility. The rotation of the *tert*-butyl in the R1 position gives rise to a couple of distinct conformations, one with C4 in *anti* position with respect to C1, and the other with C1 and C4 eclipsed (*syn*). The optimized structure of the *syn* conformation of diastereomer **b**, labeled as **b-AC'**, is represented in Figure 4.5. The **b-AC** geometry corresponds to the *anti* conformation. Both isomers can be easily distinguished inspecting the C1-C2-C3-C4 dihedral angle, which has a value of 178.4° in **b-AC** and -0.2° in **b-AC'**. The *anti* arrangement is more stable than the *syn* for both **a** and **b** diastereomers by *ca.* 1 kcal/mol. The existence of the *anti* and *syn* conformations was taken into account in the calculation of the transition states because R1 is close to the site in which the substrate is enantioselectively oxidized. The rotation of the *tert*-butyl substituent in the R2 position was not considered since it will be probably irrelevant due to its far location with respect to vanadium and the reactive center. The rotation of *tert*-butyl R3 was also ignored since their possible arrangements are three equivalent staggered conformations.

As in the model system, the flipping of the five-membered metallacycle containing V, N and O5 gives rise to two distinct arrangements. The flipping of **a-AC** leads to isomer **a-AC'** (see Figure 4.5). The main structural difference between **a-AC** and **a-AC'** is given by the N-V-O5-C8 dihedral angle which has a value of -29.2° in **a-AC** and -3.1° in **a-AC'**. This fluxional process implies significant energy changes in the **a** diastereomer of *ca.* 6-7

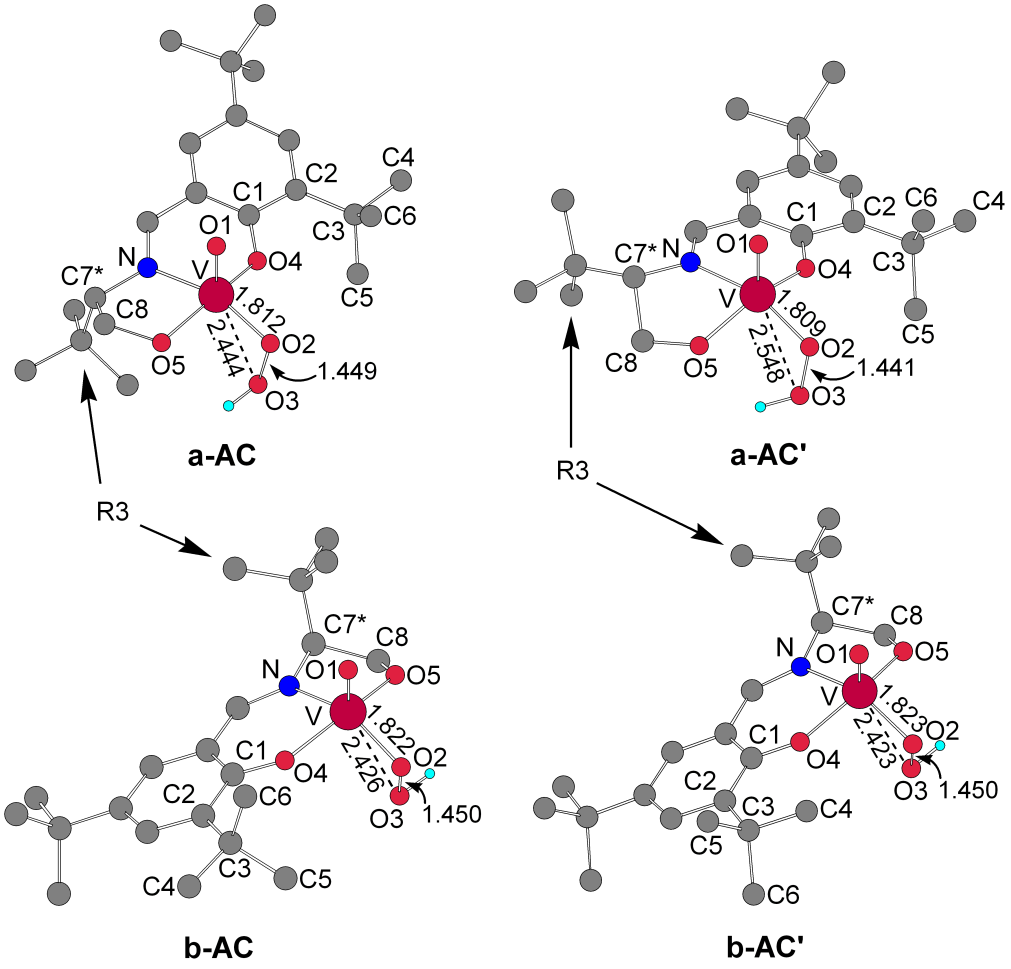

Figure 4.5: Isomers of the real catalyst. All hydrogens, except the peroxidic, were removed for clarity.

kcal/mol. For instance, **a-AC'** is less stable than **a-AC** by 6.3 kcal/mol. These energy differences become much smaller in the case of diastereomer **b**. Both **b-AC** and **b-AC'** become less stable by the flipping of the metallacycle but only by 0.3 kcal/mol. Hence, in the subsequent reactivity study, the existence of these conformations was neglected in the case of diasteromer **a** but taken into account in the case of **b**.

In summary, the calculation of the catalytic species in the real system revealed that the most stable complexes are **a-AC** and **b-AC**. This diastereomeric η^1-hydroperoxovanadium species have distinct conformations with similar energies associated with the rotation of the R1 *tert*-butyl, and the flipping of the five-membered vanadacycle.

4.3.2 Enantioselectivity with ligand A

Enantioselectivity was theoretically evaluated for ligand **A** by optimizing the structures of the transition states for the oxidation step. According to the previous model study (**article I**) this step determines the final stereochemical outcome of the reaction. Four diastereoisomeric approaches of (*t*-Bu)S-S(*t*-Bu) to the catalyst were considered: two (one pro-R and one pro-S) for each diastereomeric form (**a** and **b**) of the catalyst. In the case of diastereoisomer **a** two conformations of the catalyst, associated with the rotation of the *tert*-butyl in the R1 position, were considered. The other possible conformations derived from the flipping of the five-membered vanadacycle were discarded due to their poor stability. As in the model study (see section 3.3.3), three sources of conformational flexibility were considered in the calculation of the possible transition states: 1) the rotation of the nascent bond, S1-O2, associated to the different orientations of the substrate with respect to the catalyst, 2) the rotation of the S1-S2 bond associated to the distinct conformations of the substrate and 3) the two possible configurations of S1. Overall, 24 geometries of the transition state (2 conformers of the catalyst x 3 orientations x 2 conformations x 2 configurations) are in principle possible. Nevertheless, the geometry optimizations converged only in twelve cases. The other non converged structures suffered high steric hindrance between the substrate and the catalyst. The most stable pro-R and pro-S transition states, labeled

as **a-ATSR** and **a-ATSS** respectively, are represented in Figure 4.6. Both transition states correspond to the oxidation of bis(*tert*-butyl) disulfide by complex **a-AC** (see Figure 4.5). As in the model system the oxidation is a concerted process involving the formation of the S1-O2 bond and the cleavage of the O2-O3 bond (see section 3.3.2). These transformations are clearly indicated by the S1-O2 bond distance, which is reduced from infinite in the reactants side to 2.099 Å in **a-ATSR** (2.149 Å in the model), and the O2-O3 distance, which is elongated from 1.449 Å in **a-AC** to 1.850 Å in **a-ATSR** (1.829 Å in the model). The **a-ATSR** geometry confirms that R1 and R3 are clearly close and far respectively from the reactive center of the catalyst in which S1 is oxidized.

The most stable transition state, **a-ATSR**, is pro-R in total agreement with the experimental results[174] (see Figure 4.1). Since **a-ATSR** and **a-ATSS** are the most stable pro-R and pro-S transition states, the energy gap between them can be used to evaluate enantioselectivity combining equations 1.2 and 1.3 (see chapter 1). The **a-ATSR** geometry is more stable than **a-ATSS** by 2.4 kcal/mol. This energy difference gives rise to a theoretical enantioselectivity of 97% ee at 298 K. This value is moderately above the experimental result (82% ee) but as it will be shown below, the prediction improves when the other diastereomer of the catalyst, **b**, is considered. The higher stability of **a-ATSR** with respect to **a-ATSS** can be easily understood comparing their structures. In fact, the only relevant difference between both geometries is the absolute configuration of S1. In **a-ATSR** the *tert*-butyl group attached to S1 is oriented towards the left empty pocket of the catalyst. In contrast with this, such *tert*-butyl points towards the right in **a-ATSS** standing in the same region occupied by the R1 *tert*-butyl of the catalyst. Hence, the lower stability of **a-ATSS** is due to the steric repulsions between the *tert*-butyl of the substrate connected to S1 and the *tert*-butyl of the catalyst in the R1 position. This result accounts for the relevant role of R1 in the modulation of enantioselectivity found experimentally[174] (see Figure 4.1).

The reactivity of diastereomer **b** was explored computing the corresponding transition states. Only the orientation and conformation of the substrate preferred for the **a** diastereomer were taken into account. Nevertheless, the

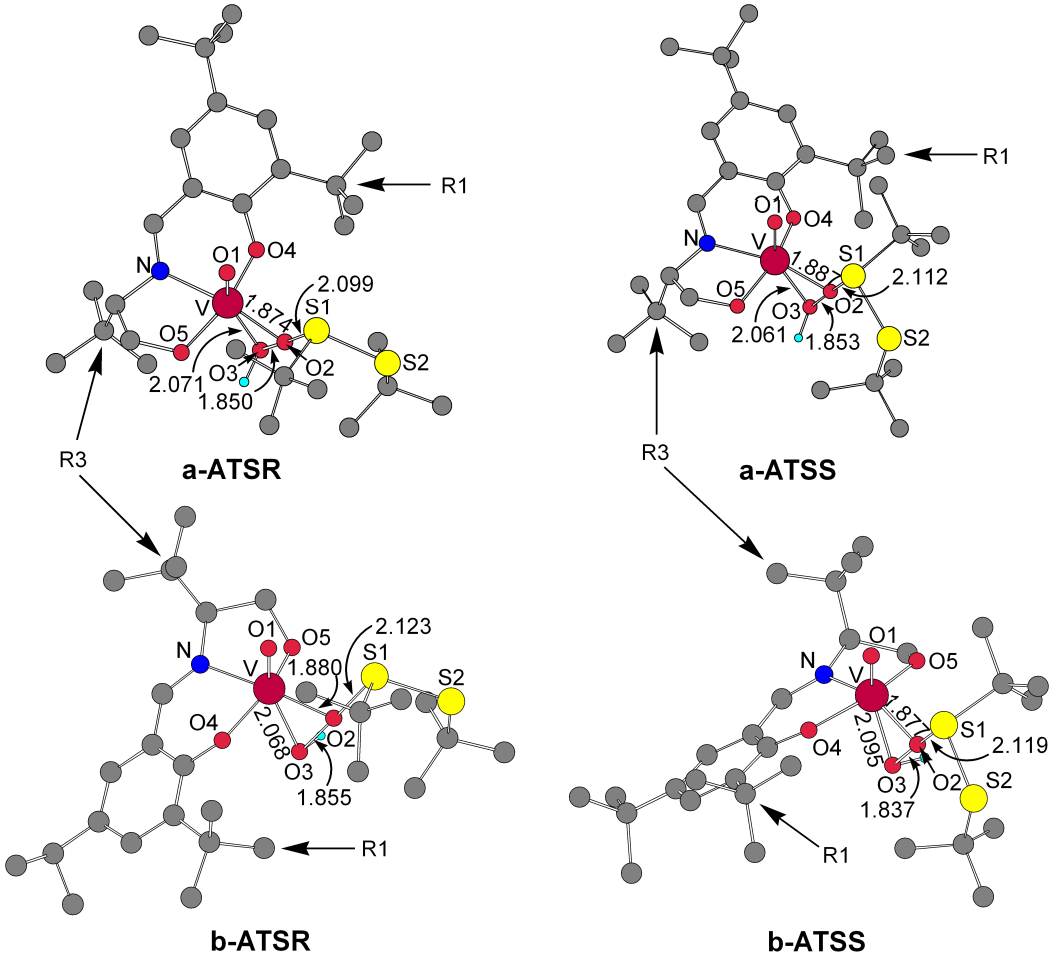

Figure 4.6: Selected transition states for ligand **A**. All hydrogens, except the peroxidic, were removed for clarity.

four possible conformations of catalyst **b** were considered in this case, because small energy differences between them were found. These conformations are derived from the rotation of *tert*-butyl R1 and the flipping of the five-membered metalacycle. For each conformation, the two possible approaches of the substrate, namely the pro-R and pro-S, were explored and a total number of eight saddle points were thus optimized. These geometry optimizations converged in five cases. The most stable pro-R and pro-S transition states associated to form **b**, labeled as **b-ATSR** and **b-ATSS** respectively, are represented in Figure 4.6. The lowest-energy saddle point, **b-ATSS**, is connected to the **b-AC'** isomer of the real catalyst (see Figure 4.5). This transition state corresponds to the oxidation of (*t*-Bu)S-S(*t*-Bu) as the S1-O2 (2.119 Å) and O2-O3 (1.837 Å) bond distances, very similar to those found in the model system and in **a-ATSR**, pointed out.

The relative energy of **b-ATSS** is 1.2 kcal/mol lower than that of **b-ATSR**. The comparison of geometries **b-ATSS** and **b-ATSR** indicated that in this case the S pathway is preferred due to the same intramolecular interactions found for diasteromer **a**. While in **b-ATSS** the *tert*-butyl attached to S1 lies on an empty pocket of the catalyst, in **b-ATSR** such *tert*-butyl is within the same region occupied by *tert*-butyl R1 giving rise to steric repulsions. Interestingly, while these repulsive interactions are found in the right side of catalyst **a**, in catalyst **b** they are originated in the left side due to the inversion of the chiral vanadium center from **a** to **b**. Hence, whereas the **a** form of the catalyst is pro-R, **b** is pro-S. Furthermore, the participation of catalyst **b** is quite important since the energy gap between the most stable pro-R and pro-S transition states ($\Delta E_{R/S}$) is significantly reduced when form **b** is taken into account. When only form **a** is considered (**a-ATSR** and **a-ATSS** transition states) $\Delta E_{R/S}$ is 2.4 kcal/mol. In contrast with this, $\Delta E_{R/S}$ is 1.8 kcal/mol when **b** is also considered (**a-ATSR** and **b-ATSS** transition states). The reduction of $\Delta E_{R/S}$ implies a decrease in the theoretical enantioselectivity from 97% ee to 90% ee, a value remarkably closer to the experimental result (82% ee). These data revealed that the existence of an additional diasteromeric form of the catalyst implies a reduction of enantioselectivity, which would be increased if somehow form **a** could be isolated and used apart from form **b**. Furthermore, comparison of geometries

a-ATSR and **b-ATSS** shows that the main structural difference between these transition states is the relative position of *tert*-butyl R3. Thus, such substituent is able to modulate the energy gap between the pro-R and pro-S transition states connected to **a** and **b** respectively. This explains why R3 has an important influence upon enantioselectivity in spite of being far from the reactive center of the catalyst (see Figure 4.1).

4.3.3 Enantioselectivity with ligands B, C and D

The theoretical enantioselectivity with ligands **B**, **C** and **D** was computed searching the corresponding transition states. For each ligand the pro-R and pro-S diastereomeric approaches of the substrate to both the **a** and **b** forms of the catalyst were considered. Four saddle points were thus computed for each ligand. The conformation and orientation of the substrate (rotation of the S1-O2 and S1-S2 bonds) and the arrangement of the catalyst (*anti*/*syn* conformations and flipping of the five-membered vanadacycle) were not sistematically explored. Instead of this, the structural preferences found in this regard for ligand **A** were assumed to be the same for ligands **B**, **C** and **D**. The structural features of the transition states were in all cases very similar to those found for ligand **A**. The transition state nature of each geometry was confirmed comparing the key geometrical parameters involved in the oxidation process (S1-O2 and O2-O3 bond distances) with those found for the model system. As for ligand **A**, for all other ligands the most stable saddle point was a pro-R geometry connected to diastereomer **a**, while the first and second most stable pro-S transition states were associated to forms **b** and **a** respectively. These results indicated that the whole set of **A**-**D** ligands is pro-R in total agreement with the experimental results[174] (see Figure 4.1).

The transition states found for ligand **B** were almost identic to those found for ligand **A**. The energy differences between the pro-R and pro-S transition states were also the same. Hence, the theoretical enantioselectivities for **A** and **B** have the same value, which is in good agreement with the enantiomeric excess rise of only 1% ee when going from **A** to **B** found experimentally[174] (see Figure 4.1). Since the sole difference between ligands A and B is given by the R2 substituent (*t*-Bu in **A** and H in **B**), these results

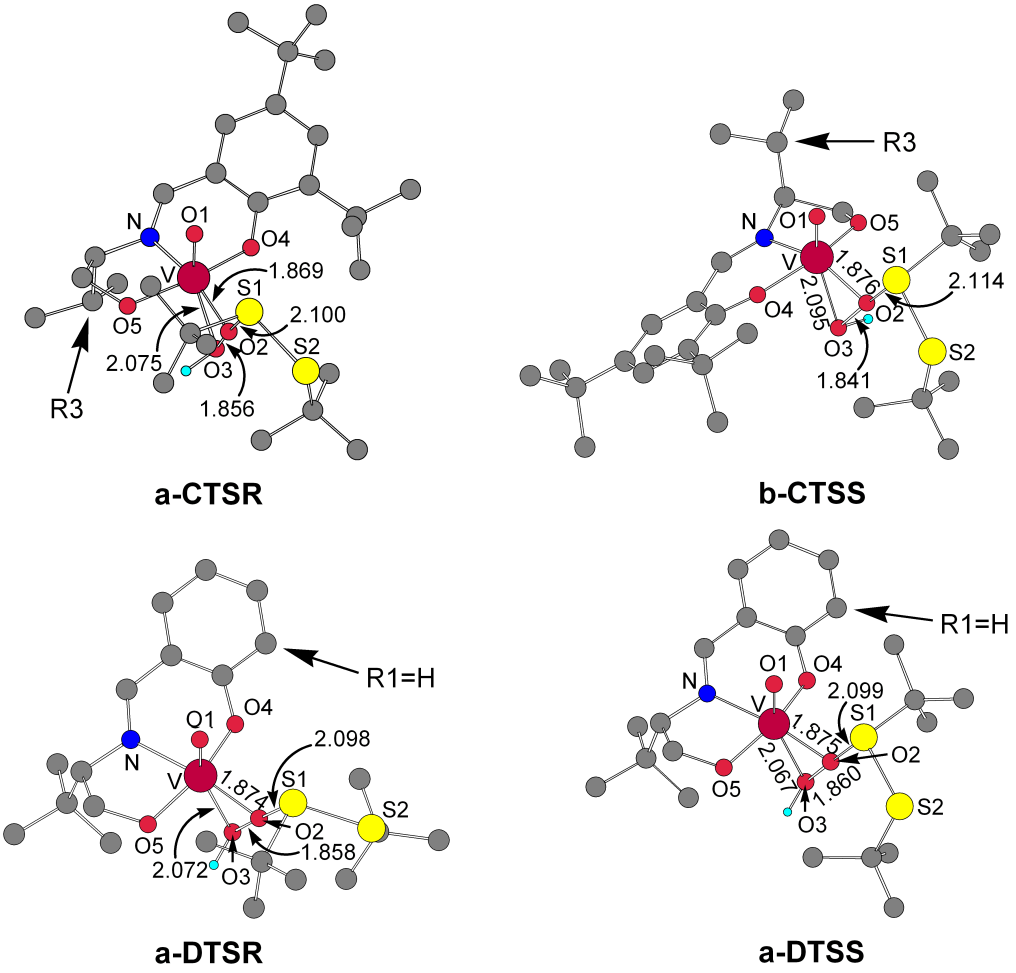

Figure 4.7: Selected transition states for ligands **C** and **D**. All hydrogens, except the peroxidic, were removed for clarity.

confirm that R2 has no influence upon enantioselectivity. The optimized geometries of the transition states showed that the null effect of R2 is due to 1) the remote location of this substituent with respect to the reaction center of the catalyst and 2) the lack of relevant structural differences associated to R2 between the pro-R and pro-S transition states.

In the case of ligand **C**, important energy changes with respect to ligand **A** were found. The most relevant change was found between the pro-R and pro-S transtition states connected to **a** (**a-CTSR**) and **b** (**b-CTSS**) respectively (see Figure 4.7). The energy difference between these saddle points, which was 1.8 kcal/mol for ligand **A**, is now 1.1 kcal/mol. Since this value corresponds to the minimum energy gap between the pro-R and pro-S pathways, enantioselectivity decreases from 90% ee (ligand **A**) to 74% ee (ligand **C**), in good agreement with the experimental results[174] (see Figure 4.1). Since the only difference between ligands **A** and **C** is given by R3, our computational results can be used to rationalize the effect of this substituent on enantioselectivity. The **a-CTSR** and **b-CTSS** geometries show that although R3 is far from the site of chemistry, this substituent is able to modulate the energy difference between diastereomers **a** (pro-R) and **b** (pro-S), and thus the enantiomeric excess, because the main structural difference between these transition states is given by the relative position of R3. The reduction of the steric bulk in the oxo face of catalyst **b** by the replacement of R3=*t*-Bu by R3=*i*-Pr implies a decrease in the energy difference between the **a** pro-R and the **b** pro-S transition states.

The energy differences between the pro-R and pro-S transition states found for ligand **D** were also significantly different than those found for **A**. In this case both ligands differ in the nature of R1 and R2 which are *t*-Bu in **A** and H in **D**. Since we already demonstrated that R2 has no effect on enantioselectivity, the results obtained for ligand **D** can be used to explain the effect of R1. The main change in the relative energies was found for the gap between the pro-R and pro-S transition states connected to diastereomer **a**, labeled as **a-DTSR** and **a-DTSS** respectively (see Figure 4.7). With ligand **D** this gap is reduced from 2.4 kcal/mol (ligand **A**) to 0.3 kcal/mol and becomes the narrowest separation between the pro-R and pro-S pathways. Enantioselectivity is consequently reduced from 90% ee (ligand **A**) to 21%

Ligand	R1	R2	R3	exp. % ee	theor. % ee	ΔE_A	ΔE_{AB}
A	*t*-Bu	*t*-Bu	*t*-Bu	82%	90%	2.4	1.8
B	*t*-Bu	**H**	*t*-Bu	83%	90%	2.4	1.8
C	*t*-Bu	*t*-Bu	***i*-Pr**	60%	74%	2.7	1.1
D	**H**	H	*t*-Bu	46%	21%	0.3	0.3

Table 4.1: Theoretical and experimental enantioselectivities and energy differences, in kcal/mol, between the most stable pro-R and pro-S transition states.

ee, in reasonable agreement with the experimental results (see Figure 4.1). The comparison of geometries **a-DTSR** and **a-DTSS** showed the origin of this drop in enantiomeric excess: while with ligand **A** the left and right sides of the catalyst were well differentiated by R1=*t*-Bu, with ligand **D** (R1=H) both sides are sterically similar.

4.3.4 Origin of Enantioselectivity

The experimental and theoretical enantioselectivities for the different **A**, **B**, **C** and **D** ligands used in the Ellman's vanadium-catalyzed sulfoxidation[174] are collected in Table 4.1. Our predicted values are in general in good agreement with the experimental results and, except for ligand **D**, the differences are lower than 15% ee. In fact, the exact reproduction of the empirical values is very difficult since such differences on the enantiomeric excess are associated to errors in the calculation of the energy of tenths of kcal/mol. In general, the predicted enantiomeric excees is higher than the experimental. Nevertheless, the empirical tendence consisting of a significant reduction of enantioselectivity with ligands **C** and **D** with respect to **A** and **B** is clearly reproduced by our calculations (see Figure 4.8). These results show the ability of our computational method to test *in silico* the efficiency of a given Schiff base ligand.

Our computational study revealed that two diastereomers of the catalyst, namely **a** and **b**, are possible. Both species, that in solution will probably be in equilibrium, catalyze the enantioselective oxidation of (*t*-Bu)S-S(*t*-Bu)

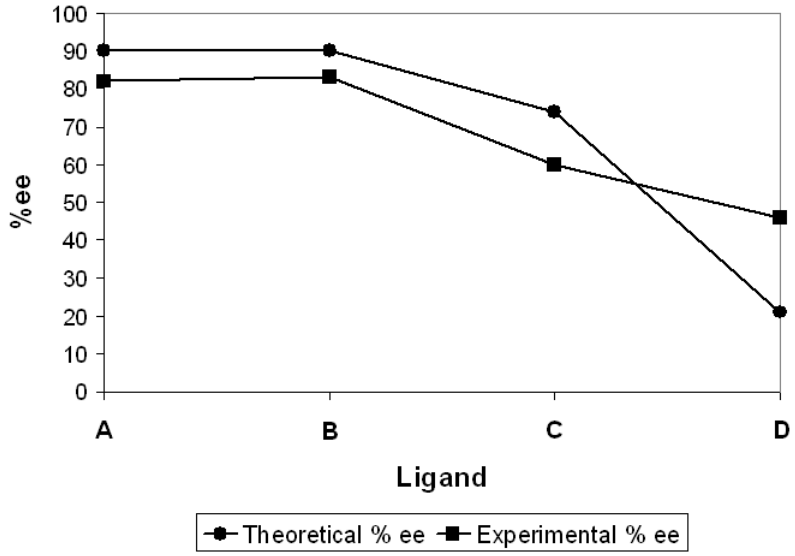

Figure 4.8: Correlation between theoretical and experimental enenatioselectivities.

with hydrogen peroxide. Nevertheless, while form **a** is pro-R, **b** is pro-S (see Figure 4.9). The enantioselectivity induced by **a** and **b** is given by the energy difference between the most stable pro-R and pro-S transition states associated to each diastereomer: ΔE_A for **a** and ΔE_B for **b**. ΔE_B can be neglected in the calculation of enantiomeric excess, since the pro-R saddle point connected to **b** is always the less stable one. In contrast with this, the energy difference between the **a** pro-R transition state and the **b** pro-S transition state, ΔE_{AB}, is quite important. Enantioselectivity is controlled by ΔE_{AB} since for ligands **A**, **B** and **C** $\Delta E_{AB} < \Delta E_A$ (see Table 4.1). Only for ligand **D** both ΔE_A and ΔE_{AB} are equally important since in this particular case $\Delta E_A = \Delta E_{AB}$.

The analysis of the variation of ΔE_A and ΔE_{AB} together with the comparison of the associated transition states allows a rational interpretation of enantioselectivity (see Figure 4.9). ΔE_A, is controlled by substituent R1. When the steric bulk of a *tert*-butyl substituent (ligand **A**) is eliminated placing a hydrogen in this position (ligand **D**) there is a clear reduction of ΔE_A from 2.4 kcal/mol to 0.3 kcal/mol (see Table 4.1). This effect is related to

the steric repulsions between the substrate and the catalyst in the oxidation transition state. ΔE_{AB} is sensitive to the nature of R3 substituent. The steric bulk reduction from *tert*-butyl (ligand **A**) to *iso*-propyl (ligand **C**) implies a decrease of ΔE_{AB} from 1.8 kcal/mol to 1.1 kcal/mol. This effect can be associated to the intrinsic stability of the catalyst which apparently depends on the steric bulk introduced on the oxo face. In contrast with this, R2 has no effect in neither ΔE_A nor ΔE_{AB} which are unaffected by the replacement of *tert*-butyl (ligand **A**) by hydrogen (ligand **B**) in this position. The irrelevant role of R2 can be understood taking into account that this substituent has no interaction with the substrate, and is not related with any structural difference between **a** and **b**. Furthermore, the energy differences collected in Table 4.1 revealed that the effects of R1 and R3 are somehow coupled. This fact is especially clear in the case of ligand **D** in which the replacement of *tert*-butyl R1 (ligand **A**) by hydrogen implies a reduction not only of ΔE_A, but also of ΔE_{AB} from 1.8 to 0.3 kcal/mol. The interpretation of this effect is not straightforward but nevertheless it has no effect on the stereochemical outcome of the reaction for ligands **A**-**D**.

The theoretical model represented in Figure 4.9 suggests that ligand **A**, which according to Ellman is the ligand inducing the highest enantioselectivity,[174] could be improved applying the following rational strategy: 1) enantioselectiviy is first increased reducing the participation of the pro-S **b** form of the catalyst ($\Delta E_{AB} > \Delta E_A$) and then 2) the pro-R character of form **a** (ΔE_A) is amplified. The first point can be accomplished through the increase of the value of ΔE_{AB} by reinforcing the steric bulk in the R3 position of the ligand. The goal of the second point can be achieved amplifying ΔE_A through the introduction of substituents bulkier than *tert*-butyl in R1.

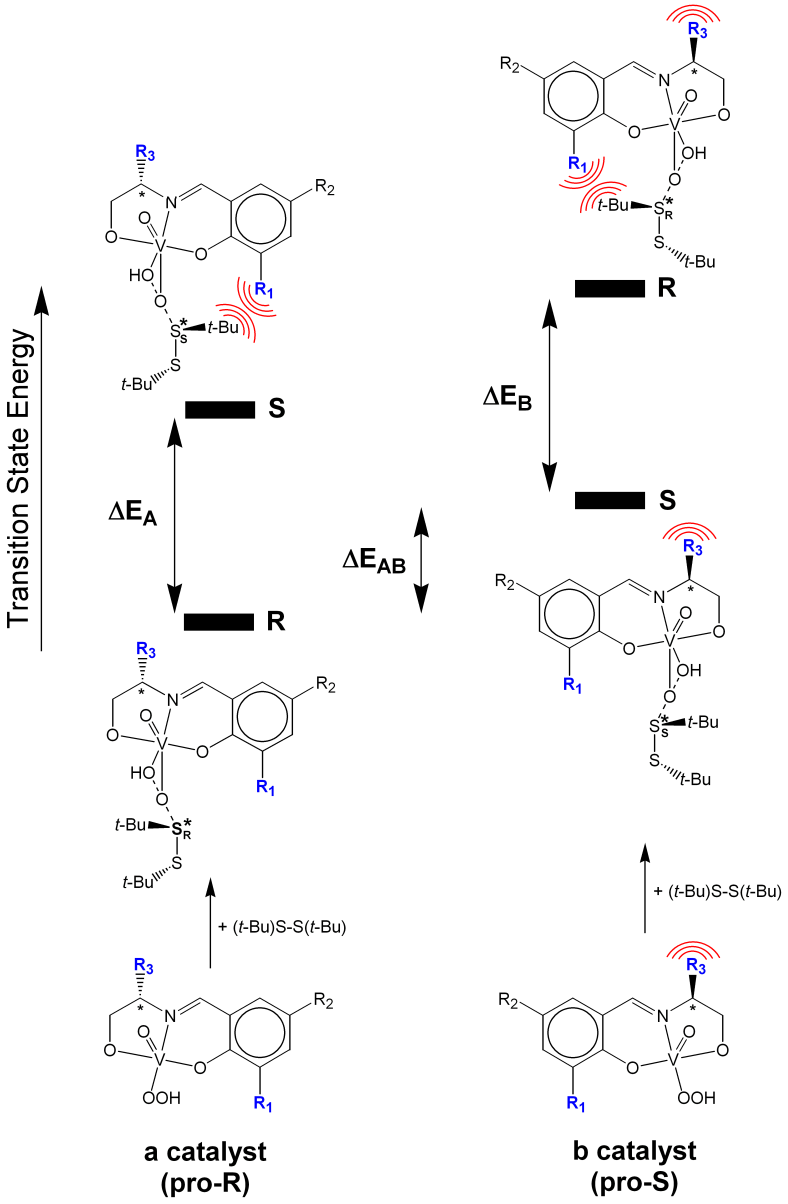

Figure 4.9: Origin of enantioselectivity.

Chapter 5

Mechanism of the Dynamic Kinetic Resolution of Sulfinyl Chlorides

The DAG method developed by Khiar[162] (see Figure 5.1) is one of the most important methods used in the synthesis of chiral sulfoxides. The mechanism of this reaction, based on the nucleophilic substitution on sulfur derivatives, was theoretically studied considering a model sytem. The interconversion of both enantiomers of the sulfinyl chloride (**article III**) and their transformation into chiral sulfinate esters (**article IV**) were explored. The role of the base in both processes was also investigated. The results of this study gave a deep mechanistic insight not only for the DAG method, but also for other synthetic methods based on the dynamic kinetic resolution (DKR) of sulfinyl chlorides. The knowledge acquired in this preliminar work was subsequently applied to the study of the real system in which the origin of enantioselectivity was rationalized (**article V**), as will be explained in the next chapter.

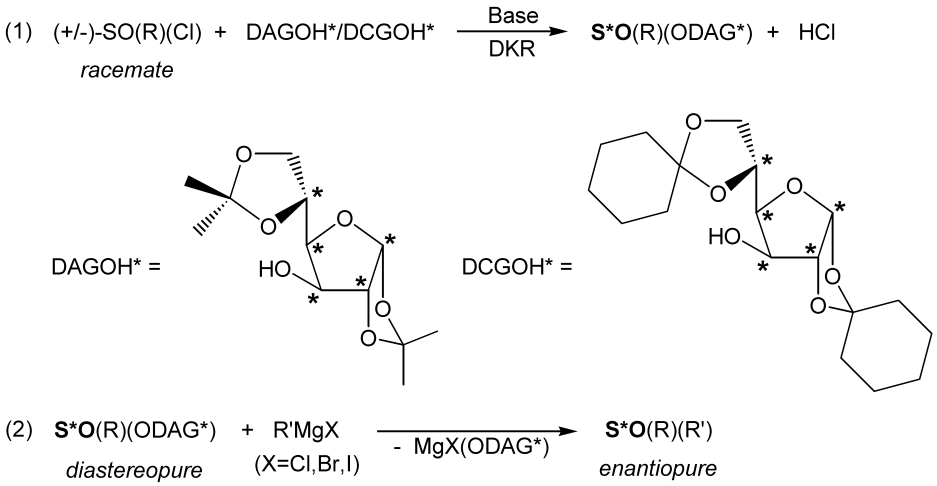

Figure 5.1: The DAG method.

5.1 Introduction

5.1.1 Dynamic Kinetic Resolution of Sulfinyl Chlorides

One of the most important methods used in the synthesis of chiral sulfoxides is the nucleophilic substitution on sulfur derivatives[71] (see section 1.2.3). Two of the most prominent examples of this methodology are the DAG method and the cinchona-assisted DKR. These synthetic methods are based on the general scheme represented in Figure 5.2. In a first step, an optically active sulfinate ester (S*O(R)(OR')) is obtained by DKR of a sulfinyl chloride racemate ((+/-)-S*O(R)(Cl)) in the presence of an alcohol and a base. The dynamic kinetic resolution[242,243] process consists of the combination of two chemical transformations: 1) the fast interconversion of both enantiomers of the sulfinyl chloride, which allows the obtention of yields higher than 50% and 2) the reaction of the alcohol with the sulfinyl chloride giving rise to the sulfinate ester. The by-product of the latter reaction, HCl, is allways neutralized *in situ* with some basic compound. The major stereoisomer of SO(R)(OR') is obtained through the fastest reaction channel. In the final step, this stereoisomer is separated from the minor reaction product and

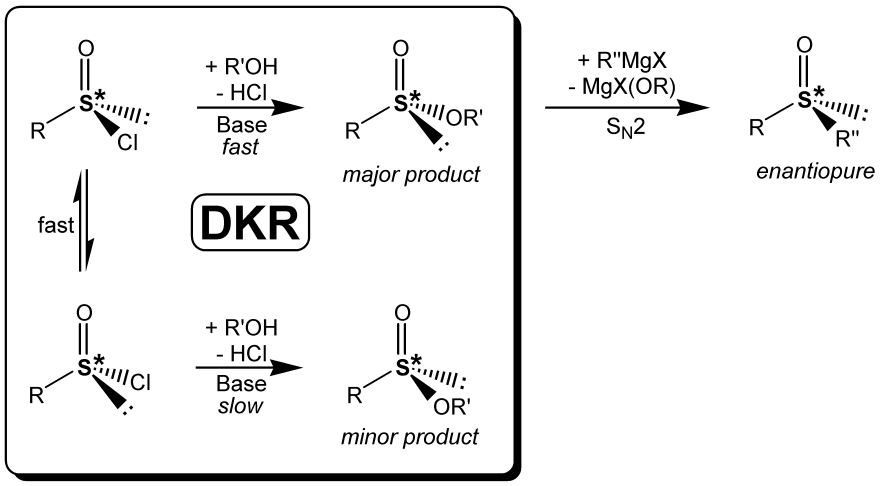

Figure 5.2: DKR of sulfinyl chlorides.

transformed into an optically active sulfoxide by addition of a Grignard reagent. This second step proceeds through a S_N2 mechanism with total inversion of configuration in most cases,[150,151] *i.e.* if the sulfinate ester substrate is completely diastereopure then the chiral sulfoxide is obtained with very high enantiomeric excess (>99%). Hence, the successful application of these synthetic methods is only possible when the formation of the major sulfinate ester is highly diastereoselective.

In the DAG method (see Figure 5.1), originally reported by Khiar,[162] a chiral sugar derivative called DAGOH (DiAcetone-D-Glucose) was used as alcohol. DCGOH (DiCyclohexylidene-D-Glucose) was also tested as chiral alcohol and the results were very similar to those obtained with DAGOH.[163,164] The reaction was performed with stoichiometric amounts of nitrogenated organic bases like pyridine or triethylamine, which were used to neutralize HCl. Several racemic alkyl sulfinyl chlorides were transformed into the corresponding optically active sulfinate esters of DAGOH. The addition of Grignard reagents to these species leads to chiral sulfoxides with high yields (>83%) and enantioselectivities (>99% ee).[162] The method was subsequently applied to the synthesis of C_2-symmetric bis-sulfoxides.[163,164] These compounds were used as bidentate ligands to prepare Pd(II) and Ru(II) complexes.[164] The DAG method has been also used in the synthesis of several chiral sulfoxides

with synthetic[99–101,244] and pharmacologic[245,246] interest.

The other relevant synthetic method based on the dynamic kinetic resolution of sulfinyl chlorides is the cinchona-assisted DKR recently developed by Ellman (see Figure 5.3).[147,165] This method consists of the DKR of *tert*-butyl sulfinyl chloride with benzylic alcohols and using chiral amines as catalysts. The HCl by-product was neutralized using proton sponge. The main advantage introduced by this method is that the only source of chirality, the base, is used in small catalytic amounts. In the original work, the best results (99% of yield with 80% ee[147]) were obtained with the peptide represented in Figure 5.3. The results were later improved (yields and enantiomeric excesses higher than 90%) using the cinchona alkaloid quinidine as catalyst.[165] Shibata and Toru also applied cinchona alkaloids to the DKR of sulfinyl chlorides. In this case however, the cinchona alkaloids were used in stoichiometric amounts. The best results (yields up to 92% and enantiomeric excesses up to 95% ee) were obtained in the DKR of *p*-toluenesulfinyl chloride with *tert*-butanol using quinidine acetate as cinchona alkaloid.[166] As in the DAG method, the sulfinate esters obtained with these synthetic approaches can be subsequently transformed into chiral sulfoxides by addition of Grignard reagents.

5.1.2 Previous Mechanistic Studies

One of the most interesting features of the DAG method and the cinchona-assisted DKR consists of the dramatic effects of the base on the diastereoselective synthesis of the sulfinate ester. In the cinchona-assisted DKR, the enantiomeric excess depends strongly on the structure of the cinchona alkaloid.[147,165,166] More interestingly, in the DAG method, the structural modification of the base, which is non chiral, can be used not only to tune the diastereomeric excess but also to select the desired absolute configuration of the sulfinyl sulfur in SO(R)(OR').[162–164] This enantiodirecting effect of the base in the DAG method will be further commmented and studied in the next chapter. These experimental results showed that the base should play a central mechanistic role in the formation of the sulfinate ester. Nevertheless, the mechanistic details of the interconversion of both enantiomers of SO(Cl)(R) and their subsequent transformation into SO(R)(OR') were unknown.

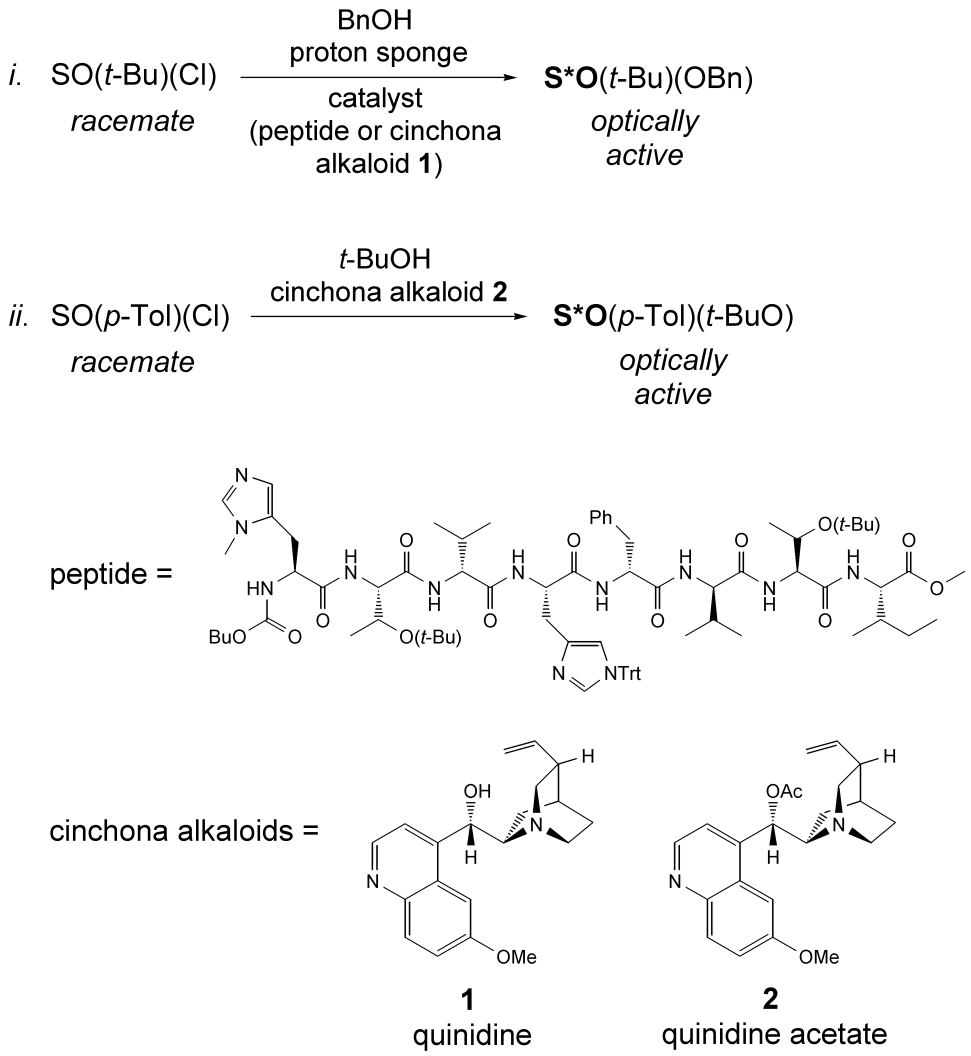

Figure 5.3: Dynamic kinetic resolution of chlorides by Ellman (i) and Shibata and Toru (ii).

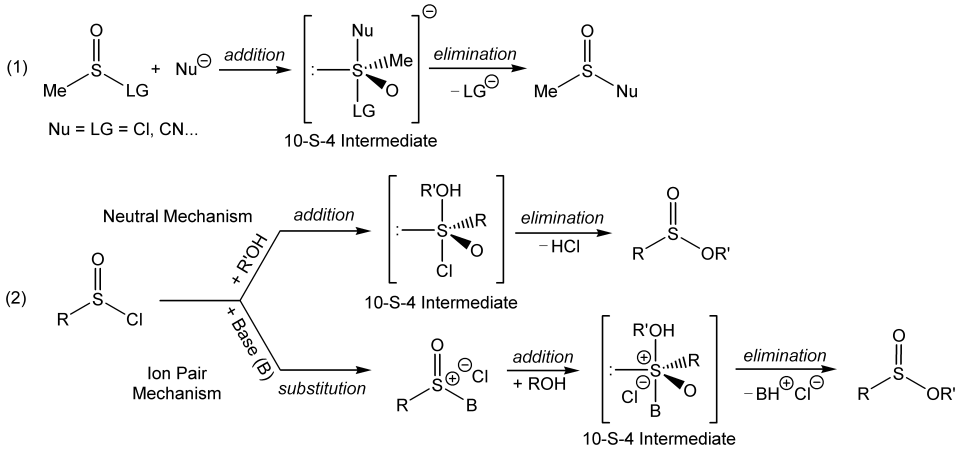

Figure 5.4: Mechanism proposed by Bachrach (1) and the reaction pathways considered in our study (2).

Chiral amines and sulfoxides can undergo thermal racemization through a process known as pyramidal inversion, in which both tetrahedral enantiomers are interconverted through a non chiral planar transition state (see section 1.1.1). In principle, this process is a plausible mechansim for the interconversion of R-SO(Cl)(R) and S-SO(Cl)(R) involved in the DKR of sulfinyl chlorides (see Figure 5.2). Several theoretical[247–250] and experimental[251–254] studies on the inversion of amines showed that in most cases this process is very fast at room temperature. In the case of sulfoxides the situation is the same only in some specific cases. Experimental studies have shown that the pyramidal inversion of some arenethiolsulfinates,[255] allyl,[256] vinyl[257] and benzyl[258] sulfoxides occurs under mild conditions. In contrast with this, Mislow demonstrated that the inversion of several dialkyl, diaryl and alkyl aryl sulfoxides is significantly fast only above 200 °C.[60] To the best of our knowledge, there was not any previous study on the inversion of sulfinyl chlorides. We thus decided to carry out a theoretical study on the pyramidal inversion of these compounds considering the eventual participation of the base.

The other important reaction involved in the DKR of sulfinyl chlorides is the addition of the alcohol leading to the sulfinate ester product (see Figure 5.2). In this process, Cl is displaced by OR' and the absolute configuration of the sulfinyl sulfur in S*O(R)(OR') is decided. The configuration of the final

chiral sulfoxide is also decided in this step, since the subsequent addition of Grignard reagents proceeds with total inversion of configuration.[150,151] The nucleophilic substitution on sulfur derivatives has been theoretically studied by Bachrach.[259,260] In a recent study this mechanism was analyzed for the particular case of methanesulfinyl derivatives considering the addition of small anions equal to the leaving group[261] (see Figure 5.4). According to this study the reaction follows an addition/elimination mechanism. The first step consists of the addition of the nucleophile giving rise to a hypervalent 10-S-4 (10 electrons with 4 substituents sulfur) intermediate. In the subsequent step the reaction product is obtained by elimination of the leaving group. The mechanism postulated by Bachrach is in principle a feasible reaction pathway for the addition of R'OH to SO(Cl)(R). Nevertheless, this mechanistic model does not clarify how the base participates in the reaction. The addition of alcohols to sulfinyl chlorides was theoretically studied in a model system considering an addition/elimination mechanism analogous to that proposed by Bachrach.[261] Two different starting points were taken into account: 1) the alcohol reacts directly with the sulfinyl chloride (neutral mechanism) and 2) the base displaces chlorine in an initial step giving rise to an ionic species that subsequently reacts with DAGOH, as proposed by Khiar[162] (ion pair mechanism).

5.2 Computational Details

All calculations were done with the DFT Becke3LYP hybrid functional[208,209] as implemented in the Gaussian03 code.[262] The 6-31G(d) basis set[214,215] was used to describe nitrogen, oxygen, carbon and hydrogen atoms. In the case of sulfur and chlorine, the ten innermost electrons of these atoms were replaced with an effective core potential.[212] The valence double-ζ basis set associated to the pseudopotential in the program,[262] with the contraction labeled as LANL2DZ, was used for these two elements and supplemented with a d shell.[213] All elements involved in the system were thus described with a double-ζ quality basis set including polarization d functions. The suitability of this basis set was confirmed expanding it through the addition of diffuse functions for chlorine.[263] This was done in the study of the pyramidal

inversion of SO(Cl)(Me) (article **III**) since quite long S-Cl bonds were found, which suggested a strong anionic character for chlorine.

All geometries were fully optimized and subsequently classified as minima or transition states by vibrational analysis. The nature of the transition states was further confirmed relaxating their structures towards reactants and products by means of IRC calculations.[264] The alcohols and trialkyl amines used in the DAG method and the cinchona-assisted DKR were modeled as methanol and trimethyl amine respectively. Although this was a quite drastic simplification of the real system, the electronic effects governing the reaction mechanism were preserved. In the theoretical study of the chloride displacement by alcohol (**article IV**) solvent effects were taken into account with the CPCM method.[265] The free energy in solution ($G_{(sol)}$) of each stationary point was computed using equation 5.1 and considering the solvent used in most experiments: toluene (ϵ=2.379). The CPCM energies (G_{CPCM}), computed by single point calculations on the gas phase optimized geometries, account for the free energies of solvation but without including the thermal and entropy contributions of the solute. These contributions were computed as the difference between the potential and Gibbs free energies ($G_{(g)}$-$E_{(g)}$) found for the solute in gas phase, and added to G_{CPCM} in order to obtain $G_{(sol)}$.

$$G_{(sol)} = G_{CPCM} + (G_{(g)} - E_{(g)}) \tag{5.1}$$

5.3 Results and Discussion

5.3.1 Pyramidal inversion of SO(Cl)(Me)

The pyramidal inversion of SO(Cl)(Me) is in principle a reasonable mechanism for the racemization of sulfinyl chlorides involved in the DAG method and the cinchona-assisted DKR. This process was thus theoretically studied. The computational model used in this study was initially validated exploring the pyramidal inversion of methyl (*p*-methyl)-phenyl sulfoxide (SO(*p*-MePh)(Me)) for which experimental data was available.[60] The geometries of this species and the inversion transition state were optimized. Accord-

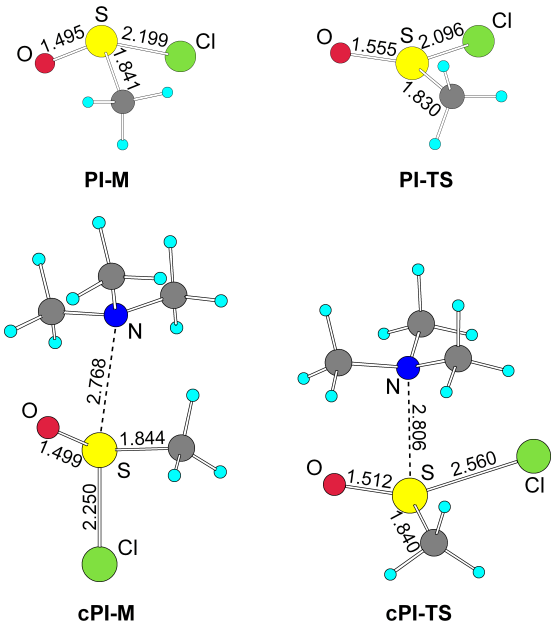

Figure 5.5: Stationary points involved in the pyramidal inversion of SO(Cl)(Me).

ing to our results, the pyramidal inversion of SO(*p*-MePh)(Me) implies a free energy barrier of 41.4 kcal/mol. This result confirmed the suitability of our theoretical model since exactly the same barrier was found by Mislow.[60] The structural transformations involved in the inversion of SO(*p*-MePh)(Me) were analogous to those found in the case of methyl sulfinyl chloride, which will be explained in detail below.

The pyramidal inversion of SO(Cl)(Me) was explored computing the corresponding transition state. The optimized geometries of SO(Cl)(Me) and the saddle point, labeled as **PI-M** and **PI-TS** respectively, are represented in Figure 5.5. The pyramidal inversion of SO(Cl)(Me) involves the planarization of the sulfoxide. In this process, the pyramidal geometry of the sulfinyl sulfur in the reactant is transformed into planar trigonal in the transition state. This geometrical transformation is clearly indicated by the Cl-S-O-Me dihedral angle which has a value of 99.8° in **PI-M** and 180.0° in **PI-TS**. The unique imaginary frequency of **PI-TS** consists of the oscilation of sulfur above and below the (O)(Cl)(Me) plane, which is fully consistent with the

pyramidal inversion process. The inversion also involves the contraction of the S-Me (from 1.841 Å in **PI-M** to 1.830 Å in **PI-TS**) and S-Cl (from 2.199 Å in **PI-M** to 2.096 Å in **PI-TS**) bonds and the elongation of the S-O (from 1.495 Å in **PI-M** to 1.555 Å in **PI-TS**) bond . The energy barrier found for the **PI-M** $\longrightarrow$ **PI-TS** transformation was 63.4 kcal/mol. This value, clearly higher than that measured for SO(*p*-MePh)(Me) ($\Delta G^{\ddagger}$=41.4 kcal/mol), indicated that the pyramidal inversion of methyl sulfinyl chloride is not a feasible racemization mechanism.

The hypothetic participation of the base, trimethylamine, in the pyramidal inversion of SO(Cl)(Me) was explored. The structure of **PI-TS** was reoptimized as a transition state putting a molecule of NMe_3 interacting with sulfur from above the (O)(Cl)(Me) plane. This calculation converged into the transition state **cPI-TS** (see Figure 5.5). As in **PI-TS**, the unique imaginary frequency of this saddle point consists of the oscilation of sulfur above and below the (O)(Cl)(Me) plane. Furthermore, the IRC-driven relaxation of **cPI-TS** towards reactants and products converged into van der Waals complexes like **cPI-M** in which the base appears bound to SO(Cl)(Me) through long S-N bonds. In these complexes, the absolute configuration of SO(Cl)(Me) is different in each side of the reaction. Hence, we concluded that this process consists of a base-assisted pyramidal inversion of SO(Cl)(Me). The **cPI-M** $\longrightarrow$ **cPI-TS** transformation involves the elongation of the S-O (from 1.499 Å in **cPI-M** to 1.512 Å in **cPI-TS**), S-Cl (from 2.250 Å in **cPI-M** to 2.560 Å in **cPI-TS**) and S-N (from 2.768 Å in **cPI-M** to 2.806 Å in **cPI-TS**) bonds. In this case, the S-Me bond is almost unaffected. Interestingly, **cPI-TS** has a distorted trigonal bipyramid (TBP) geometry with oxygen and chlorine in the axial positions, and methyl, the base and the lone electron pair of sulfur on the equatorial plane. These structural features are reflected on the axial O-S-Cl angle of 153.0° and the equatorial Me-S-NMe_3 angle of 95.9°. The Berry pseudorotation[266,267] of 10-S-4 hypervalent sulfur intermediates[268,269] has been proposed as a DKR mechanism.[162] Nevertheless, our study shows that 1) hypervalency is apparently avoided as indicated by the very long S-N bond distances and 2) the TBP species do not participate in the inversion process as intermediates but as transition states. Surprisingly, we found that trimethylamine catalyzes the inversion of SO(Cl)(Me) since it reduces the

barrier of this process from 63.4 kcal/mol to 22.3 kcal/mol. Hence, the base-catalyzed pyramidal inversion of methyl sulfinyl chloride was postulated as a feasible DKR mechanism.

The base-free and base-catalyzed pyramidal inversions of the model reaction product, SO(OMe)(Me), were also investigated. In this case, the participation of the base induces a decrease of the energy barrier from 64.1 to 42.7 kcal/mol. These results showed that the reduction of the inversion barrier by trimethylamine is clearly larger for SO(Cl)(Me) ($\Delta\Delta G^{\ddagger}$=40.5 kcal/mol) than for SO(OMe)(Me) ($\Delta\Delta G^{\ddagger}$=21.4 kcal/mol). The still high barrier found for the base-catalyzed inversion of SO(OMe)(Me), very similar to that reported for SO(*p*-MePh)(Me) ($\Delta G^{\ddagger}$=41.4 kcal/mol[60]), confirmed the optical stability of this compound. This is in total agreement with the experimental results since the racemization of the reaction product in the presence of the base was never observed.

The optimized geometries revealed that the base-assisted pyramidal inversion of SO(X)(Me) involves a clear elongation of the S-X bond for both X=Cl and X=OMe. Hence, the higher strength of the S-OMe bond with respect to S-Cl can be associated to the much lower energy barrier found for the base-catalyzed inversion of SO(Cl)(Me) with respect to SO(OMe)(Me). The base-catalyzed inversion of SO(*p*-MePh)(Me) was also investigated in order to infer whether the base has also a catalytic effect upon the racemization of aryl alkyl sulfoxides. In this case however, all attempts to converge the inversion transition state failed.

5.3.2 Chloride displacement by alcohol

Neutral mechanism

The addition-elimination mechanism proposed by Bachrach[261] (see Figure 5.4) was explored for the particular reaction in which methanol displaces the chlorine of SO(Cl)(Me). We started this study considering the neutral pathway. The transition state corresponding to the addition of methanol to SO(Cl)(Me), labeled as **NM-TS**, is represented in Figure 5.6. The imaginary frequency of **NM-TS** involves the formation of the S-O1 bond and the elongation of the S-Cl bond. Interestingly, this process is accompained by

the transfer of the hydroxylic hydrogen of methanol to the sulfinyl oxygen of SO(Cl)(Me). In fact, no transition state could be located without the participation of this additional process. The IRC-driven relaxation of **NM-TS** towards reactants and products conducted to species **NM-I1** and **NM-I2**, respectively. **NM-I1** is a complex of methanol associated with methyl sulfinyl chloride through a hydrogen bond between H and O2. **NM-I2** is a complex of SOH(Me)(OMe) associated with chloride. The **NM-I1** $\longrightarrow$ **NM-TS** $\longrightarrow$ **NM-I2** reaction pathway involves a hydrogen transfer from methanol to the sulfinyl group of SO(Cl)(Me) since H appears bound to O1 in **NM-I1**, with a O1-H bond distance of 0.972 Å, and to O2 in **NM-I2**, with a O2-H bond distance of 0.981 Å. In **NM-TS** H is located close to the midpoint between O1 and O2, as the O1-H (1.311 Å) and O2-H (1.159 Å) distances indicated. The H,O1,S,O2 set of atoms are in a coplanar arrangement as indicated by the H-O1-S-O2 dihedral angle of 1.7°. Furthermore, the shortening of the S-O1 bond distance from 3.015 Å in **NM-I1** to 1.818 Å in **NM-I2** through 2.138 Å in **NM-TS** pointed out the formation of the S-OMe bond. Simultaneously, the S-Cl bond distance is elongated from 2.188 Å in **NM-I1** to 2.340 Å in **NM-I2**, through 2.207 Å in **NM-TS**. The evolution of these geometrical parameters can be interpreted in two different manners: 1) the reaction is an addition in which methanol binds with sulfur leading to the formation of a hypervalent 10-S-4 intermediate (preservation of the S-Cl bond) or 2) the reaction is a S_N2 nucleophilic substitution in which Cl is the leaving group and methanol the nucleophile (rupture of the S-Cl bond).

The three stationary points involved in the addition step have a distorted trigonal bipyramid geometry around sulfur. In all cases the axial positions are occupied by OMe and Cl, and the equatorial plane contains Me, O2 and the lone electron pair of sulfur. This relative distribution of substituents around sulfur is clearly indicated by the geometrical parametes of **NM-I2**: the O1-S-Cl axial and C-S-O2 equatorial angles are 176.0° and 103.2° respectively, and the C-S-O2-O1 and C-S-O2-Cl dihedral angles are -88.9° and 88.4° respectively. The other isomers of these trigonal bipyramid geometries were explored without success.

The long S-Cl bond distance in **NM-I2** suggested that this species might have some degree of ion pair character. This possiblity was explored ana-

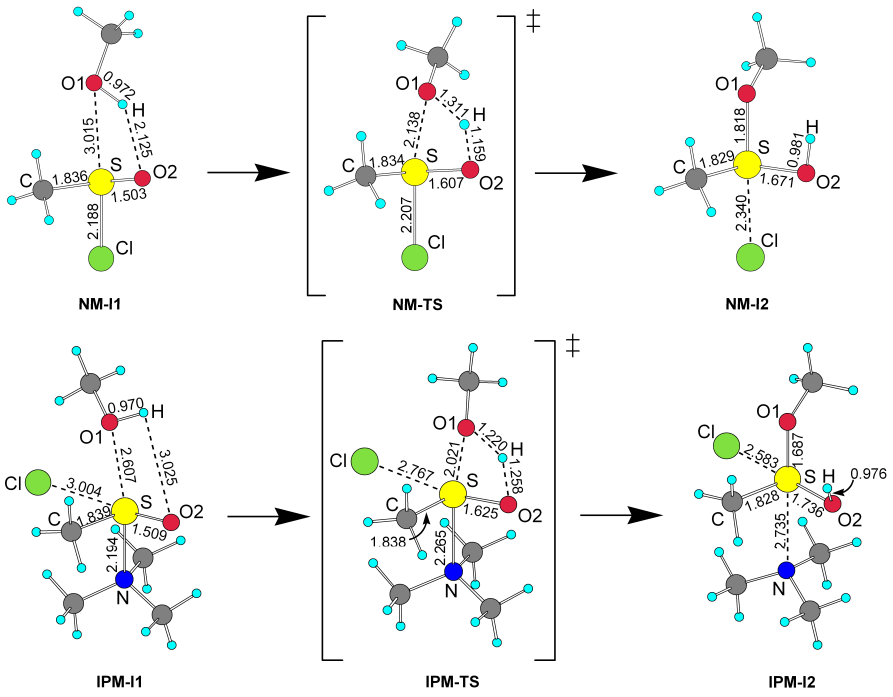

Figure 5.6: Stationary points involved in the addition of methanol to SO(Cl)(Me).

lyzing the evolution of the chloride Mulliken charge (q_{Cl}) along the reaction pathway. The rising of q_{Cl} from -0.240 a.u. in **NM-I1** to -0.407 in **NM-I2** indicated that the elongation of the S-Cl bond is accompained with its polarization. Thus, **NM-I2** is characterized by a significant degree of charge separation. These results highlighted the necessity of introducing solvent effects in the theoretical model, as we did.

The **NM-I2** intermediate gives rise to the final reaction product, SO(OMe)(Me), by elimination of HCl (see Figure 5.4). The transition state of this reaction was computed and the corresponding transition vector consists of the rotation of the S-O2(H) bond coupled with the shortening of the S-O1 bond and the cleavage of the S-Cl bond. This process is also accompanied by a hydrogen transfer from O2 to Cl in which the O2-H bond is broken and a new H-Cl bond is formed. The free energy barrier in solution of this reaction is 19.1 kcal/mol, clearly lower than that found for the previous addition step (26.8 kcal/mol). Furthermore, the absolute configuration of sulfur in **NM-I2** is retained in the elimination. Hence, the stereochemical outcome of the reaction is decided in the addition step. All these data pointed out that the most important step of the mechanism is the addition of methanol to SO(Cl)(Me) and the elimination step was thus not considered in any further extent.

The relative Gibbs free energies in solution of all stationary points are given in the energy profile represented in Figure 5.7. The formation of **NM-I1** from infinitely separated reactants is moderately endergonic by +2.6 kcal/mol due to the entropy loss of this associative process. This unfavourable entropic effect is also present in **NM-TS** and **NM-I2** since both stationary points involve the association of methanol to SO(Cl)(Me). The **NM-I2** intermediate is less stable than reactants by +17.2 kcal/mol. The poor stability of **NM-I2** can be associated to the charge separation involved in the elongation of the S-Cl bond commented above. The overall reaction is slightly endergonic by +1.1 kcal/mol. The relative energy of **NM-TS** implies that the addition step has an energy barrier of 26.8 kcal/mol. The relatively high energy of the transition state is probably due to the strain present in the plane constituted by the S,O1,H,O2 set of atoms. The ideal O1-H-O2 arrangement for a proton transfer is linear. However this is not

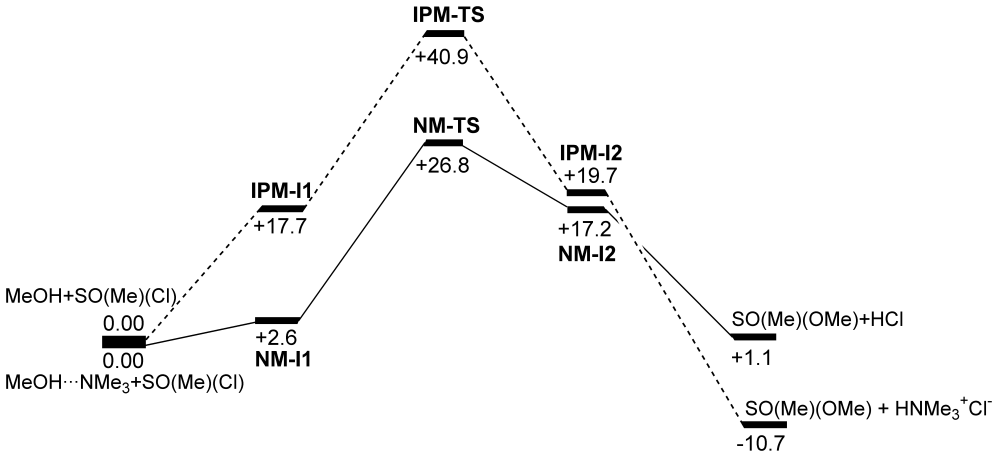

Figure 5.7: Profiles of free energy in solution for the neutral (solid line) and ion pair (dotted line) mechanisms.

fully compatible with the simultaneous formation of the S-O1 bond and the O1-H-O2 angle is distorted to 134.8°. The tetrahedral sp^3 geometry of O1 is also distorted as indicated by the S-O1-H angle of 63.6°.

Ion pair mechanism

The addition of methanol to SO(Cl)(Me) through the ion pair reaction pathway (see Figure 5.4) was also explored. The initial displacement of chlorine by the base was investigated at the thermodynamic level. The formation of the totally separated charged products, namely $SO(NMe_3)(Me)^+$ and Cl^-, is very endergonic. The $SO(Cl)(Me) + NMe_3 \longrightarrow SO(NMe_3)(Me)^+ + Cl^-$ reaction is characterized by $\Delta G_{(sol)}$=+72.3 kcal/mol. This unfavourable factor is only avoided by the formation of an ion pair in which both charged fragments are in close proximity to each other, like in the optimized addition transition state, label as **IPM-TS** (see Figure 5.6). As in the neutral mechanism, the transition vector of this saddle point consists of the formation of the S-O1 bond coupled with a hydrogen transfer from O1 to O2. In contrast with the neutral mechanism, this process is accompanied by the elongation of the S-NMe_3 bond *trans* to S-O1. The IRC-driven relaxation of **IPM-TS** towards reactants and products converged into **IPM-I1** and **IPM-**

I2 respectively (see Figure 5.6). The **IPM-I1** intermediate is a complex of methanol associated with Cl···SO(NMe_3)(Me), characterized by long S···O1 and H···O2 distances. The **IPM-I2** species is a complex of NMe_3 associated with Cl···SOH(OMe)(Me). The **IPM-I1** $\longrightarrow$ **IPM-TS** $\longrightarrow$ **IPM-I2** reaction pathway implies three different processes: 1) the formation of the S-OMe bond, as indicated by the shortening of the S-O1 distance from 2.607 Å in **IPM-I1** to 2.021 Å in **IPM-TS**, 2) the transfer of H from O1 to O2, as indicated by the elongation of the O1-H bond from 0.970 Å in **IPM-I1** to 1.220 Å in **IPM-TS** and the shortening of the O2-H bond from 3.025 Å in **IPM-I1** to 1.258 Å in **IPM-TS** and 3) the elongation of the S-NMe_3 bond, as indicated by the S-N distances of 2.194 Å in **IPM-I1** and 2.265 Å in **IPM-TS**. In **IPM-I2** the S-O1, S-N and O2-H bond distances of 1.687 Å, 2.735 Å and 0.976 Å respectively, pointed out that the S-O1 bond is formed, the S-NMe_3 bond is elongated and H is bound to O2. The initial displacement of Cl by NMe_3 giving rise to **IPM-I1** was not explored in detail since as will be explained below, the addition energy barrier of the ion pair mechanism is higher than that of the neutral mechanism.

In contrast with the neutral reaction pathway, in this case sulfur is interacting with an additional ligand, namely the Cl counteranion. Hence, the five-coordinated trigonal bipyramid geometries are replaced by octahedral structures. The octahedral geometry of sulfur is found all along the ion pair pathway and in all cases O1 is *trans* to N, O2 is *trans* to Cl and C is *trans* to the lone electron pair. These structural features are clearly reflected on the geometrical parameters of **IPM-I2** in which the O1-S-N and O2-S-Cl bond angles are 174.1° and 178.1° resepectively. Moreover, all ligands in *cis* form L-S-L bond angles close to 90°. The other isomers of these octahedral geometries were explored without success.

In both **IPM-I1** and **IPM-I2** the S-Cl distances longer than 2.5 Å indicated that there is no covalent bond between S and Cl. The long S-O1 distance in **IPM-I1** and the long S-N distance in **IPM-I2** pointed out that, as in the neutral mechanism, the 10-S-4 hypervalency is apparently avoided in this reaction system. Moreover, the long S-Cl distances suggested the presence of charge separation. This was confirmed inspecting the Mulliken charges of chlorine (q_{Cl}). The maximum charge separation was found for

IPM-I1 which has the longest S-Cl distance (3.004 Å) combined with the largest polarization (q_{Cl}=-0.686 a.u.). The values of q_{Cl} for **IPM-TS** (-0.648 a.u.) and **IPM-I2** (-0.565 a.u.) are also clearly above the largest value of q_{Cl} found in the neutral mechanism (-0.407 a.u.). These results showed the highest degree of charge separation of the species involved in the ion pair mechanism with respect to the neutral pathway.

The profile of free energy in solution for the ion pair mechanism is represented in Figure 5.7. The formation of the **IPM-I1** and **IPM-I2** intermediates from reactants (MeOH···NMe_3 + SO(Cl)(Me)) is clearly endergonic by +17.7 and +19.7 kcal/mol respectively. The relative energies of all species involved in the ion pair pathway are clearly above those found for the neutral mechanism. The poor stability of **IPM-I1**, **IPM-TS** and **IPM-I2** is probably due to the higher degree of charge separation in comparison with the neutral pathway. Moreover, the low polarity of the solvent (toluene, with ϵ=2.379) did not favour the charge separation. The energy barrier for the addition of methanol is 40.9 kcal/mol, clearly higher than that found for the neutral mechanism (26.8 kcal/mol). As in **NM-TS**, the O1-H-O2 moiety of **IPM-TS** has a strained non-linear arrangemenet. The ion pair mechanism is only favoured over the neutral pathway at the thermodynamic level. The overall reaction is exergonic by -10.7 kcal/mol due to the formation of the $HNMe_3{}^+Cl^-$ ion pair. Nevertheless, the formation of this compound is also possible as a final step of the neutral mechanism through a simple acid/base reaction between HCl and NMe_3.

In principle, the participation of the base in the ion pair mechanism can be used to define a tentative model able to explain the effect of the base on enantioselectivity. Nevertheless, in the addition transition state, **IPM-TS**, trimethylamine stands *trans* to O1(Me) and thus far from the position that will be occupied by the chiral alcohol in the real system. Moreover, the energy profiles of Figure 5.7 showed that the neutral mechanism is clearly favoured over the ion pair mechanism at the kinetic level by a difference of 14.1 kcal/mol in the addition energy barrier. These results suggested that the base should be involved in the mechanism in a different manner.

5.3.3 Chloride displacement by alcohol. Effect of the base

Neutral mechanism

The most peculiar feature found in both the neutral and ion pair mechanisms is the fact that the addition step involves a hydrogen transfer from methanol to the sulfinyl oxygen of SO(Cl)(Me). This process involves the presence of a proton in between the O1 and O2 oxygens in the transition state (see Figure 5.6). Furthermore, the high relative energies of the **NM-TS** (+26.8 kcal/mol) and **IPM-TS** (+40.9 kcal/mol) saddle points, can be associated with the bent O1-H-O2 arrangement. These results suggested the possibility that the barrier of the addition can be lowered by the base through the interaction of its nitrogen with the transferred hydrogen. This possibility was initially explored for the neutral mechanism which, as commented above, is the most favoured reaction pathway. The reoptimization of **NM-TS** with one molecule of NMe_3 interacting with H converged into **baNM-TS** (see Figure 5.8). This transition state is very similar to that found for the base-free neutral mechanism. The O1-S-O2-H dihedral angle of -12.8° showed that this set of atoms is almost coplanar. The shorter S-O1 (1.993 Å) and longer S-Cl (2.422 Å) bond distances in **baNM-TS** with respect to **NM-TS** (2.138 Å) and 2.207 Å respectively) showed that the former transition state is more product-like than the latter. The main structural difference is given by the relative position of H. As in the neutral pathway, H is in between O1 and O2 as indicated by the similar O1-H and O2-H bond distances of 1.908 Å and 1.843 Å respectively. Nevertheless, while the shape of the O1-S-O2-H arrangement in **NM-TS** is rather triangular, in **baNM-TS** the shape of this plane is more close to a square. Moreover, in **baNM-TS** H appears clearly bound to the nitrogen of the base through a N-H bond characterized by a short distance of 1.056 Å.

The transition vector associated to the single imaginary frequency of **baNM-TS** consists of the shortening of the S-O1 bond coupled with the elongation of the S-Cl bond. This vibration is consistent with the addition of methanol to SO(Cl)(Me). As in **NM-TS**, H is also transferred from O1 to O2 but now its movement is followed by NMe_3 which is bound to this

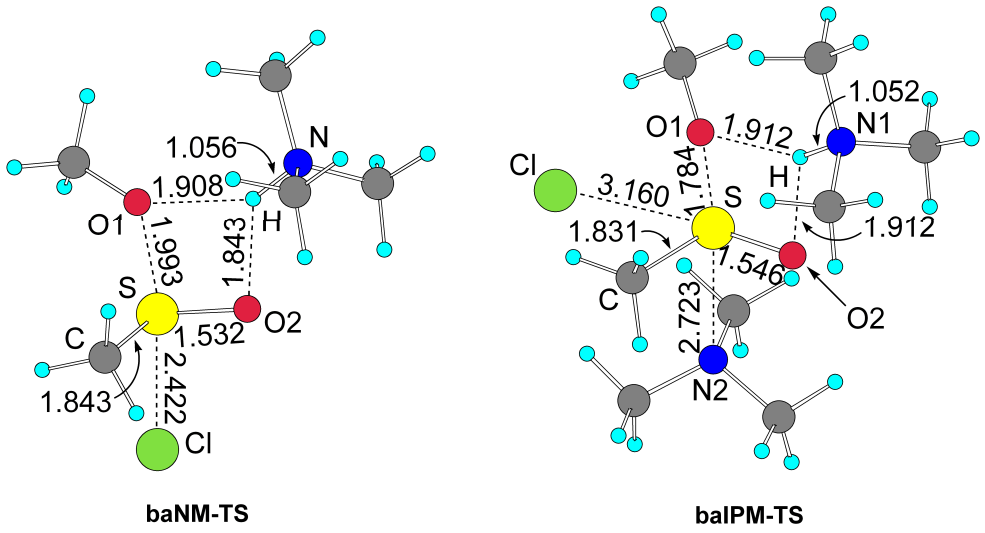

Figure 5.8: Addition transition states for the base-assisted neutral (left) and ion pair (right) mehanisms.

hydrogen. The IRC-driven relaxation of **baNM-TS** towards reactants and products converged into **baNM-I1** and **baNM-I2** respectively. These intermediates are analogous to those found in the base-free pathway. The **baNM-I1** intermediate is a complex in which MeOH is weakly bound to SO(Cl)(Me) through a long S-O1 bond. In this species, trimethylamine is associated with the acidic hydrogen of methanol through a hydrogen bond characterized by a distance of 1.798 Å. The **baNM-I2** intermediate is a complex in which $HNMe_3^+$ is bound to the sulfinyl oxygen of SO(Cl)(Me)(OMe) through a hydrogen bond of 1.798 Å. The shortening of the S-O1 distance from 2.713 Å (**baNM-I1**) to 1.925 Å (**baNM-I2**) and the increase of the S-Cl distance from 2.225 Å (**baNM-I1**) to 2.440 Å (**baNM-I2**) indicated the formation of a new S-OMe bond coupled with the elongation of the S-Cl bond.

As in the base-free neutral pathway, all species directly involved in the addition process have a trigonal bipyramid geometry in which the apical positions are occupied by O1 and Cl. The equatorial plane contains O2, C and the lone electron pair of sulfur. These structural features are reflected in the geometrical parameters of **baNM-TS**. The axial O1-S-Cl angle is 170.1°,

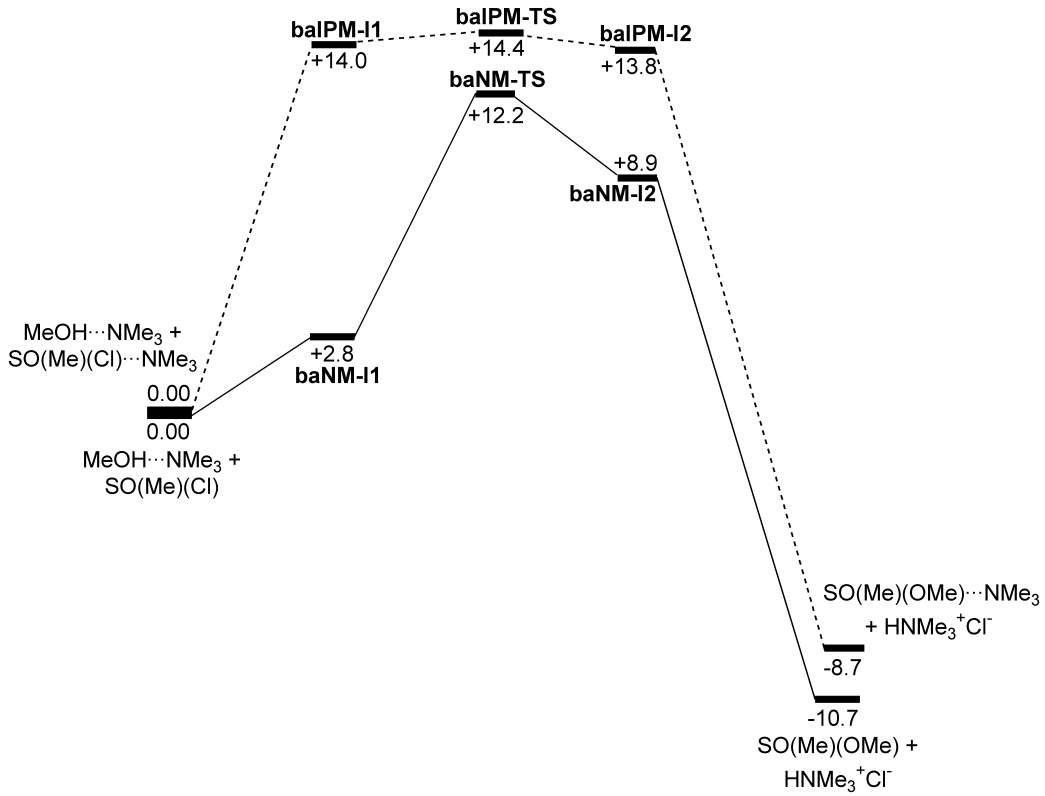

Figure 5.9: Profiles of free energy in solution for the base-assisted neutral (solid line) and ion pair (dotted line) mechanisms.

and O1 stands perpendicular to the plane defined by S, C and O2 as indicated by the O1-S-C and O1-S-O2 angles of 89.7° and 91.3° respectively. The 10-S-4 hypervalency is again apparently avoided by sulfur. The S-Cl bond has remarkably long distances in both **baNM-TS** (2.422 Å) and **baNM-I2** (2.440 Å). These long distances are associated with a significant degree of charge separation. The Mulliken charge of chlorine (q_{Cl}) has a maximum negative value of -0.507 a.u. in **baNM-I2**, which is moderately higher than the maximum value found in the base-free mechanism (-0.407 a.u.). These data indicated that the species involved in the neutral mechanism also have some ion pair character when the base participates in the addition process.

The free energy in solution profile for the base-assisted neutral pathway is represented in Figure 5.9. The formation of **baNM-I1** is moderately

endergonic by +2.8 kcal/mol, probably due to the entropically unfavoured associative character of this step. The other intermediate, **baNM-I2**, is also less stable than reactants, in this case by +8.9 kcal/mol. The low stability of **baNM-I2** can be atributed to the charge separation given by the elongation of the S-Cl bond. The decomposition of this intermediate into products (SO(OMe)(Me)+$HNMe_3^+$) is clearly favoured at the thermodynamic level since it is exergonic by -10.7 kcal/mol. The relative energy of **baNM-TS** showed that the base-assisted addition has an energy barrier of +12.2 kcal/mol, clearly lower than that found in the base-free neutral pathway (+26.8 kcal/mol). These results showed that the base assists the addition step reducing its energy barrier by 14.6 kcal/mol. This effect can be rationalized comparing the structures of **NM-TS** and **baNM-TS**. The much lower relative energy of **baNM-TS** can be assigned to the N-H bond between trimethylamine and the hydrogen transferred from O1 to O2. Furthermore, the N-H bond also reduces the strain of the H-O1-S-O2 plane that characterizes **NM-TS**.

Ion pair mechanism

As in the neutral pathway, the addition of methanol to SO(Cl)(Me) in the ion pair mechanism involves a hydrogen transfer between O1 and O2 (see Figure 5.6). Thus, the base should be in principle also able to reduce the addition energy barrier of the ion pair mechanism. This possibility was explored reoptimizing the structure of **IPM-TS** with an additional molecule of trimethylamine interacting with H. This calculation converged into **baIPM-TS** (see Figure 5.8), which is quite similar to **IPM-TS**. The most relevant difference is that H is now bound to the nitrogen of the base, with an N-H bond distance of 1.052 Å. On the other hand, H is located in between O1 and O2 as indicated by the identic O1-H and O2-H bond distances of 1.912 Å. The S-O1 and S-NMe_3 bond distances of 1.784 Å and 2.723 Å respectively, suggested that **baIPM-TS** corresponds to the simultaneous formation of the S-OMe bond and elongation of the S-NMe_3 bond, which was confirmed by the analytic calculation of frequencies. Moreover, the transition vector of **baIPM-TS** also involves the transfer of H from O1 to O2. In contrast

with **IPM-TS**, H is bound to N and trimehtylamine follows the transfer movement of H. The nature of this process was also confirmed by the relaxation of **baIPM-TS** towards reactants and products, which converged into **baIPM-I1** and **baIPM-I2** respectively. **baIPM-I1** consists of a complex in which MeOH···NMe_3 is weakly bound to Cl···$SO(NMe_3)(Me)$ through a long S-O1 bond of 2.427 Å. In this intermediate the axial base is strongly bound to sulfur as indicated by the S-N2 bond distance of 2.240 Å. On the other hand, H is bound to O1 as indicated by the O1-H bond distance of 1.005 Å. In **baIPM-I2** the two molecules of trimethyl amine are weakly bound to Cl···SO(OMe)(Me), one through a hydrogen bond with a H-N1 bond distance of 1.825 Å, and the other to sulfur through a long S-N2 bond of 2.769 Å. O1 is strongly bound to sulfur, and H to O2, as indicated by the S-O1 and O2-H bond distances of 1.692 Å and 1.024 Å respectively.

As in the non-assisted ion pair mechanism, sulfur has an octahedral geometry in all species directly involved in the addition process. In these structures O1 is *trans* to N2, O2 is *trans* to Cl and C is *trans* to the lone electron pair. These *trans* relationships are clearly indicated by the O1-S-N2 and O2-S-Cl bond angles of 168.6° and 172.9° respectively, both very close to 180°. As in the other reaction pathways, the 10-S-4 hypervalency is apparently avoided. In the **baIPM-I1** and **baIPM-I2** intermediates, and also in the transition state, the S-Cl bond is clearly broken as indicated by S-Cl bond distances longer than 2.7 Å. The associated charge separation reaches its maxiumum in **baIPM-TS** with a q_{Cl} value of -0.721 a.u. and a S-Cl bond distance of 3.160 Å. The higher values of q_{Cl} with respect to the **IPM-I1** $\longrightarrow$ **IPM-TS** $\longrightarrow$ **IPM-I2** pathway, in which the maximum negative value of q_{Cl} was -0.686 a.u., pointed out that the direct participation of the base in the hydrogen transfer from O1 to O2 increased the ion pair character of the system.

The free energy in solution profile for the NMe_3-assisted ion pair mechanism is represented in Figure 5.9. Both **baIPM-I1** and **baIPM-I2** intermediates are clearly less stable than reactants by 14.0 and 13.8 kcal/mol respectively. The endergonic character of the formation of these species can be understood taking into account the associative process involved, unfavoured at the entropic level, and the charge separation associated with the broken S-Cl bond. The overall reaction is exergonic by -8.7 kcal/mol. In this case, the

energy profile for the **baIPM-I1** ⟶ **baIPM-TS** ⟶ **baIPM-I2** transformation is very flat. The relative energy of **baIPM-TS** indicated that the addition has an energy barrier of +14.4 kcal/mol, clearly lower than that of the non-assisted ion pair pathway (+40.9 kcal/mol). These results pointed out that the base also assists the addition of methanol to SO(Cl)(Me) in the ion pair mechanism through a reduction of the energy barrier of 26.5 kcal/mol, clearly larger than that found for the neutral pathway (14.6 kcal/mol). Nevertheless, the relative energy of **ba-IPM-TS** is moderatly higher than that of **ba-NM-TS**, showing that the base-assisted neutral mechanism is kinetically favoured over the base-assisted ion pair mechanism.

The identification of the transition states corresponding to the base-assisted addition of methanol, **baNM-TS** and **baIPM-TS**, constitute a very valuable starting point for the modelization of the base effects upon enantioselectivity because 1) it gives a mechanistic role to the base and 2) it implies a close proximity of the base to the reaction center in which the absolute configuration of sulfur is decided. The energy profiles represented in Figure 5.9 showed that the lowest base-assisted pathway corresponds to the neutral mechanism. Therefore, the subsequent study on the origin of the enantioselectivity reversal in the DAG method, that will be discussed in the next chapter, was carried out considering a transition state geometry analogous to **baNM-TS**, in which methanol was replaced by DAGOH.

Chapter 6

Origin of the enantioselectivity reversal in the DAG method

6.1 Introduction

The DAG synthetic method developed by Khiar[162–164] (see Figure 6.1) is of particular interest due to the possibility of select the final absolute configuration of sulfur just changing the nature of the base, and without any modification of the chiral resolving agent (DAGOH). In asymmetric synthesis, the reversal of enantioselectivity can be achieved modifying the substrate[270,271] or the nature of a given catalyst by changing the ligand[272,273] or the metal.[274,275] Nevertheless, the application of these strategies is usually challenging, especially without a detailed knowledge of the origin of enantioselectivity. Therefore, the reversal of enantioselectivity is in most cases performed by just inverting the absolute configuration of the chiral source. However, although this strategy is in principle much easier and efficient, its application is sometimes not possible because the other stereoisomer of the chiral auxiliary or ligand used in the synthesis is either expensive or not accessible. This is the case of the DAG method: while the enantiomer of DAGOH represented in Figure 6.1 is easily obtained from natural and cheap D-glucose, the other enantiomer is very expensive. The enantiodirecting effect of the base is thus very convenient.

The base-driven reversal of enantioselectivity was first observed when

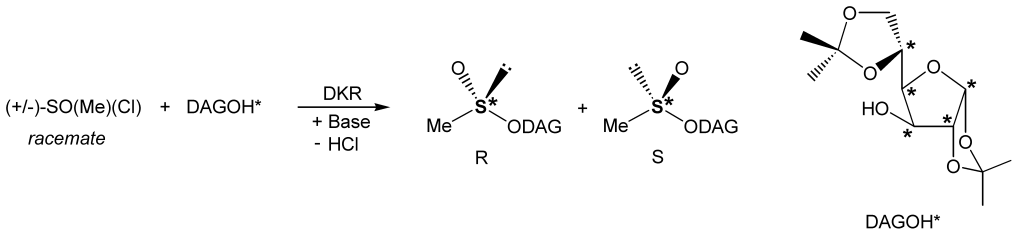

Base	R/S	% de
pyridine	93/7	86
DMAP	78/22	56
imidazole	82/18	64
i-Pr_2NEt	2/98	96
collidine	2/98	96
DMA	37/63	26
NEt_3	2/98	96

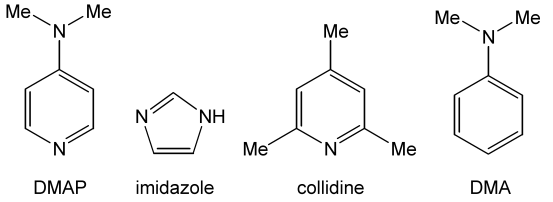

Figure 6.1: Influence of the base on the enantioselectivity of the DAG synthetic method.

the DAG method was applied to the dynamic kinetic resolution (DKR) of methyl sulfinyl chloride[162] (see Figure 6.1). When the base was planar and aromatic (pyridine, DMAP and imidazole) the final configuration of sulfur in the sulfinate ester product was R. In contrast with this, the S enantiomer was obtained using much bulkier bases like *i*-Pr_2NEt, DMA or NEt_3. This finding was quite puzzling since in principle the base was only added to the reaction mixture in order to neutralize the HCl by-product. The mechanistic role of the base in the DKR of sulfinyl chlorides was clarified in our previous studies (articles **III** and **IV**). These studies showed that the base is able to reduce the energy barrier of both the pyramidal inversion of the sulfinyl chloride and the subsequent addition of the alcohol. In the latter case, the base is in close proximity to the reaction center in which the stereogenic sulfur of the product is generated. Nevertheless, the modelization of the system supressed the chirality of DAGOH and the origin of enantioselectivity was thus not explored. This issue was tackled in a QM/MM study on the real system (**article V**) taking into account the main conclusion of the previous mechanistic study (**article IV**): the Cl displacement by the alcohol follows an

addition/elimination neutral pathway in which the base reduces the energy barrier of the rate-determining addition step. Pyridine and collidine were considered as bases since they promote opposite enantioselectivities in spite of their similarity. Collidine is planar and aromatic as pyridine and all other pro-R bases, but nevertheless it leads to the major formation of the S enantiomer.

6.2 Computational Details

The study on the real system was carried out by means of the hybrid QM/MM ONIOM method.[276] The system was divided in two parts, one computed at a quantum mechanical level (QM part) and the other at a molecular mechanics level (MM part). The QM/MM partition is represented in Figure 6.2. For both pyridine and collidine, the nitrogenated aromatic ring was computed at the QM level. In the particular case of collidine, the three metyhl groups were included in the MM part of the calculation. Only the C-OH fragment of DAGOH was considered at the QM level. The rest of DAGOH was included in the MM partition. All calculations were done with Gaussian03[262] at the ONIOM(Becke3LYP:UFF) level, *i.e.* the Becke3LYP hybrid density functional[208,209] was used for the QM part, and the UFF force filed[229] was used for the MM part. The QM part was computed with the same basis set used in the mechanistic studies discussed in the previous chapter.

The geometeries were fully optimized with the sole exception of the link bonds between the QM and MM parts. All energies given in the following sections are relative energies in gas phase. Frequencies were not computed but the nature of all transition states was confirmed comparing their structures with that found in the study of the model system (**baNM-TS** geometry; see section 5.3.3), which was characterized by vibrational analysis and IRC calculations.

The conformational space of the system, which was found to be large and complex, was explored applying a statistical MCMM (Monte Carlo Multiple Minimum) approach[277,278] by means of the Macromodel 8.5 code.[279] The potential energy was computed using the MMFF94 force field.[280,281] All bonds able to rotate were considered in the conformational search, and the bond distances directly involved in the transition vector (S-O1, S-O2,

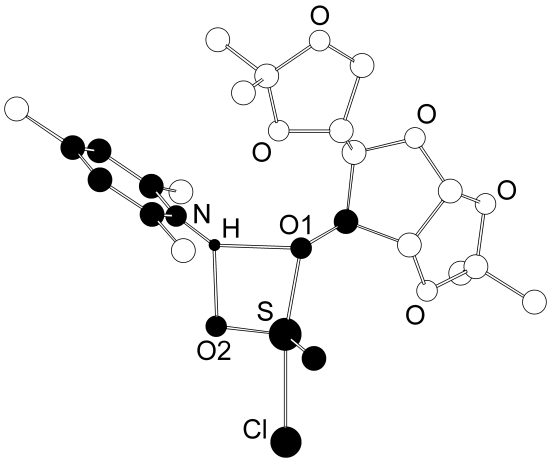

Figure 6.2: QM (black) and MM (white) partitions of the ONIOM(Becke3LYP:UFF) calculations on the collidine-assisted addition.

O1-H, O2-H and S-Cl; see Figure 6.2) were frozen. For both the pro-R and pro-S transition states, the four most stable conformations according to the MCMM search were selected and subsequently reoptimized at the ONIOM(Becke3LYP:UFF) level.

6.3 Results and Discussion

6.3.1 Pyridine-assisted addition of DAGOH

The kinetic resolution of methyl sulfinyl chloride in the presence of DAGOH and pyridine was theoretically investigated. Only the base-assisted neutral mechanism, which according to the study reported in the previous chapter is the lowest-energy reaction pathway, was considered. The origin of enantioselectivity was determined computing the pro-R and pro-S transition states corresponding to the addition of DAGOH to SO(Cl)(Me) since the absolute configuration of the product is decided in this step. The consideration of the full structure of DAGOH increased the structural complexity of the system. There are six sources of structural flexibility that give rise to a large conformational space. In contrast with the vanadium-catalyzed

asymmetric sulfoxidation (see section 4.3.1), in which both absolute configurations of two stereogenic centers (vanadium and sulfur) were possible, in the present system the only stereocenter that has two possible configurations is sulfur. These configurations were identified inspecting the Cl-S-O2-C1 dihedral angle, labeled as D1 (see Figure 6.3), and associated with the absolute configuration of SO(Cl)(Me). Since the addition process only takes place with O1 *trans* to Cl, the sulfur configuration of SO(Cl)(Me) determines the final configuration of the sulfinate ester product. DAGOH has five chiral carbons but their configurations are well defined and preserved along the reaction. The transition state corresponding to the addition of DAGOH has a higher degree of conformational flexibility in comparison with that of the vanadium-catalyzed sulfoxidation. The following four σ-bond rotations should be considered: 1) the rotation of the S-O1 nascent bond, associated to the O2-S-O1-C2 dihedral angle (D2), 2) the rotation of the O1-C2 bond, associated to the S-O1-C2-C3 dihedral angle (D3), 3) the rotation of the C3-C4 bond, associated to the C2-C3-C4-C5 dihedral angle (D4) and 4) the rotation of the N-H bond, associated to the O1-H-N-C6 dihedral angle (D5). The values of D2 and D3 are related to the relative orientation of DAG with respect to the substrate and the base. The internal conformation of DAG is given by D4. D5 is associated with the relative orientation of the base with respect to the reaction center consituted by the coplanar H-O1-S-O2 set of atoms. There is also a sixth source of structural complexity consisting of the flipping of the five-membered cycles of DAGOH.

If each one of the 6 sources of conformational flexibility mentioned above give rise to only 2 isomers, then a total number of 64 (2^6) conformers of the addition transition state are possible. Furthermore, the torsions associated to the D1-5 dihedral angles are probably strongly correlated and it is thus very difficult to assign a set of preferred values to each one. Due to this large conformational complexity, the systematic strategy used in the vanadium-catalyzed asymmetric sulfoxidation was not applied in this case. Instead, a statistical MCMM approach was adopted in order to sample the conformational space. This conformational search was performed for both the pro-R and pro-S transition states and the four most stable structures found in each case were reoptimized at the ONIOM level. The optimized geometries of the

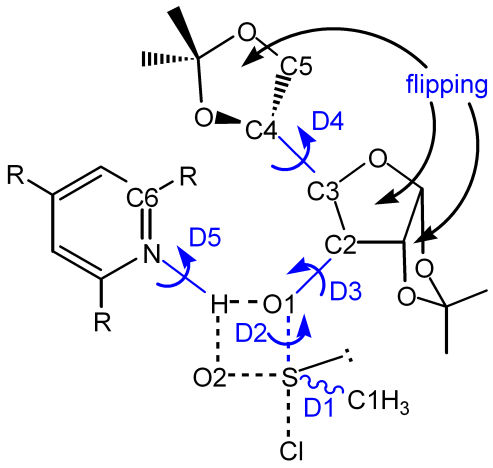

Figure 6.3: Sources of conformational flexibility in the addition transition state.

most stable pro-R and pro-S transition states, labeled as **R1-P** and **S1-P** respectively, are represented in Figure 6.4. The geometrical parameters of **R1-P** and **S1-P** involved in the formation and breaking of bonds are very similar. In **R1-P**, the S-O1 and S-Cl bond distances of 2.002 Å (1.993 Å in the model) and 2.415 Å (2.422 Å in the model) respectively pointed out the formation of the S-ODAG bond and the elongation of the S-Cl bond. As in the model, H stands attached to the nitrogen of the base and in between O1 and O2. This structural feature is clearly indicated by the N-H (1.059 Å; 1.056 Å in the model), O1-H (1.832 Å; 1.908 Å in the model) and O2-H (1.822 Å; 1.843 Å in the model) bond distances. The real transition state also has the trigonal bipyramid geometry found in the study of the model system. While the equatorial plane contains C1, O2 and the lone electron pair of sulfur, the axial positions are occupied by O1 and Cl. The axial O1-S-Cl angle is 169.0° and O1 is clearly perpendicular to both C1 and O2 as indicated by the O1-S-C1 and O1-S-O2 bond angles of 88.4° and 92.3° respectively. The H, O1, S and O2 atoms are in a coplanar arrangement as indicated by the H-O1-S-O2 dihedral angle of -0.2°. The values of all these angles are very similar to those found in the model study (see section 5.3.3). The structural similarity between the model saddle point and the ONIOM

TS	D1	D2	D3	D4	D5	E
R1-P	-90.3	131.6	138.5	-176.1	11.6	0.0
R2-P	-90.2	128.9	138.1	-171.1	10.3	0.4
R3-P	-90.4	151.3	161.2	-54.6	21.1	2.7
R4-P	-89.4	95.7	97.6	-78.0	48.4	4.3
S1-P	90.3	-159.6	89.2	173.0	-3.0	1.0
S2-P	90.4	-150.3	117.4	-168.0	-1.7	1.3
S3-P	90.6	-162.9	86.9	177.2	-22.1	1.6
S4-P	90.7	176.7	131.2	-59.1	-6.2	4.1

Table 6.1: Dihedral angles, in degrees, and relative energies, in kcal/mol, of the transition states corresponding to the pyridine-assisted addition of DAGOH. D1=Cl-S-O2-C1, D2=O2-S-O1-C2, D3=S-O1-C2-C3, D4=C2-C3-C4-C5, D5=O1-H-N-C6.

R1-P and **S1-P** geometries, confirmed that these transition states also correspond to the addition of DAGOH coupled with a hydrogen transfer from O1 to O2 and the elongation of the S-Cl bond.

The dihedral angles (D1-5) and relative energies of all pro-R (**R1-P**, **R2-P**, **R3-P** and **R4-P**) and pro-S (**S1-P**, **S2-P**, **S3-P** and **S4-P**) transition states are collected in Table 6.1. All structures are well differentiated by the values of D1-5 with only one exception given by **R1-P** and **R2-P**. These geometries only differ in the conformation of a five-membered cycle of DAGOH. The absolute value of D1 is in all cases very close to 90° indicating the perpendicular arrangement between the equatorial C1 atom and the axial Cl atom. Furthermore, D1 is negative in the pro-R transition states and positive in the pro-S, due to the inversion of the sulfur absolute configuration. In the pro-R transition states the values of the D2 dihedral angle, which gives the relative orientation of DAG with respect to the planar H-O1-S-O2 reaction center, are in all cases between 90° and 180°. These values indicated that DAG occupies the side of the H-O1-S-O2 plane opposite to that occupied by the methyl attached to sulfur (C1-methyl). The same scenario was found in the pro-S transition states and the sign of D2 was thus reversed, since the relative positions of C1 and O2 were exchanged. The only exception was found

in the case of **S4-P** (D2= 176.7°) in which DAG and C1-methyl are on the same side of the H-O1-S-O2 plane. The relative energies collected in Table 6.1 showed that the preferred orientation of DAG is associated with a value of D2 close to 120°. As will be further commented below, the rotation of the S-O1 nascent bond is not free but strongly influenced by the sp^3 character of O1. In contrast with this, the rotation of the O1-C2 bond, associated to D3, is much free and likely to be mainly controlled by steric effects. Hence, several different values of D3 were found. The rotation of the C3-C4 bond (D4) gives rise to three different rotamers: one rotamer in which C2 and C5 are in *anti* position, characterized by D4=180°, and two rotamers in which C2 and C5 are in *gauche* position, characterized by D4=60° and D4=-60°. The geometrical parameters showed that only the *gauche* conformation with D4 close to -60° is stable. This arrangement is energetically less favoured than the *anti* since it was only found in the less stable pro-R (**R3-P** and **R4-P**) and pro-S (**S4-P**) transition states. The values of D5 are in general close to 0° indicating the coplanarity of pyridine with the H-O1-S-O2 plane. In general, the relative energy of the transition states increases as D5 deviates from 0° as clearly shown by the comparison of geometries **S1-P** and **S3-P** which differ mainly in the value of D5. In this case, the rotation of the N-H bond from D5=-3.0° to D5=-22.1° implies a relative energy rise of 0.6 kcal/mol. In fact, D5 was frozen to 0° in the MCMM conformational search. DFT(B3LYP) calculations in the model system pointed out that the relative energy of the system increases by *ca.* 4 kcal/mol due to the rotation of D5 from 0° to 90°. This effect can be associated to CH···O atractive interactions between the *ortho* hydrogens of pyridine and the O1 and O2 oxygens, which are only possible when O1 and C6 are eclipsed (D5=0°). Furthermore, when the conformational search was initially performed allowing the free rotation of the N-H bond, although many conformers had D1 close to 90°, their ONIOM reoptimization allways converged with D1 very close to 0°.

The most stable transition state, **R1-P**, leads to the formation of the R enantiomer of the product in total agreement with the experimental results.[162] This saddle point is 1.0 kcal/mol more stable than **S1-P**, which is the most stable pro-S transition state. The preference for the pro-R pathway in the pyridine-assisted addition of DAGOH to SO(Me)(Cl) can be rational-

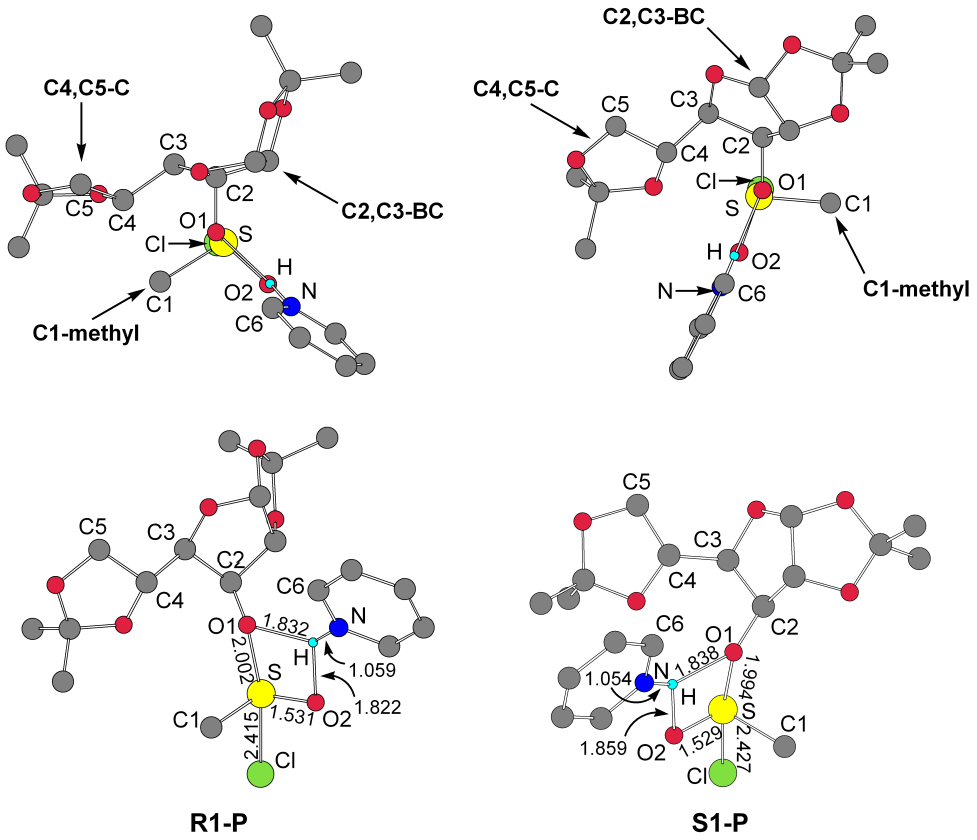

Figure 6.4: Top (above) and side (below) views of the most stable pro-R (left) and pro-S (right) transition states for the pyridine-assisted addition of DAGOH. All hydrogens, except the proton being transferred, are removed for clarity.

ized comparing the **R1-P** and **S1-P** geometries. If we look at the top view of both geometries represented in the upper part of Figure 6.4, we can divide each structure in two fragments, namely DAG and the sulfur block, connected by the O1-C2 bond. Each fragment has two sterically active regions and the arrangement between them rulles the overall energy of the structure. In the case of the sulfur block, the groups with potential steric activity are the C1-methyl (left side in **R1-P**) and the base (right side in **R1-P**). Their positions are inverted in **S1-P**. The C1-methyl group happens to be more sterically active because the base, being coplanar with the H-O1-S-O2 plane, stays always away from DAGOH. DAGOH is constituted by two well differentiated molecular fragments linked by the C3-C4 bond: a bicycle consisting of two fused 5-membered cycles, that will be referred as **C2,C3-BC**, and a single 5-membered cycle, that will be referred as **C4,C5-C**. The size and thus the steric bulk of **C2,C3-BC** is clearly larger than that of **C4,C5-C**. In both **R1-P** and **S1-P** the **C4,C5-C** and **C2,C3-BC** fragments of DAGOH are on the left and right sides of the H-O1-S-O2 plane respectively. In contrast with this, due to the opposite configuration of sulfur, C1-methyl stands on the left in **R1-P** but on the right in **S1-P**. The lower stability of **S1-P** in comparison with **R1-P** can be thus associated with the close proximity between C1-methyl and the bulkiest fragment of DAGOH, namely **C2,C3-BC**, in the former transition state. The presence of steric repulsions between C1-methyl and **C2,C3-BC** was clearly indicated by the values of the D2 dihedral angle which showed that these fragments are always on opposite sides of the H-O1-S-O2 reaction center. As the absolute value of D2 increases from 131.6° in **R1-P** to 159.6° in **S1-P** (see Table 6.1) the C1-methyl gets closer to **C2,C3-BC**. The D2=131.6° conformation is not possible in **S1-P** since it involves the overlapping of DAGOH with the base. Furthermore, the rotation of the nascent S-O1 bond, characterized by the value of D2, is restricted by the tetrahedral sp^3 structure of O1. According to the model study, the sp^3 character of O1 is preserved in the addition process (see section 5.3.3). The values of the H-O1-C2 bond angle (131.7° in **R1-P** and 152.3° in **S1-P**) and of the H-O1-S-C2 dihedral angle (-131.8° in **R1-P** and 156.2° in **S1-P**) indicated that the sp^3 character of O1 is higher in **R1-P** than in **S1-P** since in the former geometry these values are clearly closer to the ideal sp^3 tetrahe-

dral angles of 110° (H-O1-C2) and 120° (H-O1-S-C2). All these data justify the lower relative energy of **R1-P**. Furthermore, the energy associated to the variation of these angles is computed at the QM level and in fact the full energy difference between **R1-P** and **S1-P** was given by the QM part of the ONIOM calculation.

6.3.2 Collidine-assisted addition of DAGOH

The addition of DAGOH to methyl sulfinyl chloride in the presence of collidine was explored considering the neutral pathway. Enantioselectivity was theoretically evaluated by computing the most stable pro-R and pro-S transition states. As in the case of pyridine, all sources of structural complexity, namely the two possible configurations of sulfur (D1), the rotation of four σ-bonds (D2-5) and the flipping of the 5-membered cycles of DAGOH (see Figure 6.3), were considered. The conformational space was also inspected with a MCMM statistical approach and the four most stable pro-R and pro-S transition states were then recomputed at the ONIOM level. The most stable pro-R and pro-S transition states, labeled as **R1-C** and **S1-C** respectively, are represented in Figure 6.5. As in the case of pyridine, the geometrical parameters of the reaction center are very similar in both structures and also similar to the values found in the study of the model system, suggesting that these transition sates correspond to the addition of DAGOH to methyl sulfinyl chloride. In **R1-C**, the formation of the S-ODAG bond and the elongation of the S-Cl bond are indicated by the the S-O1 and S-Cl bond distances of 1.975 Å and 2.442 Å respectively. The similar O1-H and O2-H bond distances (1.781 Å and 1.872 Å respectively) pointed out that there is a hydrogen transfer between O1 and O2. Furthermore, the N-H bond distance of 1.061 Å indicated that the transferred hydrogen is bound to collidine. The geometry of sulfur in **R1-C** is trigonal bipyramid with O1 and Cl in the axial positions, and C1, O2 and the lone electron pair of sulfur on the equatorial plane. Moreover, the atoms of the reaction center H, O1, S and O2 are coplanar as indicated by the H-O1-S-O2 dihedral angle of -7.5°.

The relative energies and D1-5 dihedral angles of the most stable pro-R (**R1-C**, **R2-C**, **R3-C** and **R4-C**) and pro-S (**S1-C**, **S2-C**, **S3-C** and **S4-**

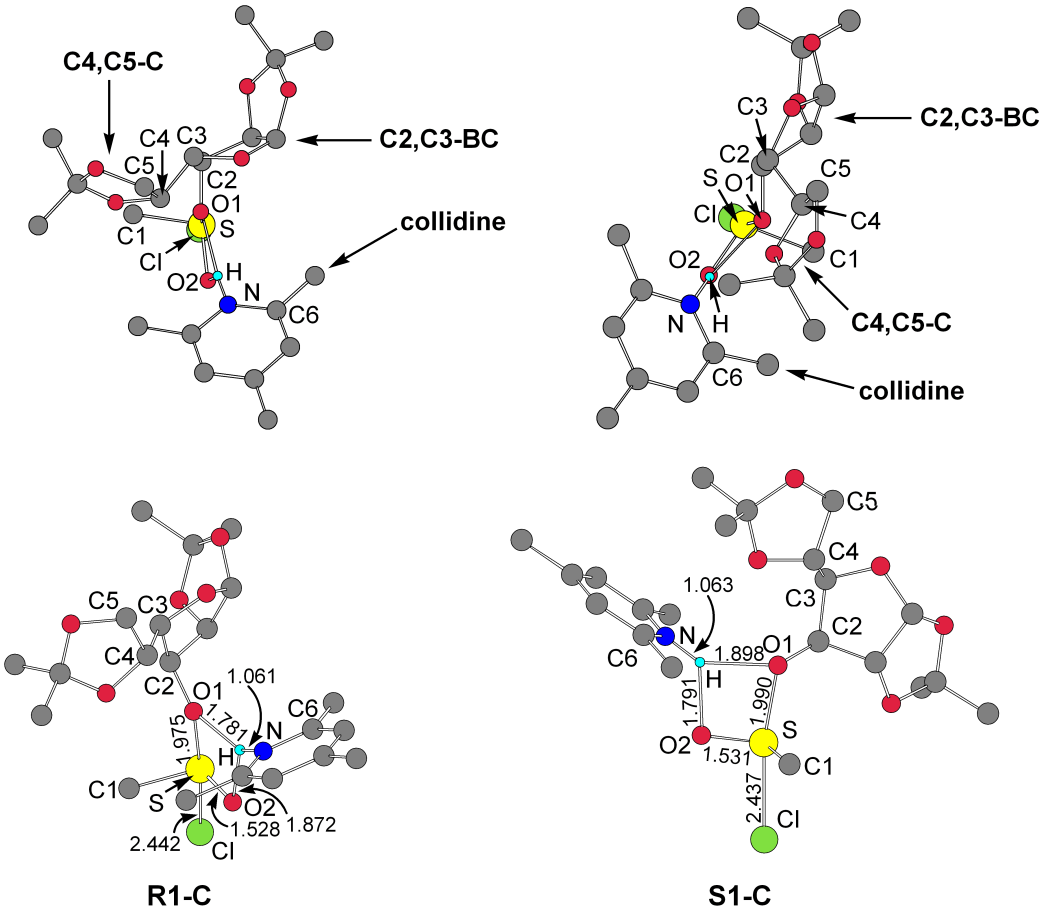

Figure 6.5: Top (above) and side (below) views of the most stable pro-R (left) and pro-S (right) transition states for the collidine-assisted addition of DAGOH. All hydrogens, except the proton being transferred, are removed for clarity.

C) transition states involving collidine as base are collected in Table 6.2. All the pro-R geometries are differentiated by the D1-5 dihedral angles. In contrast with this, the values of these parameters are very similar in both **S1-C** and **S2-C**, and the same happens for **S3-C** and **S4-C**. **S1-C** and **S2-C** only differ in the conformation of the collidine methyls and because of this their relative energies are different by only 0.1 kcal/mol. A more significant structural difference was found between **S3-C** and **S4-C**, consisting of a different conformation of the rings of DAGOH. As in the case of pyridine, the values of D1 are very close to 90° due to the trigonal bypiramid geometry of sulfur. Moreover, all pro-R transition states have a negative value of D1 while positive values are found in the pro-S geometries due to the opposite absolute configuration of sulfur. In all pro-S transition states, the negative values of D2 close to -138° pointed out that DAG is oriented towards the face of the H-O1-S-O2 plane opposite to that occupied by C1-methyl. The same orientation of DAG was found in the pro-R transition state as indicated by the positive values of D2 lower than 180°. In this case, the rotation of the O1-C2 bond (D3) gives rise to three different orientations characterized by values of D3 close to 90°, 160° and 180°. As in the pyridine-assisted addition, the *gauche* conformation of the C3-C4 bond characterized by a value of D4 close to -60° is less favoured than the *anti* conformation (D4 close to 180°). The pro-R transition states having the *gauche* arrangement (**R3-C** and **R4-C**) are less stable by $\geq$3 kcal/mol than those having the *anti* arrangement (**R1-C** and **R2-C**). The main difference with respect to the case of pyridine is given by the dihedral angle D5, which measures the relative orientation of collidine with respect to the H-O1-S-O2 square plane. Pyridine is coplanar with this plane as shown by the values of D5 very close to 0° in all transition states (see Table 6.1). In contrast with this, the aromatic plane of collidine is clearly perpendicular to H1-O1-S-O2 as indicated by the absolute values of D5, close to 90° in all geometries. In general, as D5 deviates from 90° the relative energy rises as demonstrated by the geometries **S1-C** and **S3-C** which differ mainly in the value of D5. In this case, the variation of D5 from -88.9° (**S1-C**) to -71.1° (**S3-C**) implies an energy increase of 1.0 kcal/mol. The different orientation of collidine in the addition transition state is due to the replacement of the *ortho* hydrogens of pyridine by much bulkier methyl

TS	D1	D2	D3	D4	D5	E
R1-C	-89.2	173.2	171.9	-168.2	-86.5	2.2
R2-C	-90.2	158.9	160.6	-174.1	-101.2	2.3
R3-C	-90.2	105.9	90.7	-84.9	-122.8	5.2
R4-C	-92.5	145.6	172.0	-78.7	-119.9	9.6
S1-C	89.9	-139.6	171.3	167.8	-88.9	0.0
S2-C	89.9	-138.6	169.9	166.8	-91.5	0.1
S3-C	89.6	-138.2	177.3	-176.3	-71.7	1.0
S4-C	89.5	-136.4	-179.3	178.6	-78.8	1.3

Table 6.2: Dihedral angles, in degrees, and relative energies, in kcal/mol, of the transition states corresponding to the collidine-assisted addition of DAGOH. D1=Cl-S-O2-C1, D2=O2-S-O1-C2, D3=S-O1-C2-C3, D4=C2-C3-C4-C5, D5=O1-H-N-C6

groups. The atractive CH···O interactions given by pyridine when D5=0° are consequently replaced by repulsive Me-O1 and Me-O2 steric interactions that are avoided with D5=90°. All attempts to optimize an addition transition state with D5 close to 0° failed. As will be explained below, this change in the relative orientation of the base is closely related with the origin of the enantioselectivity reversal.

In contrast with the case of pyridine, the relative energies collected in Table 6.2 showed that the most stable pro-S transition state, **S1-C**, is favoured over the most stable pro-R transition state, **R1-C**, by 2.2 kcal/mol. The preference for the pro-S pathway when the base is collidine can be rationalized comparing the optimized geometries of **R1-C** and **S1-C** (see Figure 6.5). Since the structure of DAG is the same regardless of the base used in the reaction, the steric model proposed for DAG in the pyridine-assisted addition should be exactly the same in the collidine-assisted pathway. As in the saddle points found for pyridine, while the **C4,C5-C** ring is on the left side of both the pro-R and pro-S transition states, the much bulkier **C2,C3-BC** bicycle is on the right side. Also as in **R1-P** and **S1-P** (see Figure 6.4), the inversion of sulfur implies that C1-methyl is on the left in the pro-R transition state and on the right in the pro-S. Nevertheless, with collidine the

bulkiest fragment attached to sulfur is not the C1-methyl but instead the H-O1-S-O2 plane bound to the base through H. The non coplanar arrangement of collidine with respect to H-O1-S-O2 implies that the *ortho* methyls occupy the left and right sides of the H-O1-S-O2 plane pointing towards DAG. Thus, the critical interactions between DAG and the rest of the system will imply collidine instead of C1-methyl. In **R1-C**, collidine and **C2,C3-BC**, which are the bulkiest fragment around sulfur and the bulkiest part of DAG respectively, are found in close proximity to each other since they occupy the same side of the transition state. The steric repulsions between **C2,C3-BC** and the *ortho*-methyl of collidine attached to C6 are evaluated in the MM part of the calculation, and in fact, a significant portion of the energy difference between **R1-C** and **S1-C** (0.8 of 2.2 kcal/mol) corresponds to the MM energy. The rest of the ONIOM energy difference (1.4 kcal/mol), which comes from the QM part, can be asigned as in the case of pyridine to the O2-S-O1-C2 (D2) dihedral angle related with the sp^3 character of O1. This angle is clearly more closed in the favoured pro-S transtion state, **S1-C**, than in **R1-C**, as indicated by the values of D2 (-139.6° and 173.2° respectively). In **R1-C** the nascent S-O1 bond rotates towards a O2,C2-*anti* conformation in order to reduce the steric hindrance between DAG and collidine originated on the right side of the H-O1-S-O2 plane. As commented above for pyridine, the rise of the absolute value of D2 implies a distorsion of the O1 sp^3 geometry that increases the QM energy of the system.

6.3.3 Origin of the enantioselectivity reversal

The relative energies found in the case of pyridine (see Table 6.1) showed that the most stable pro-R and pro-S transition states are **R1-P** and **S1-P** respectively. Furthermore, **R1-P** was more stable than **S1-P** and thus the R enantiomer of the product should be the major reaction product, in total agreement with the experimental results. The energy gap between **R1-P** and **S1-P** is 1.0 kcal/mol, which corresponds to a theoretical enantiomeric excess at -78 °C of 85% ee (see equations 1.2 and 1.3 in chapter 1), very close to the experimental value of 86% ee (see Figure 6.1). In the case of collidine, the relative energies collected in Table 6.2 showed that the most stable

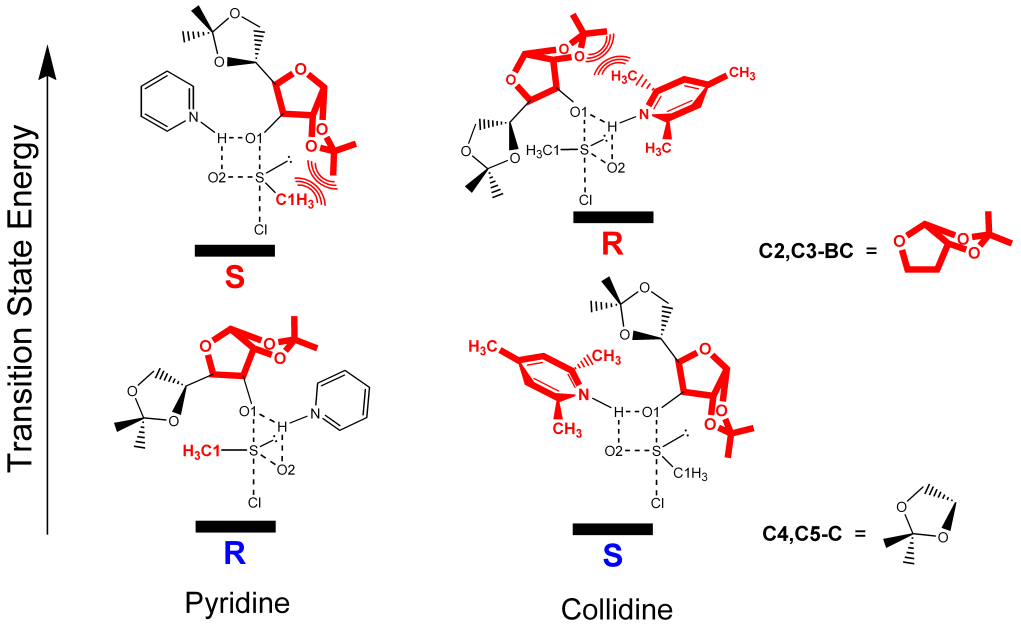

Figure 6.6: Origin of the enantioselectivity reversal in the DAG method.

pro-S transition state, **S1-C**, is favoured over the most stable pro-R transition state, **R1-C**, by 2.2 kcal/mol. This energy gap implies a theoretical enantiomeric excess of 99% ee, which is quite close to the experimental value (96 % ee). Hence, the theoretical model predicts that the enantioselectivity reached with collidine is slightly better than that obtained with pyridine. Nevertheless, the important result is that the calculations reproduced the most relevant feature of the DAG asymmetric method, namely the enantioselectivity reversal induced by the nature of the base. Our results showed that while the preferred reaction pathway is the pro-R when the base is pyridine, with collidine the fastest addition corresponds to the pro-S pathway. This enantioselectivity reversal can be rationalized comparing the structures and relative energies of the most stable pro-R and pro-S transition states found for pyridine and collidine.

Our calculations showed that the addition transition state has a trigonal bipyramid geometry in which DAGOH and Cl occupy the axial positions. The other fragments attached to sulfur lie on the equatorial plane of the molecule. These fragments are C1-methyl and O2 which are in *cis* posi-

tion, and thus in close proximity, with respect to DAGOH. The OH group of DAGOH is directly involved in the H-O1-S-O2 reaction center. The rest of the molecule (DAG) consists of the chiral auxiliary that discriminates the pro-R and pro-S pathways through diastereomeric interactions with the groups attached to sulfur (see the steric model represented in Figure 6.6). Since the O1-*trans*-Cl arrangement is an electronic requirement of the addition process, the axial positions of O1 and Cl are fixed. Hence, the two possible chiral environments around sulfur are interconverted exchanging the relative positions of C1-mehtyl and O2 on the equatorial plane. DAG is able to recognize and differentiate these two configurations thanks to its chiral structure which is clearly divided in two parts that introduce different degrees of steric hindrance. These two parts are the **C4,C5-C** cycle and the much bulkier **C2,C3-BC** bicycle. In all transition states, DAGOH occupies both sides of the H-O1-S-O2 plane in such a manner that **C2,C3-BC** and **C4,C5-C** are always on the right and left sides of this plane respectively. Hence, the preferred diastereomeric pathway will be that one having the less bulky substituent of the sulfur block in the right side. This substituent is O2 with pyridine since the whole base-H-O1-S-O2 set of atoms is in a coplanar arrangement in which the base stands far from DAGOH. With collidine, this substituent becomes the bulkiest one due to the alkylation and subsequent rotation of the base. Therefore, with pyridine the most stable transition state is that with O2 on the right side while for collidine is that with O2 on the left side, and obviously while the former transition state leads to the R enantiomer of the product, the latter gives rise to the S enantiomer. In summary, our results revealed that the replacement of pyridine by collidine induces a reversal of enantioselectivity due to an inversion of the chiral distribution of steric bulk around sulfur.

The steric model represented in Figure 6.6 can be used to tackle the optimization of the DAG method in a rational fashion. Regardless of the base used to neutralize the HCl by-product, enantioselectivity would rise by increasing the steric bulk of DAGOH and particulary that of the **C2,C3-BC** fragment. In the case of sterically inactive pro-R bases like pyridine, enantioselectivity can be improved introducing substituents bulkier than methyl in the starting sulfinyl chloride substrate. In the case of sterically active

pro-S bases like collidine, enantioselectivity would improve using much more sterically hindered bases.

Chapter 7

Conclusions

The main conclusions of the DFT(B3LYP) study on the reaction mechanism of the vanadium-catalyzed oxidation of 1,2-dimethyl disulfide by hydrogen peroxide were the following:

- There are two possible types of oxovanadium(+V) complexes which differ on how the oxidant is bound to the metal. In the most stable isomer, H_2O_2 is coordinated to vanadium as a monoanionic hydroperoxo HOO^- ligand in a η^1 fashion. In the other isomer, 4.4 kcal/mol above, H_2O_2 is bound to the metal as a dianionic peroxo OO^{2-} ligand in a η^2 mode.

- The vanadium-assisted oxidation of MeS-SMe follows a direct oxygen transfer mechanism, in which the oxidation process occurs in a single concerted step. This process, in which the absolute configuration of sulfur is decided, is the rate-determining step of the mechanism and consists of an electrophilic attack of the vanadium-coordinated peroxidic oxygen upon a sulfur of the substrate. The insertion pathway, in which MeS-SMe coordinates to vanadium prior to the oxidation, is not feasible.

- The η^1-hydroperoxo complex catalyzes the oxidation of the substrate reducing the energy barrier from 40.4 to 26.7 kcal/mol. The η^2-peroxo isomer catalyzes the sulfoxidation process as well, but through a higher energy barrier of 29.2 kcal/mol.

The main conclusions of the IMOMM(B3LYP:MM3) study on the origin of enantioselectivity in the vanadium-catalyzed sulfoxidation of 1,2-bis(*tert*-butyl) disulfide by hydrogen peroxide were the following:

- There are two diastereomers of the η^1-hydroperoxo catalyst, namely **A** and **B**, in which vanadium has opposite absolute configurations. **A** is more stable than **B** by 1.9 kcal/mol, but both isomers can catalyze the oxidation of 1,2-bis(*tert*-butyl) disulfide by hydrogen peroxide.

- Enantioselectivity depends on two energy gaps: 1) the energy difference between the pro-R and pro-S transition states connected to **A** (ΔE_A) and 2) the energy difference between the **A** pro-R and the **B** pro-S transition states (ΔE_{AB}).

- ΔE_A is sensitive to the nature of substituent R1. The steric bulk decrease from *t*-Bu to H in this position reduces ΔE_A from 2.4 to 0.3 kcal/mol.

- ΔE_{AB} depends on the nature of substituent R3. The replacement of *t*-Bu by the less bulky *i*-Pr group in this position reduces the value of ΔE_{AB} from 1.8 to 1.1 kcal/mol.

The main conclusions of the DFT(B3LYP) study on the reaction mechanism of the dynamic kinetic resolution (DKR) of methyl sulfinyl chloride by methanol in the presence of trimethylamine were:

- Trimethylamine catalyzes the racemization of methyl sulfinyl chloride. The energy barrier of the pyramidal inversion of this compound is reduced by the base from 63.4 to 22.3 kcal/mol.

- The chloride displacement by methanol in methyl sulfinyl chloride follows an addition/elimination mechanism. The addition step, in which the absolute configuration of sulfur is decided, involves the formation of the S-OMe bond and the elongation of the S-Cl bond.

- The addition process is coupled with a hydrogen transfer of the acidic hydrogen of methanol to the oxygen of methyl sulfinyl chloride. The

base reduces the energy barrier of the addition through the formation of a N-H bond with the transferred hydrogen.

- The lowest-energy pathway corresponds to the base-assisted neutral mechanism, in which methanol reacts directly with methyl sulfinyl chloride. The base reduces the energy barrier of the addition from 26.8 to 12.2 kcal/mol.

- Trimethylamine can also assist the addition of methanol in the ion pair mechanism, in which chloride is initially displaced by the base, but in this case the energy barrier is higher (14.4 kcal/mol).

The main conclusions of the ONIOM(B3LYP:UFF) study on the DAG method were:

- Both pyridine and collidine assist the hydrogen transfer involved in the addition of DAGOH to methyl sulfinyl chloride. While with pyridine the major product of the reaction is the R enantiomer, with collidine the major product is the S enantiomer.

- The R product is obtained in the reaction assisted by pyridine because in the pro-R transition state there is a favourable match between the bulkiest side of DAGOH and the little steric bulk of pyridine.

- Collidine is much more sterically active because it takes an arrangement perpendicular to that of pyridine. This results in an inversion of selectivity leading to the S enantiomer.

Bibliography

[1] Eliel, E. L.; Wilen, S. H.; Mander, L. N. *Stereochemistry of Organic Compounds*; John Wiley & Sons: New York, 1994.

[2] Kurihara, N.; Miyamoto, J.; Paulson, G. D.; Zeeh, B.; Skidmore, M. W.; Hollingworth, R. M.; Kuiper, H. A. *Pure Appl. Chem.* **1997,** *69,* 2007.

[3] Mellin, G. W.; Katzenstein, M. *N. Engl. J. Med.* **1962,** *267,* 1184.

[4] Tomaszewski, J.; Rumore, M. M. *Drug Dev. Ind. Pharm.* **1994,** *20,* 119.

[5] Thayer, A. M. *Chem. Eng. News* **2006,** *84,* 29.

[6] Veghini, D.; Henling, L. M.; Burkhardt, T. J.; Bercaw, J. E. *J. Am. Chem. Soc.* **1999,** *121,* 564.

[7] Hata, S.; Iguchi, M.; Iwasawa, T.; Yamada, K.-i.; Tomioka, K. *Org. Lett.* **2004,** *6,* 1721.

[8] Masuno, M. N.; Young, D. M.; Hoepker, A. C.; Skepper, C. K.; Molinski, T. F. *J. Org. Chem.* **2005,** *70,* 4162.

[9] Davis, F. A.; Chen, B. C. *Chem. Rev.* **1992,** *95,* 919.

[10] Klibanov, A. M. *Acc. Chem. Res.* **1990,** *23,* 114.

[11] Pamies, O.; Backvall, J.-E. *Chem. Rev.* **2003,** *103,* 3247.

[12] Wentworth, P.; Janda, K. D. In *Comprehensive Asymmetric Catalysis*; Jacobsen E. N.; Pfaltz, A.; Yamamoto, H. Eds.; Springer: Berlin, 1999; p. 1403.

[13] Knowles, W. S.; Sabacky, M. J. *Chem. Commun.* **1968,** *22,* 1445.

[14] Knowles, W. S. *Acc. Chem. Res.* **1983,** *16,* 106.

[15] Knowles, W. S. *J. Chem. Educ.* **1986,** *63,* 222.

[16] Michaelson, R. C.; Palmero, R.; Sharpless, K. B. *J. Am. Chem. Soc.* **1977,** *99,* 1990.

[17] Katsuki, T.; Sharpless, K. B. *J. Am. Chem. Soc.* **1980,** *102,* 5974.

[18] Miyashita, A.; Yasuda, A.; Takaya, H.; Toriumi, K.; Ito, T.; Souchi, T.; Noyori, R. *J. Am. Chem. Soc.* **1980,** *102,* 7932.

[19] Noyori, R.; Hashiguchi, S. *Acc. Chem. Res.* **1997,** *30,* 97.

[20] Knowles, W. S. *Angew. Chem. Int. Ed. Engl.* **2002,** *41,* 1998.

[21] Sharpless, K. B. *Angew. Chem. Int. Ed. Engl.* **2002,** *41,* 2024.

[22] Noyori, R. *Angew. Chem. Int. Ed. Engl.* **2002,** *41,* 2008.

[23] Collins, A. N.; Sheldrake, G.; Crosby, J. *Chirality in Industry: The Commercial Manufacture and Applications of Optically Active Compounds*; John Wiley & Sons: New York, 1995.

[24] Thayer, A. *Chem. Eng. News* **2005,** *83,* 55.

[25] Hawkins, J. M.; Watson, T. J. N. *Angew. Chem. Int. Ed. Engl.* **2004,** *43,* 3224.

[26] Thayer, A. *Chem. Eng. News* **2005,** *83,* 49.

[27] Aoyama, H.; Tokunaga, M.; Kiyosu, J.; Iwasawa, T.; Obora, Y.; Tsuji, Y. *J. Am. Chem. Soc.* **2005,** *127,* 10474.

[28] Birman, V. B.; Jiang, H. *Org. Lett.* **2005,** *7,* 3445.

[29] Paetzold, J.; Backvall, J. E. *J. Am. Chem. Soc.* **2005,** *127,* 17620.

[30] Ros, A.; Magriz, A.; Dietrich, H.; Fernandez, R.; Alvarez, E.; Lassaletta, J. M. *Org. Lett.* **2006,** *8,* 127.

[31] Leach, A. R. *Molecular Modelling*; Prentice Hall: Harlow, 2001.

[32] Levine, I. N. *Quantum Chemistry*; Prentice Hall: Harlow, 1999.

[33] Rappe, A. K.; Casewit, C. J. R. *Molecular Mechanics Across Chemistry*; University Science Books: New York, 1997.

[34] Norrby, P.-O.; Rasmussen, T.; Haller, J.; Strassner, T.; Houk, K. N. *J. Am. Chem. Soc.* **1999,** *121,* 10186.

[35] Jensen, F.; Norrby, P.-O. *Theor. Chem. Acc.* **2003,** *109,* 1.

[36] Gao, J. *Acc. Chem. Res.* **1996,** *29,* 298.

[37] Monard, G.; Merz, K. M., J. *Acc. Chem. Res.* **1999,** *32,* 904.

[38] Maseras, F. In *Computational Organometallic Chemistry*; Cundari, T., Ed.; Marcel Decker: New York, 2001, p 159.

[39] Ujaque, G.; Maseras, F. *Struct. Bond.* **2004,** *112,* 117.

[40] Koch, W.; Holthausen, M. C. *A Chemist's Guide to Density Functional Theory*; Wiley-VCH: Weinheim, 2001.

[41] Torrent, M.; Sola, M.; Frenking, G. *Chem. Rev.* **2000,** *100,* 439.

[42] Ziegler, T.; Autschbach, J. *Chem. Rev.* **2005,** *105,* 2695.

[43] Allemann, C.; Gordillo, R.; Clemente, F. R.; Cheong, P. H.-Y.; Houk, K. N. *Acc. Chem. Res.* **2004,** *37,* 558.

[44] Musaev, D. G.; Morokuma, K. In *Theoretical Aspects of Transition Metal Catalysis*; Frenking, G. Ed.; Springer: Berlin, 2005; p. 1.

[45] Sakaki, S.; Musashi, Y. In *Computational Modeling of Homogeneous Catalysis*; Maseras, F.; Lledós, A. Eds.; Kluwer: Dordrecht, 2002; p. 79.

[46] Michalak, A.; Ziegler, T. In *Theoretical Aspects of Transition Metal Catalysis*; Frenking, G. Ed.; Springer: Berlin, 2005; p. 145.

[47] Clot, E.; Eisenstein, O. In *Computational Modeling of Homogeneous Catalysis*; Maseras, F.; Lledós, A. Eds.; Kluwer: Dordrecht, 2002; p. 137.

[48] Deubel, D. V.; Loschen, C.; Frenking, G. In *Theoretical Aspects of Transition Metal Catalysis*; Frenking, G. Ed.; Springer: Berlin, 2005; p. 109.

[49] Solà, M.; Duran, M.; Torrent, M. In *Computational Modeling of Homogeneous Catalysis*; Maseras, F.; Lledós, A. Eds.; Kluwer: Dordrecht, 2002; p. 269.

[50] Sundermann, A.; Uzan, O.; Martin, J. M. L. *Chem. Eur. J.* **2001,** *7,* 1703.

[51] Braga, A. A. C.; Morgon, N. H.; Ujaque, G.; F., M. *J. Am. Chem. Soc.* **2005,** *127,* 9298.

[52] Álvarez, R.; Faza, O. N.; López, C. S.; de Lera, A. R. *Org. Lett.* **2006,** *8,* 35.

[53] Landis, C. R.; Hilfenhaus, P.; Feldgus, S. *J. Am. Chem. Soc.* **1999,** *121,* 8741.

[54] Feldgus, S.; Landis, C. R. *J. Am. Chem. Soc.* **2000,** *122,* 12714.

[55] Dapprich, S.; Ujaque, G.; Maseras, F.; Lledós, A.; Musaev, D. G.; Morokuma, K. *J. Am. Chem. Soc.* **1996,** *118,* 11660.

[56] Ujaque, G.; Maseras, F.; Lledós, A. *J. Am. Chem. Soc.* **1999,** *121,* 1317.

[57] Matsubara, T.; Koga, N.; Ding, Y.; Musaev, D. G.; Morokuma, K. *Organometallics* **1997,** *16,* 1065.

[58] Carbo, J. J.; Maseras, F.; Bo, C.; van Leeuwen, P. W. N. M. *J. Am. Chem. Soc.* **2001,** *123,* 7630.

[59] Magistrato, A.; Woo, T. K.; Togni, A.; Rothlisberger, U. *Organometallics* **2004,** *23,* 3218.

[60] Rayner, D. R.; Gordon, A. J.; Mislow, K. *J. Am. Chem. Soc.* **1968,** *90,* 4854.

[61] Lindberg, P.; Brandstrom, A.; Wallmark, B.; Mattson, H.; Rikner, L.; Hoffman, K.-J. *Med. Res. Rev.* **1990,** *10,* 1.

[62] Renfrey, S.; Featherstne, J. *Nature Rev. Drug Discov.* **2002,** *1,* 175.

[63] Cotton, H.; Elebring, T.; Larsson, M.; Li, L.; Sörensen, H.; von Unge, S. *Tetrahedron: Asymmetry* **2000,** *11,* 3819.

[64] Brown, T. J.; Chapman, R. F.; Cook, D. C.; Hart, T. W.; McLay, I. M.; Jordan, R.; Mason, J. S.; Palfreyman, M. N.; Walsh, R. J. A.; Withnall, M. T.; Aloup, J.-C.; Cavero, I.; D., F.; James, C.; Mondot, S. *J. Med. Chem.* **1992,** *35,* 3613.

[65] Schenk, W. A.; Durr, M. *Chem. Eur. J.* **1997,** *3,* 713.

[66] Ortega, M. P.; Garcia, M. D. C.; Gijon, M. A.; Casa-Juana, M. F. D.; Priego, J. G.; Crespo, M. S.; Sunkel, C. *J. Pharmacol. Exp. Ther.* **1990,** *255,* 28.

[67] Nakajima, N.; Enomoto, T.; Matsuura, N.; Ubukata, M. *Bioorg. Med. Chem. Lett.* **1998,** *8,* 3331.

[68] Chooi, S. Y. M.; Leung, P. H.; Sim, K. Y.; Tan, K. S.; Kon, O. L. *Tetrahedron: Asymmetry* **1994,** *5,* 49.

[69] Okamoto, K.; Nishito, T. *J. Biol. Chem.* **1995,** *270,* 7816.

[70] Carreño, M. C. *Chem. Rev.* **1995,** 1717.

[71] Fernández, I.; Khiar, N. *Chem. Rev.* **2003,** *103,* 3651.

[72] Solladie, G.; Maestro, M. C.; Rubio, A.; Pedregal, C.; Carreño, M. C.; Garcia Ruano, J. L. *J. Org. Chem.* **1991,** *56,* 2317.

[73] Solladie, G.; Huser, N.; Garcia Ruano, J. L.; Adrio, J.; Carreño, M. C.; Tito, A. *Tetrahedron Lett.* **1994,** *35,* 5297.

[74] Solladie, G.; Lohse, . *J. Org. Chem.* **1993,** *58,* 4555.

[75] Solladie, G.; Almario, A. *Tetrahedron: Asymmetry* **1995,** *5,* 1717.

[76] Solladie, G.; Ziani-Chérif, C. *J. Org. Chem.* **1993,** *58,* 2181.

[77] Solladie, G.; Ziani-Chérif, C.; Jesser, F. *Tetrahedron Lett.* **1992,** *33,* 931.

[78] Kosugi, H.; Kanno, O.; Uda, H. *Tetrahedron: Asymmetry* **1994,** *5,* 1139.

[79] Posner, G. H.; Asirvatham, E. *J. Org. Chem.* **1985,** *50,* 2591.

[80] Posner, G. H.; Kogan, T. P.; Haines, S. R.; Frye, L. L. *Tetrahedron Lett.* **1984,** *25,* 2627.

[81] Lee, A. W. M.; Chan, W. H.; Lee, Y.-K. *Tetrahedron Lett.* **1991,** *32,* 6861.

[82] Lee, A. W. M.; Chan, W. H.; Tao, Y.; Lee, Y. K. *J. Chem. Soc. Perkin Trans. 1* **1994,** 477.

[83] Posner, G. H.; Mallamo, J. P.; Miura, K. *J. Am. Chem. Soc.* **1981,** *103,* 2886.

[84] Corey, E. J.; Weigel, L. O.; Chamberlin, A. R.; Cho, H.; Hua, D. H. *J. Am. Chem. Soc.* **1980,** *102,* 6613.

[85] Pyne, S. G.; Dikic, B. *J. Org. Chem.* **1990,** *50,* 1932.

[86] Hua, D. H.; Sinai-Zingde, G.; Venkataraman, S. *J. Am. Chem. Soc.* **1985,** *107,* 4088.

[87] Hua, D. H.; Venkataraman, S.; Ostrander, R. A.; Sinai, G.-Z.; McCann, P. J.; Coulter, M. J.; Xu, M. R. *J. Org. Chem.* **1988,** *53,* 507.

[88] Hua, D. H.; Bharati, S. N.; Robinson, P. D.; Tsujimoto, A. *J. Org. Chem.* **1990,** *50,* 2128.

[89] Ferreira, J. T. B.; Marques, J. A.; Marino, J. P. *Tetrahedron: Asymmetry* **1994,** *5,* 641.

[90] Kosugi, H.; Miura, Y.; Kanna, H.; Uda, H. *Tetrahedron: Asymmetry* **1993,** *4,* 1409.

[91] Marino, J. P.; Bogdan, S.; Kimura, K. *J. Am. Chem. Soc.* **1992,** *114,* 5566.

[92] Takahashi, T.; Iyobe, A.; Arai, Y.; Koizumi, T. *Synlett* **1989,** 189.

[93] Arai, Y.; Hayashi, Y.; Yamamoto, M.; Takayama, H.; Koizumi, T. *Chem. Lett.* **1987,** 185.

[94] Gibbs, R. A.; Okamura, W. H. *J. Am. Chem. Soc.* **1988,** *110,* 4062.

[95] Gibbs, R. A.; Bartels, K.; Lee, R. W. K.; Okamura, W. H. *J. Am. Chem. Soc.* **1989,** *111,* 3717.

[96] Takayama, H.; Hayashi, K.; Koizumi, T. *Tetrahedron Lett.* **1986,** *27,* 5509.

[97] James, B. R.; McMillan, R. S.; Reimer, K. *J. Med. Chem.* **1976,** *1,* 439.

[98] Petra, D. G. I.; Kamer, P. C. J.; Spek, A. L.; Schoemaker, H. E.; van Leeuwen, P. W. N. M. *J. Org. Chem.* **2000,** *65,* 3010.

[99] Khiar, N.; Fernández, I.; Alcudia, F. *Tetrahedron Lett.* **1993,** *34,* 123.

[100] Owens, T. D.; Hollander, F. J.; Oliver, A. G.; Ellman, J. A. *J. Am. Chem. Soc.* **2001,** *123,* 1539.

[101] Carreño, M. C.; García-Ruano, J. L.; Maestro, M. C.; Martín Cabrejas, L. M. *Tetrahedron: Asymmetry* **1993,** *4,* 727.

[102] Priego, J.; Mancheño, O. G.; Cabrera, S.; Carretero, J. C. *J. Org. Chem.* **2002,** *67,* 1346.

[103] Allen, J. V.; Bower, J. F.; Williams, J. M. J. *Tetrahedron: Asymmetry* **1994,** *5,* 1895.

[104] Hiroi, K.; Suzuki, Y.; Abe, I.; Kawagishi, R. *Tetrahedron* **2000,** *56,* 4701.

[105] Light, D. R.; Waxman, D. J.; Walsh, C. T. *Biochemistry* **1982,** *21,* 2490.

[106] Andersson, M.; Willetts, A.; Allenmark, S. *J. Org. Chem.* **1997,** *62,* 8544.

[107] Ozaki, S.; Matsui, T.; Watanabe, Y. *J. Am. Chem. Soc.* **1997,** *119,* 6666.

[108] Cashman, J. R.; Olsen, L. D.; Boyd, D. R.; McMordie, R. A. S.; Dulop, R.; Dalton, H. *J. Am. Chem. Soc.* **1992,** *114,* 8772.

[109] Holland, H. L.; Brown, F. M.; Laksmaiah, G.; Larsen, B. G.; Patel, M. *Tetrahedron: Asymmetry* **1997,** *8,* 683.

[110] Buist, P. H.; Marecak, D. M. *J. Am. Chem. Soc.* **1992,** *114,* 5073.

[111] Schultz, P. G.; Lerner, R. A. *Science* **1995,** *269,* 1835.

[112] Nimri, S.; Keinan, E. *J. Am. Chem. Soc.* **1999,** *121,* 8978.

[113] Davis, F. A.; Weismiller, M. C.; Murphy, C. K.; Reddy, R. T.; Chen, B. C. *J. Org. Chem.* **1992,** *57,* 7274.

[114] Davis, F. A.; Reddy, R. T.; Han, W.; Carroll, P. J. *J. Am. Chem. Soc.* **1992,** *114,* 1428.

[115] Hamann, H. J.; Hoft, E.; Mostowicz, D.; Mishnev, A.; Urbanczyk-Lipkoswska, Z.; Chmielewski, M. *Tetrahedron* **1997,** *53,* 185.

[116] Adam, W.; Korb, M. N.; Roschmann, K. J.; Saha-Moller, C. R. *J. Org. Chem.* **1998,** *63,* 3423.

[117] Bolm, C.; Muñiz, K.; Hildebrand, J. P. In *Comprehensive Asymmetric Catalysis*; Jacobsen E. N.; Pfaltz, A.; Yamamoto, H. Eds.; Springer: Berlin, 1999; p. 697.

[118] Rouhi, A. M. *Chem. Eng. News* **2003,** *81,* 56.

[119] Johnson, R. A.; Sharpless, K. B.; In *Catalytic Asymmetric Synthesis*; Ojima, I., Ed.; Wiley-VCH: New York, 1993; p. 227.

[120] Pitchen, P.; Deshmukh, M. N.; Duñach, E.; Kagan, H. B. *J. Am. Chem. Soc.* **1984,** *106,* 8188.

[121] Zhao, S. H.; Samuel, O.; Kagan, H. B. *Tetrahedron* **1987,** *43,* 5135.

[122] Brunel, J. M.; Kagan, H. B. *Synlett* **1996,** 404.

[123] Pitchen, P.; France, C. J.; McFarlane, I. M.; Newton, C. G.; Thompson, D. M. *Tetrahedron Lett.* **1994,** *35,* 485.

[124] Pitchen, P. In *Chirality in Industry II*; Collins, A. N., Sheldrake, G. N., Crosby, J., Eds.; John Wiley & Sons: New York, 1997; p. 381.

[125] Davis, F. A.; Kern, J. R.; Kurtz, J. L.; Pfister, J. R. *J. Am. Chem. Soc.* **1988,** *110,* 7873.

[126] Miyashita, K.; Nishimota, M.; Ishino, T.; Murafuji, H.; Obika, S.; Muraoka, O.; Imanishi, T. *Tetrahedron* **1997,** *53,* 4279.

[127] Di Furia, F.; Modena, G.; Seraglia, R. *Synthesis* **1984,** 325.

[128] Bortolini, O.; Di Furia, F.; Licini, G.; Modena, G.; Rossi, M. *Tetrahedron Lett.* **1986,** *27,* 6257.

[129] Komatsu, N.; Hashizume, M.; Sugita, T.; Umeura, S. *J. Org. Chem.* **1993,** *58,* 4529.

[130] Donnoli, M. I.; Superchi, M. I.; Rosini, C. *J. Org. Chem.* **1998,** *63,* 9392.

[131] Martyn, L. J. P.; Pandaraju, S.; Yudin, A. K. *J. Organomet. Chem.* **2000,** *98,* 603.

[132] Di Furia, F.; Licini, G.; Modena, G.; Motterle, R.; Nugent, W. *J. Org. Chem.* **1996,** *61,* 5175.

[133] Bonchio, M.; Licini, G.; Di Furia, F.; Mantovani, S.; Modena, G.; Nugent, W. *J. Org. Chem.* **1999,** *64,* 1326.

[134] Darensbourg, D. J.; Mackiewicz, R. M.; Phelps, A. L.; Billodeaux, D. R. *Acc. Chem. Res.* **2004,** *37,* 836.

[135] McGarrigle, E. M.; Gilheany, D. G. *Chem. Rev.* **2005,** *105,* 1563.

[136] Colombo, A.; Marturano, G.; Pasini, A. *Gazz. Chim. Ital.* **1986,** 35.

[137] Nakajima, K.; Kojima, M.; Fujita, J. *Chem. Lett.* **1986,** 1483.

[138] Palucki, M.; Hanson, P.; Jacobsen, E. N. *Tetrahedron Lett.* **1992,** *33,* 7111.

[139] Noda, K.; Hosoya, N.; Irie, R.; Yamashita, Y.; Katsuki, T. *Tetrahedron* **1994,** *50,* 9609.

[140] Saito, B.; Katsuki, T. *Tetrahedron Lett.* **2001,** *42,* 3873.

[141] Bolm, C.; Binewald, F. *Angew. Chem. Int. Ed. Engl.* **1995,** *34,* 2640.

[142] Legros, J.; Bolm, C. *Angew. Chem. Int. Ed. Engl.* **2003,** *42,* 5487.

[143] Legros, J.; Bolm, C. *Angew. Chem. Int. Ed. Engl.* **2004,** *43,* 4225.

[144] Legros, J.; Bolm, C. *Chem. Eur. J.* **2005,** *11,* 1086.

[145] Bryliakov, K. P.; Talsi, E. P. *Angew. Chem. Int. Ed. Engl.* **2004,** *43,* 5228.

[146] Mekmouche, Y.; Hummel, H.; Ho, R. Y. N.; Que, L.; Schünemann, V.; Thomas, F.; Trautwein, A. X.; Lebrun, C.; Gorgy, K.; Leprête, J.-C.; Collomb, M.-N.; Deronzier, A.; Fontecave, M.; Ménage, S. *Chem. Eur. J.* **2002,** *8,* 1196.

[147] Evans, J. W.; Fierman, M. B.; Miller, S. J.; Ellman, J. A. *J. Am. Chem. Soc.* **2004,** *126,* 8134.

[148] Andersen, K. K. *Tetrahedron Lett.* **1962,** 93.

[149] Andersen, K. K.; Gaffield, W.; Papanikolaou, N. E.; Foley, J. W.; Perkins, R. I. *J. Am. Chem. Soc.* **1964,** *86,* 5637.

[150] Mislow, K.; Ternay, A.; Melillo, J. T. *J. Am. Chem. Soc.* **1963,** *85,* 2329.

[151] Alexrod, M.; Bickert, P.; Jacobus, J.; Green, M.; Mislow, K. *J. Am. Chem. Soc.* **1968,** *90,* 4835.

[152] Mioskowski, C.; Solladie, G. *Tetrahedron Lett.* **1975,** 3341.

[153] Solladie, G.; Hutt, J.; Girardin, A. *Synthesis* **1987,** 173.

[154] Drabowicz, J.; Kielbasinski, P.; Mikolajczyk, M. In *The Chemistry of Sulfones and Sulfoxides*; Patai, S., Rappaport, Z., Stirling, C., Eds.; Wiley & Sons: New York, 1988; Chapter 8.

[155] Whitesell, J. K. *Chem. Rev.* **1992,** *92,* 953.

[156] Whitesell, J. K.; Wong, M.-S. *J. Org. Chem.* **1991,** *4552,*.

[157] Evans, D. A.; Kandor, S. W.; Jones, T. K.; Clardy, J.; Stout, T. J. *J. Am. Chem. Soc.* **1990,** *112,* 7001.

[158] Evans, D. A.; Faul, M. M.; Colombo, L.; Bisaha, J. J.; Clardy, J.; Cherry, D. *J. Am. Chem. Soc.* **1992,** *114,* 5977.

[159] Bueno, A. B.; Carreno, M. C.; Garcia Ruano, J. L.; Gomez Arrayas, R.; Zarzuelo, M. M. *J. Org. Chem.* **1997,** *62,* 2139.

[160] Oppolzer, W. *Pure Appl. Chem.* **1990,** *62,* 1241.

[161] Oppolzer, W.; Froelich, O.; Wiaux-Zamar, C.; Bernardinelli, G. *Tetrahedron Lett.* **1997,** *38,* 2825.

[162] Fernández, I.; Khiar, N.; Llera, J. M.; Alcudia, F. *J. Org. Chem.* **1992,** *57,* 6789.

[163] Khiar, N.; Alcudia, F.; Espartero, J.; Rodríguez, L.; Fernández, I. *J. Am. Chem. Soc.* **2000,** *122,* 7598.

[164] Khiar, N.; Araujo, C. S.; Alcudia, F.; Fernández, I. *J. Org. Chem.* **2002,** *67,* 345.

[165] Peltier, H. M.; Evans, J. W.; Ellman, J. A. *Org. Lett.* **2005,** *7,* 1733.

[166] Shibata, N.; Matsunaga, M.; Nakagawa, M.; Fukuzumi, T.; Nakamura, S.; Toru, T. *J. Am. Chem. Soc.* **2005,** *127,* 1374.

[167] Shibata, N.; Matsunaga, M.; Nakagawa, M.; Fukuzumi, T.; Nakamura, S.; Toru, T. *Org. Lett.* **2005,** *7,* 1465.

[168] Wudl, F.; Lee, T. B. K. *J. Am. Chem. Soc.* **1973,** *95,* 6349.

[169] Benson, S. C.; Snider, J. K. *Tetrahedron Lett.* **1991,** *32,* 5885.

[170] Rebiere, F.; Kagan, H. B. *Tetrahedron Lett.* **1989,** *30,* 3659.

[171] Rebiere, F.; Samuel, O.; Ricard, L.; Kagan, H. B. *J. Org. Chem.* **1991,** *56,* 5991.

[172] Rebiere, F.; Riant, O.; Kagan, H. B. *Tetrahedron: Asymmetry* **1990,** *1,* 199.

[173] Rebière, F.; Riant, O.; Ricard, L.; Kagan, H. B. *Angew. Chem. Int. Ed. Engl.* **1993,** *32,* 568.

[174] Cogan, A. D.; Liu, G.; Kim, K.; Backes, B. J.; Ellman, J. A. *J. Am. Chem. Soc.* **1998,** *120,* 8011.

[175] Butler, A.; Walker, J. V. *Chem. Rev.* **1993,** *93,* 1937.

[176] Raugei, S.; Carloni, P. *J. Phys. Chem. B* **2006,** *110,* 3747.

[177] Bolm, C.; Schlingloff, G.; Bienewald, F. *J. Mol. Cat. A: Chem.* **1997,** *117,* 347.

[178] Bolm, C.; Bienewald, F. *Synlett* **1998,** 1327.

[179] Vetter, A. H.; Berkessel, A. *Tetrahedron Lett.* **1998,** *39,* 1741.

[180] Skarzewski, J.; Ostrycharz, E.; Siedlecka, R. *Tetrahedron: Asymmetry* **1999,** *10,* 3457.

[181] Skarzewski, J.; Wojazczynska, E.; Turowska-Tyrk, I. *Tetrahedron: Asymmetry* **2002,** *13,* 369.

[182] Jeong, Y. C.; Choi, S.; Hwang, Y. D.; Anh, K. *Tetrahedron Lett.* **2004,** *45,* 9249.

[183] Jeong, Y. C.; Hwang, Y. D.; Choi, S.; Anh, K. *Tetrahedron: Asymmetry* **2005,** *16,* 3497.

[184] Drago, C.; Caggiano, L.; Jackson, R. F. W. *Angew. Chem. Int. Ed. Engl.* **2005,** *44,* 7221.

[185] Cucciolito, M. E.; Del Litto, R.; Roviello, G.; Ruffo, F. *J. Mol. Cat. A: Chem.* **2005,** *236,* 176.

[186] Ellman, J. A.; Owens, T. D.; Tang, T. P. *Acc. Chem. Res.* **2002,** *35,* 984.

[187] Weix, D. J.; Ellman, J. A. *Org. Lett.* **2003,** *5,* 1317.

[188] Kagan, H. B. In *Catalytic Asymmetric Synthesis*; Ojima, I., Ed.; Wiley-VCH: New York, 1993; p. 203.

[189] Bonchio, M.; Calloi, S.; Di Furia, F.; Licini, G.; Modena, G.; Moro, S.; Nugent, W. *J. Am. Chem. Soc.* **1997,** *119,* 6935.

[190] Bonchio, M.; Licini, G.; Modena, G.; Bartolini, O.; Moro, S.; Nugent, W. *J. Am. Chem. Soc.* **1999,** *121,* 6258.

[191] Smith, T. S.; Pecoraro, V. L. *Inorg. Chem.* **2002,** *41,* 6754.

[192] ten Brink, H. B.; Tuynman, A.; Dekker, H. L.; Hemrika, W.; Izumi, Y.; Oshiro, T.; Schoemaker, H. E.; Wever, R. *Inorg. Chem.* **1998,** *37,* 6780.

[193] Zampella, G.; Fantucci, P.; Pecoraro, V. L.; De Gioia, L. *J. Am. Chem. Soc.* **2005,** *127,* 953.

[194] Butler, A.; Clague, M. J.; E., M. G. *Chem. Rev.* **1994,** *94,* 625.

[195] Curci, R.; Di Furia, F.; Testi, R.; Modena, G. *J. Chem. Soc. Perkin Trans. 2* **1972,** 752.

[196] Blum, S. A.; Bergman, R. G.; Ellman, J. A. *J. Org. Chem.* **2003,** *68,* 150.

[197] Karpyshev, N. N.; Yakovleva, O. D.; Talsi, E. P.; Bryliakov, K. P.; Tolstikova, O. V.; Tolstikov, A. G. *J. Mol. Cat. A: Chem.* **2000,** *157,* 91.

[198] Bryliakov, K. P.; Karpyshev, N. N.; Fominsky, S. A.; Tolstikov, A. G.; Talsi, E. P. *J. Mol. Cat. A: Chem.* **2001,** *171,* 73.

[199] Rösch, N.; Di Valentin, C.; Yudanov, I. V. In *Computational Modeling of Homogeneous Catalysis*; Maseras, F.; Lledós, A. Eds.; Kluwer: Dordrecht, 2002; p. 289.

[200] DiValentin, C.; Gandolfi, P.; Gisdakis, R.; Rösch, N. *J. Am. Chem. Soc.* **2001,** *123,* 2365.

[201] Wu, Y. D.; Lai, D. K. W. *J. Am. Chem. Soc.* **1995,** *52,* 11327.

[202] Wu, Y. D.; Sun, J. *J. Org. Chem.* **1998,** *63,* 1752.

[203] Deubel, D. V.; Sundermeyer, J.; Frenking, G. *J. Am. Chem. Soc.* **2000,** *122,* 10101.

[204] Deubel, D. V.; Sundermeyer, J.; Frenking, G. *Org. Lett.* **2001,** *3,* 329.

[205] Hroch, A.; Gemmecker, G.; Thiel, W. R. *Eur. J. Inorg. Chem.* **2000,** 1107.

[206] Simonnet-Jegat, C.; Secheresse, F. *Chem. Rev.* **2001,** *101,* 2601.

[207] Jörgensen, K. A. *J. Chem. Soc. Perkin Trans. 2* **1994,** 117.

[208] Becke, A. D. *J. Chem. Phys.* **1993,** *98,* 5648.

[209] Lee, C.; Parr, R. G.; Yang, W. *Phys. Rev.* **1988,** *37,* B785.

[210] Frisch, M. J.; Trucks, G. W.; Schlegel, H. B.; Scuseria, G. E.; Robb, M. A.; Cheeseman, J. R.; Zakrzewski, V. G.; Montgomery, J. A.; Jr. Stratmann, R. E.; Burant, J. C.; Dapprich, S.; Millam, J. M.; Daniels, A. D.; Kudin, K. N.; Strain, M. C.; Farkas, O.; Tomasi, J.; Barone, V.; Cossi, M; Cammi, R.; Mennucci, B.; Pomelli, C.; Adamo, C.; Clifford, S.; Ochterski, J.; Petersson, G. A.; Ayala, P. Y.; Cui, Q.; Morokuma, K.; Malick,D. K.; Rabuck, A. D.; Raghavachari, K.; Foresman, J. B.; Cioslowski, J.; Ortiz, J. V.; Stefanov, B. B.; Liu, G.; Liashenko, A. Piskorz, P.; Komaromi, I.; Gomperts, R.; Martin, R. L.; Fox, D. J.; Keith, T. Al-Laham, M. A.; Peng, C. Y.; Nanayakkara, A.; Gonzalez, C.; Challacombe, M.; Gill, P M. W.; Johnson, B.; Chen, W.; Wong, M. W.; Andres, J. L.; Gonzalez, C.; Head-Gordon, M.; Replogle, E. S.; Pople, J. A., *Gaussian* (Gaussian, Inc., Pittsburgh PA, 1998).

[211] Hay, P. J.; Wadt, W. R. *J. Chem. Phys.* **1985,** *82,* 299.

[212] Wadt, W. R.; Hay, P. J. *J. Chem. Phys.* **1985,** *82,* 284.

[213] Höllwarth, A.; Böhme, M.; Dapprich, S.; Ehlers, A. W.; Gobbi, A.; Jonas, V.; Köhler, K. F.; Stegmann, R.; Veldkamp, A.; Frenking, G. *Chem. Phys. Lett.* **1993,** *208,* 237.

[214] Hehre, W. J.; Ditchfield, R.; Pople, J. A. *J. Phys. Chem.* **1972,** *56,* 2257.

[215] Hariharan, P. C.; Pople, J. A. *Theor. Chim. Acta* **1973,** *28,* 213.

[216] Reed, A. E.; Weinhold, F. *J. Chem. Phys.* **1983,** *78,* 4066.

[217] Reed, A. E.; Weinstock, R. B.; Weinhold, F. *J. Chem. Phys.* **1985,** *83,* 735.

[218] Francl, M. M.; Pietro, W. J.; Hehre, W. J.; Binkley, J. S.; Gordon, M. S.; Defrees, D. J.; Pople, J. A. *J. Phys. Chem.* **1982,** *77,* 3654.

[219] Clark, T.; Chandrasekhar, J.; Spitznagel, G. W.; Schleyer, P. v. R. *J. Comput. Chem.* **1983,** *3,* 294.

[220] Miertu, S.; Scrocco, E.; Tomasi, J. *Chem. Phys.* **1981,** *55,* 117.

[221] Bach, R. D.; Wolber, G. J.; Coddens, B. A. *J. Am. Chem. Soc.* **1984,** *106,* 6098.

[222] Baboul, A. G.; Schlegel, H. B.; Glukhovtsev, M. N.; Bach, R. D. *J. Comput. Chem.* **1998,** *19,* 1353.

[223] Lipkowitz, K. B.; D'Hue, C. A.; Sakamoto, T.; Stack, J. N. *J. Am. Chem. Soc.* **2002,** *124,* 14255.

[224] Maseras, F.; Morokuma, K. *J. Comput. Chem.* **1995,** *16,* 1170.

[225] Allinger, N. L., *MM3(92)*; QCPE: Bloomington, IN, 1992.

[226] Allinger, N. L.; Yuh, Y. H.; Lii, J. H. *J. Am. Chem. Soc.* **1989,** *111,* 8551.

[227] Maseras, F. *Chem. Commun.* **2000,** 1821.

[228] Gundertofte, K.; Liljefors, T.; Norrby, P. O. *J. Comput. Chem.* **1996,** *17,* 429.

[229] Rappé, A. K.; Casewit, C. J.; Colwell, D. S.; Goddard, W. A.; Skiff, W. N. *J. Am. Chem. Soc.* **1992,** *114,* 10024.

[230] Balcells, D.; Drudis-Solé, G.; Besora, M.; Dölker, N.; Ujaque, G.; Maseras, F.; Lledós, A. *Faraday Discuss.* **2003,** *124,* 429.

[231] Gu, Y.; Kar, T.; Scheiner, S. *J. Am. Chem. Soc.* **1999,** *121,* 9411.

[232] Baures, P. W.; Beatty, A. M.; Dhanasekaran, M.; Helfrich, B. A.; Perez-Segarra, W.; Desper, J. *J. Am. Chem. Soc.* **2002,** *124,* 11315.

[233] Kar, T.; Scheiner, S. *J. Phys. Chem. A.* **2004,** *108,* 9161.

[234] Moller, C.; Plesset, M. S. *Phys. Rev.* **1934,** *46,* 618.

[235] Krishnan, R.; Binkley, J. S.; Seeger, R.; Pople, J. A. *J. Chem. Phys.* **1980,** *72,* 650.

[236] Brunel, J. M. *Chem. Rev.* **2005,** *105,* 857.

[237] Chen, Y.; Yekta, S.; Yudin, A. K. *Chem. Rev.* **2003,** *103,* 3155.

[238] Noyori, R.; Takaya, H. *Acc. Chem. Res.* **1990,** *23,* 345.

[239] Berthod, M.; Mignani, G.; Woodward, G.; Lemaire, M. *Chem. Rev.* **2005,** *105,* 1801.

[240] S., V. N.; Kuppuraj, G.; Rajagopal, S. *Coord. Chem. Rev.* **2005,** *249,* 1249.

[241] Canali, L.; Sherrington, D. C. *Chem. Soc. Rev.* **1999,** *28,* 85.

[242] Huerta, F. F.; Minidis, A. B. E.; Bäckvall, J. *Chem. Soc. Rev.* **2001,** *30,* 321.

[243] Pellissier, H. *Tetrahedron* **2003,** *59,* 8291.

[244] Tokunoh, R.; Sodekoa, M.; Ace, K.; Shibasaki, M. *Tetrahedron Lett.* **1995,** *44,* 8035.

[245] Zhang, Y.; Talay, P.; Cho, C.-G.; Posner, G. H. *Proc. Natl. Acad. Sci. USA* **1992,** *89,* 2399.

[246] Zhang, Y.; Talay, P.; Cho, C.-G.; Posner, G. H. *J. Am. Chem. Soc.* **1992,** *114,* 5946.

[247] Kincaid, J. F.; Henriques, J. *J. Am. Chem. Soc.* **1940,** *62,* 1474.

[248] Bushweller, C. H.; Anderson, W. G.; Stevenson, P. E.; Burkey, D. L.; O'Neil, J. W. *J. Am. Chem. Soc.* **1974,** *96,* 3892.

[249] Kost, D.; Raban, M. *J. Am. Chem. Soc.* **1982,** *104,* 2960.

[250] Lee, J. S. *J. Phys. Chem. A.* **1997,** *101,* 8762.

[251] Morgan, W. R.; Leyden, D. E. *J. Am. Chem. Soc.* **1970,** *92,* 4527.

[252] Forsyth, D.; Zhang, W.; Hanley, J. *J. Org. Chem.* **1996,** *61,* 1284.

[253] Wash, P.; Renslo, A.; Rebek, J. *Angew. Chem. Int. Ed. Engl.* **2001,** *40,* 1221.

[254] Naik, A.; Ferro, M.; Worman, J. *Org. Lett.* **2002,** *4,* 1059.

[255] Koch, P.; Fava, A. *J. Am. Chem. Soc.* **1968,** *90,* 3867.

[256] Bickart, P.; Carson, F. W.; Jacobus, J.; Miller, E. G. *J. Am. Chem. Soc.* **1968,** *90,* 4869.

[257] Yuste, F.; Ortiz, B.; Pérez, I.; Rodríguez-Hernández, A.; Sánchez-Obregón, R.; Walls, F.; Ruano, J. L. G. *Tetrahedron* **2002,** *58,* 2613.

[258] Miller, E.; Rayner, D. R.; Thomas, H. T.; Mislow, K. *J. Am. Chem. Soc.* **1968,** *90,* 4861.

[259] Bachrach, S. M.; Woody, J. T.; Mulhearn, D. C. *J. Org. Chem.* **2002,** *67,* 8983.

[260] Hayes, J. M.; Bachrach, S. M. *J. Phys. Chem. A.* **2003,** *107,* 7952.

[261] Norton, S. H.; Bachrach, S. M.; Hayes, J. M. *J. Org. Chem.* **2005,** *70,* 5896.

[262] Frisch, M. J.; Trucks, G. W.; Schlegel, H. B.; Scuseria, G. E.; M. A. Robb, J. R. Cheeseman, J. A. Montgomery, Jr., T. Vreven, Kudin, K. N.; Burant, J. C.; Millam, J. M.; Iyengar, S. S.; Tomasi, J.; Barone, V.; Mennucci, B.; Cossi, M.; Scalmani, G.; Rega, N.; Petersson, G. A.; Nakatsuji, H.; Hada, M.; Ehara, M.; Toyota, K.; Fukuda, R.; Hasegawa, J.; Ishida, M.; Nakajima, T.; Honda, Y.; Kitao, O.; Nakai, H.; Klene, M.; Li, X.; Knox, J. E.; Hratchian, H. P.; Cross, J. B.; Adamo, C.; Jaramillo, J.; Gomperts, R.; Stratmann, R. E.; Yazyev, O.; Austin, A. J.; Cammi, R.; Pomelli, C.; Ochterski, J. W.; Ayala, P. Y.; Morokuma, K.; Voth, G. A.; Salvador, P.; Dannenberg, J. J.; Zakrzewski, V. G.; Dapprich, S.; Daniels, A.D.; Strain, M. C.; Farkas, O.; Malick, D. K.; Rabuck, A. D.; Raghavachari, K.; Foresman, J. B.; Ortiz, J. V.; Cui, Q.; Baboul, A. G.; Clifford, S.; Cioslowski, J.; Stefanov,

B. B.; Liu, G.; Liashenko, A.; Piskorz, P.; Komaromi, I.; Martin, R. L.; Fox, D. J.; Keith, T.; Al-Laham, M. A.; Peng, C. Y.; Nanayakkara, A.; Challacombe, M.; Gill, P. M. W.; Johnson, B.; Chen, W.; Wong, M. W.; Gonzalez, A.; and Pople, J. A. *Gaussian 03* Revision C.02, Gaussian Inc., Pittsburgh PA, 2003.

[263] Check, C. E.; Faust, T. O.; Bailey, J. M.; Wright, B. J.; Gilbert, T. M.; Sunderlin, L. S. *J. Phys. Chem. A.* **2001,** *105,* 8111.

[264] Gonzalez, C.; Schlegel, H. B. *J. Chem. Phys.* **1989,** *90,* 2154.

[265] Barone, V.; Cossi, M. *J. Phys. Chem. A.* **1998,** *102,* 1995.

[266] Christe, K. O.; Dixon, D. A.; Mercier, H. P. A.; Sanders, J. C. P.; Schrobilgen, G. J.; Wilson, W. W. *J. Am. Chem. Soc.* **1994,** *116,* 2850.

[267] Taha, A. N.; True, N. S.; LeMaster, C. B.; LeMaster, C. L.; Neugebauer-Crawford, S. M. *J. Phys. Chem. A.* **2000,** *104,* 3341.

[268] Steudel, R.; Steudel, Y.; Miaskiewicz, K. *Chem. Eur. J.* **2001,** *7,* 3281.

[269] Kawashima, T. *Coord. Chem. Rev.* **2003,** *244,* 137.

[270] Feldgus, S.; Landis, C. R. *Organometallics* **2001,** *20,* 2374.

[271] Kitagawa, O.; Matsuo, S.; Yotsumoto, K.; Taguchi, T. *J. Org. Chem.* **2006,** *71,* 2524.

[272] Seebach, D.; Dahinden, R.; Marti, R. E.; Beck, A. K.; Plattner, D. A.; Kuehnle, F. N. M. *J. Org. Chem.* **1995,** *60,* 1788.

[273] Hoarau, O.; Ait-Haddou, H.; Daran, J.-C.; Cramailere, D.; Balavoine, G. G. A. *Organometallics* **1999,** *18,* 4718.

[274] Luna, A. P.; Bonin, M.; Micouin, L.; Husson, H.-P. *J. Am. Chem. Soc.* **2002,** *124,* 12098.

[275] Du, D.-M.; Lu, S.-F.; Fang, T.; Xu, J. *J. Org. Chem.* **2005,** *70,* 3712.

[276] Svensson, M.; Humbel, S.; Froese, R. D. J.; Matsubara, T.; Sieber, S.; Morokuma, K. *J. Phys. Chem.* **1996,** *100,* 19357.

[277] Chang, G.; Guida, W. C.; Still, W. C. *J. Am. Chem. Soc.* **1989,** *111,* 4379.

[278] Saunders, M.; Houk, K. N.; Wu, Y. D.; Still, W. C.; Lipton, M.; Chang, G.; Guida, W. C. *J. Am. Chem. Soc.* **1990,** *112,* 1419.

[279] MacroModel 8.5, Schrödinger L.L.C., 2003.

[280] Halgren, T. A. *J. Comput. Chem.* **1999,** *20,* 720.

[281] Halgren, T. A. *J. Comput. Chem.* **1999,** *20,* 730.

Part II

Articles I, II and III

Article I

Balcells, D.; Maseras, F.; Lledós, A. *J. Org. Chem.*, **2003**, *68*, 4265.

Article II

Balcells, D.; Maseras, F.; Ujaque, G. *J. Am. Chem. Soc.*, **2005**, *127*, 3624.

Article III

Balcells, D.; Maseras, F.; Khiar, N. *Org. Lett.*, **2004**, *6*, 2197.

Appendix. Articles IV and V

These articles have not been published yet and officially they are not part of this thesis. Nevertheless, they have been included for the sake of completeness. Article IV has been accepted for publication and Article V has been recently submitted for publication.

Article IV

Balcells, D.; Ujaque, G.; Fernandez, I.; Khiar, N.; Maseras, F. *J. Org. Chem.*, **2006**, in press.

Article V

Balcells, D.; Ujaque, G.; Fernandez, I.; Khiar, N.; Maseras, F. *submitted*.